AL.2.1992-302
c.2

AOSTRA TECHNICAL PUBLICATION SERIES #13

AOSTRA Mini-Frac Manual

FIELD TESTING, ANALYSIS AND INTERPRETATION PROCEDURES

Selim S. Hannan and Ben I. Nzekwu
May 1992

Alberta
OIL SANDS TECHNOLOGY
AND RESEARCH AUTHORITY

AOSTRA TECHNICAL PUBLICATION SERIES #13

CANADIANA
JUN 23 1992

AOSTRA
Mini-Frac Manual

FIELD TESTING, ANALYSIS AND INTERPRETATION PROCEDURES

Selim S. Hannan and Ben I. Nzekwu
May 1992

Alberta
OIL SANDS TECHNOLOGY
AND RESEARCH AUTHORITY

OTHER PUBLICATIONS IN THE AOSTRA TECHNICAL PUBLICATION SERIES

1. *Syncrude Analytical Methods For Oil Sand and Bitumen Processing*
2. *The Thermodynamic and Transport Properties of Bitumens and Heavy Oils*
3. *Aquathermolysis: A Synopsis of Work on the Chemical Reaction Between Water (Steam) and Heavy Oil Sands During Simulated Steam Stimulation*
4. *Oil Sands Composition and Behaviour Research*
5. *A Review of Analytical Methods For Bitumens and Heavy Oils*
6. *AOSTRA Technical Handbook on Oil Sands, Bitumens and Heavy Oils*
7. *Resource Characterization of the McMurray/Wabiskaw Deposit in the Athabasca Central Region of Northeastern Alberta*
8. *Resource Characterization of the McMurray/Wabiskaw Deposit in the Athabasca South Region of Northeastern Alberta*
9. *Resource Characterization of the McMurray/Wabiskaw Deposit in the Athabasca West Region of Northeastern Alberta* *
10. *Resource Characterization of the McMurray/Wabiskaw Deposit in the Athabasca Oil Sands Area: A synthesis* *
11. *Syncrude Analytical Methods Manual For Bitumen Upgrading*
12. *Fundamentals of electrokinetic and interfacial phenomenon with applications to oil sands*

---

* To be published at a future date.

AOSTRA MINI-FRAC MANUAL

Copyright 1992 by AOSTRA. All rights reserved. Printed in Canada. No part of this publication may be reproduced, stored in a retrieval system, or transmitted, in any form or by any means, electronic, mechanical, photocopying, recording, or otherwise, without the prior permission of the publisher.

ISBN 0-7732-1052-0

PUBLISHED BY
ALBERTA OIL SANDS TECHNOLOGY AND RESEARCH AUTHORITY
500 HIGHFIELD PLACE
10010 - 106 STREET
EDMONTON, ALBERTA, CANADA
T5J 3L8

PUBLISHER'S NOTE

AOSTRA TECHNICAL PUBLICATION SERIES
NUMBER 13

AOSTRA is pleased to publish this thirteenth book in a series of special publications by industry and academic authors. Like its predecessors, this publication is designed to make available, research results, analytical procedures, and engineering data on the properties and behaviour of Alberta petroleum resources that may otherwise not be available to the public.

William J. Yurko

W.J. Yurko
Chairman and Chief Executive Officer
Alberta Oil Sands Technology and Research Authority
Edmonton, Alberta, Canada

May 1992

The Alberta Oil Sands Technology and Research Authority (AOSTRA) makes no warranty, express or implied, nor assumes any legal liability or responsibility for the accuracy, completeness, or usefulness of any information, apparatus, product, or process disclosed in this publication, or represents that its use would not infringe on privately owned rights. Reference herein to any specific commercial product, process, or service by trade name, trademark, manufacturer, or otherwise, does not necessarily constitute or imply its endorsement, recommendation, or favoring by AOSTRA. The views and opinions of authors expressed herein do not necessarily reflect those of AOSTRA.

ACKNOWLEDGMENTS

We wish to express our gratitude to the management of the Calgary office of the Alberta Oil Sands Technology and Research Authority (AOSTRA) — Dr. Richard Luhning, Mr. John Scott, and Mr. William Good, for their support and encouragement during the course of this work. We would like to thank the Society of Petroleum Engineers, the Petroleum Society of CIM, and the Pergamon Press Plc. for granting us permission to reproduce some figures published originally in their journals. We thank Ms. Brenda Belland of AOSTRA Library and Information Services for her relentless effort in promptly delivering requested materials. Secretarial service provided by Ms. Beth Hill and Ms. Donna Kostuik of AOSTRA Calgary office is also acknowledged. Ms. Diane Teppan of the AOSTRA Edmonton office handled the publication. Her efforts are gratefully acknowledged.

Digitized by the Internet Archive
in 2015

https://archive.org/details/aostraminifracma00hann

TABLE OF CONTENTS

ACKNOWLEDGMENTS vii

TABLE OF CONTENTS ix

LIST OF FIGURES AND TABLES xiii

CRITICAL REVIEW xvi

PREFACE xvii

ABOUT THE AUTHORS xix

SUMMARY xxi

INTRODUCTION xxiii

OBJECTIVES OF THE MANUAL xxv

CHAPTER 1 1

- 1 **STRESS ALTERATION CAUSED BY BOREHOLE PRESENCE** 2
- 1.1 ELASTIC ANALYSIS 2
- 1.1.1 For vertical uncased borehole 2
- 1.1.2 For inclined borehole 3
- 1.2 PLASTIC ANALYSIS 4
- 1.3 EFFECT OF PRESSURE APPLIED TO AN UNCASED HOLE DURING MINI-FRAC TEST 5

CHAPTER 2 7

- 2 **THEORY OF FRACTURING** 8
- 2.1 DIFFERENCES BETWEEN MINI-FRAC AND HYDRAULIC FRACTURING STIMULATION TREATMENT (HFST) 8
- 2.2 THEORY AND EXPERIMENTAL OBSERVATIONS 8
- 2.2.1 Growth of a fracture 8
- 2.2.1.1 Fracture initiation in uncased hole 9
- 2.2.1.2 Fracture initiation in perforated cased hole 9
- 2.2.1.3 Location and orientation of a fracture in a deviated wellbore 10
- 2.2.1.4 Formation breakdown pressure (P_b) 11
- 2.2.1.5 Fracture re-opening pressure (P_{re}) 12
- 2.3 FRACTURING IN PRESENCE OR ABSENCE OF FLUID PENETRATION INTO THE FORMATION (FOR VERTICAL FRACTURES AND VERTICAL WELLBORES) 12
- 2.3.1 In the absence of fluid penetration 12
- 2.3.2 In the presence of fluid penetration 12
- 2.4 FRACTURING OF CEMENTED ROCKS AND POROUS UNCEMENTED TAR SANDS 12

CHAPTER 3 15
3 **MINI-FRAC FIELD TESTING PROCEDURE** 16
3.1 CHOICE OF INJECTION FLUID AND RATE 16
3.2 MINI-FRAC TESTS IN UNCASED AND CASED HOLES 16
3.2.1 Field test procedures 16
3.2.1.1 Equipment required to conduct a mini-frac test 17
3.2.1.2 Uncased hole testing procedure 17
3.2.1.3 Cased hole testing procedures 19
3.2.1.4 Variations due to reservoir types 19

CHAPTER 4 21
4 **ANALYSIS AND INTERPRETATION PROCEDURES OF THE RESULTS** 22
4.1 PROCEDURE FOR *IN-SITU* STRESS MEASUREMENT 22
4.1.1 Conventional procedure 22
4.1.1.1 Formation breakdown pressure (P_b) 22
4.1.1.2 Fracture re-opening pressure (P_{re}) 22
4.1.1.3 Instantaneous Shut-In Pressure (ISIP), fracture closure, and minimum *in-situ* stress from pressure–time curves 22
4.1.2 Reservoir engineering procedure 23
4.1.2.1 Understanding regimes in the presence of a fracture 23
4.1.2.2 Methods of analysis 24
4.2 PROCEDURE FOR OBTAINING RESERVOIR PARAMETERS 29
4.2.1 Determination of reservoir parameters from mini-frac test data 29
4.2.1.1 Formation transmissibility and absolute permeability 29
4.2.1.2 Skin effect 30
4.2.1.3 Wellbore storage 30
4.3 PROCEDURE FOR OBTAINING FLUID LEAK-OFF PARAMETERS 31

CHAPTER 5 33
5 **FACTORS AFFECTING MINI-FRAC TEST RESULTS** 34
5.1 RESERVOIR/GEOLOGIC FACTORS 34
5.1.1 Reservoir lithology/geomechanical behaviour of the rock 34
5.1.2 Time dependent rock deformation 35
5.1.3 Presence of natural fractures, joints, and cracks 35
5.1.4 Effect of overpressure or depleted reservoir pressure 35
5.1.5 Fluid saturation of the test interval 35
5.1.6 Influence of poro-elastic effects 35
5.2 OPERATIONAL FACTORS 35
5.2.1 Property of the fracturing fluid 35
5.2.2 Effect of injection rate 36
5.2.3 Repeated pressure cycling 36
5.2.4 Data gathering procedures 36
5.3 FRACTURE GROWTH PATTERN 36

TABLE OF CONTENTS

5.3.1 Continuation of fracture growth after shut-in 36
5.3.2 Effect of stress in the bounding layers 36
5.3.3 Fracture growth in the damaged or near wellbore region 36
5.3.4 Multiple fracture growth 37
5.3.5 Frictional pressure drop during injection through perforation 37
5.3.6 Fracture tip geometry 37
5.3.7 Fracture surface topography 37
5.4 MODE OF ANALYSIS 37
5.5 LIMITATIONS OF THE MINI-FRAC TESTS 38

CHAPTER 6 39
6 CASE STUDIES 40
6.1 CASE 1 40
6.2 CASE 2 45
6.3 CASE 3 45
6.4 CASE 4 46
6.5 ALBERTA MINI-FRAC DATA 47

CHAPTER 7 53
7 ADVANCES IN *IN-SITU* STRESS MEASUREMENTS 54
7.1 BOREHOLE ELLIPTICITY MEASUREMENT 54
7.2 ANELASTIC STRAIN RECOVERY (ASR) 54
7.3 DIFFERENTIAL STRESS ANALYSIS (DSA) 54
7.4 WAVE VELOCITY ANISOTROPY 55
7.5 COMPRESSIONAL TO SHEAR WAVE VELOCITY (V_p/V_s) ANISOTROPY 55
7.6 SHEAR WAVE POLARIZATION 55
7.7 WAVE ATTENUATION 55
7.8 BOREHOLE SLOTTING TECHNIQUE 55
7.9 BOREHOLE HOLOGRAPHIC INTERFEROMETRY 55
7.10 OVERCORING TECHNIQUE 56

REFERENCES 59

APPENDIX A — EXAMPLE CALCULATIONS OF MINI-FRAC TEST PARAMETERS 67
A1 TRANSMISSIBILITY CALCULATIONS 68
A2 SKIN FACTOR 68
A3 CALCULATION OF FLUID LEAK-OFF COEFFICIENT BY NOLTE'S METHOD 68

APPENDIX B — PRESSURE–TIME DATA OF TEST #1B 69

APPENDIX C — DEFINITION OF TERMS 71

APPENDIX D — NOMENCLATURE 73

SUBJECT INDEX / AUTHOR INDEX 75

LIST OF FIGURES AND TABLES

Figure 1–1. Superposition of stress states about a wellbore as a result of two horizontal stresses of equal magnitude.

Figure 1–2. Stress states about a borehole for regional stress ratios of σ_y/σ_x of 1.4, 2.0, and 3.0 .

Figure 1–3. Parameters used for an inclined borehole geometry.

Figure 1–4. Zones of plastic and elastic deformation around a circular borehole.

Figure 1–5. Mechanisms of plastic deformation occurring in a borehole.

Figure 1–6. Schematic diagram of the interval pressurized during mini-frac tests and the accompanying stresses.

Figure 2–1. Schematic showing resolution of in-situ stress into three mutually perpendicular principal stress components and fracture growth perpendicular to the least principal stress.

Figure 2–2. Schematic representation of the stages in the growth of a mini-frac.

Figure 3–1. Schematic diagram showing open-hole mini-frac testing equipment and well configuration.

Figure 4–1. Method of determining instantaneous shut-in pressure using tangent lines to the fall-off curve of a pressure–time record.

Figure 4–2. Flow regimes that are expected in a well with a finite conductivity fracture.

Figure 4–3. Schematic plot of mini-frac pressure fall-off data showing various flow regimes.

Figure 4–4. Interpretation of closure pressure from the change in slope of pressure versus square root of shut-in time.

Figure 4–5. Tandem square root plot used to predict minimum in-situ stress value in a mudstone interval.

Figure 4–6. Semi-log plot of pressure versus shut-in time.

Figure 4–7. Log dP versus log dt plot showing closure pressure.

Figure 4–8. Shut-in pressure determination using bi-linear pressure-decay rate method.

Figure 4–9. Profile of first two pump-in/flow-back test cycles following the first cycle of the formation breakdown.

Figure 4–10. Pressure versus flow rate plot showing closure or minimum in-situ stress.

Figure 4–11. Closure or minimum in-situ stress determination using fracture reopening method.

Figure 4–12. Determination of in-situ minimum stress from the slope of a Horner plot.

Figure 4–13. Plot showing the effect of fracture inclination on in-situ stress value.

Figure 4–14. Presence of two inflection points on the slope of the Horner plot.

Figure 4–15. Pressure fall-off data on a Horner plot to derive formation transmissibility.

Figure 4–16. Log–log plot of pressure differentials versus shut-in time data.

Figure 4–17. Nolte's type curve matching master curve.

Figure 5–1. A bar graph showing variations in breakdown, re-opening, extension, and shut-in pressures for three different lithological intervals.

Figure 5–2. Stress concentration near the tip of a crack.

Figure 6–1. SP and resistivity log response of the mini-frac test intervals. Test intervals are shown with hatched lines.

Figure 6–2. The first cycle of a mini-frac test in a mudstone unit.

Figure 6–3. The second cycle of a mini-frac test in the same mudstone unit.

Figure 6–4. The third cycle of a mini-frac test in the same mudstone unit.

Figure 6–5. The first cycle of a mini-frac test in an interbedded sand and mudstone unit.

Figure 6–6. The second cycle of a mini-frac test in the same interbedded sand and mudstone unit.

Figure 6–7. The third cycle of a mini-frac test in the same interbedded sand and mudstone unit.

Figure 6–8. The first cycle of a mini-frac test in a tar sands interval.

Figure 6–9. The second cycle of a mini-frac test in the same tar sands interval.

Figure 6–10. The third cycle of a mini-frac test in the same tar sands interval.

Figure 6–11. Horner plot of a mini-frac test performed in a mudstone interval.

Figure 6–12. Pressure versus square root of shut-in time plot to obtain fracture closure pressure.

Figure 6–13. Minimum in-situ stress from the intersection of bi-linear curves of dP/dt versus bottomhole pressure plot.

Figure 6–14. Pressure–time plot of a mini-frac test performed in an Alberta tar sands formation through a perforated well.

Figure 6–15. Variation of vertical and minimum in-situ stress in Alberta with depth.

LIST OF FIGURES AND TABLES

Table 3–1. *Results of 20* in-situ *measurements conducted by ESSO in deviated, perforated cased holes at a 454 m depth.*

Table 6–1. *Summary of mini-frac tests conducted in the McMurray Formation of the Athabasca tar sands.*

Table 6–2. *Reservoir engineering parameters estimated from mini-frac tests conducted in the McMurray Formation.*

Table 6–3. *Summary of mini-frac tests conducted in the Wabiskaw Formation.*

Table 6–4. *Summary of mini-frac tests conducted in the Clearwater Formation of Cold Lake.*

Table 6–5. *Mini-frac test results from various parts of Alberta.*

CRITICAL REVIEW

To ensure that the final manual is of the highest quality, we sought input from industry professionals with vast experience in the field of hydraulic fracturing application and analyses.

The manual has been critically reviewed by Dr. P.R (Rick) Kry (Esso Canada Research), Dr. Antonin Settari (SIMTECH Consulting Services), Dr. Mehmet Saltuklaroglu (Mobil Canada), and Mr. Harry Ripley (formerly of Halliburton Services). These reviewers have broad theoretical and practical experience in the subject matter of this manual. Suggestions provided by these reviewers, particularly to chapters two to five, have indeed been helpful. We sincerely acknowledge the contribution of these reviewers in helping us improve the quality of the manual.

PREFACE

Since the enunciation of a hydraulic fracturing theory by Hubbert and Willis (1957), and the suggestion by Fairhurst (1964) and Kehle (1964) that hydraulic fracturing techniques can be used to determine *in-situ* stress magnitude, many rock fracture studies have been published in geoscience and engineering literature. Several of these publications have addressed the use of hydraulic fracturing techniques to determine the *in-situ* stress regime in various lithologies. This application forms the basis of this mini-frac manual. Hydraulic fracturing is often being used as an attractive technology to obtain incremental production from tight formations. Heated communication between the injection and production wells, to enhance bitumen recovery, requires hydraulic fracturing of tar sands reservoirs. Methods extending hydraulic fracture technology to horizontal wells have also been reported in the literature.

The design of a large scale hydraulic fracture stimulation treatment requires a good understanding of the *in-situ* stress regime, which often is obtained by low volume and low injection rate hydraulic fracturing tests. Such tests are often referred to as micro- or mini-frac tests in the petroleum industry. The subtle difference between the micro-frac and the mini-frac test has been recognized; however, for the convenience of discussion, the term "mini-frac" is used here for both micro- and mini-frac.

We have attempted to present a comprehensive approach aimed at addressing issues that are relevant to mini-frac testing for *in-situ* stress determination. In the manual, these issues are laid out in seven chapters.

- Chapter one deals with elastic and plastic analysis of the stress alteration caused by the presence of a borehole (vertical and inclined).
- Chapter two discusses hydraulic fracturing theory for elastically as well as poro-elastically deformable rocks.
- Chapter three outlines the procedure of mini-frac field testing in cased and uncased holes.
- Chapter four describes how mini-frac test results can be analyzed and interpreted to acquire information on *in-situ* stress regime, fluid leak-off, and reservoir behavior.
- Chapter five consists of a discussion of various factors that could affect results of mini-frac tests and their analysis and interpretation.
- A comparison of the results of minimum *in-situ* stress determination by various techniques is presented in Chapter six. A number of case studies of mini-frac testing are evaluated in this chapter. This chapter also reports data from micro- and mini-frac tests conducted by oil companies in the Alberta part of the western Canadian Sedimentary Basin.
- Chapter seven briefly summarizes the other stress measurement techniques that have been proposed in the literature and compares these techniques with the mini-frac technique.

The manual represents only the current state of the published art and has been developed for the practicing engineer involved in conducting mini-frac tests in conventional as well as unconventional reservoirs. Many aspects of the manual can be used by researchers as a basis for future developments as well as by engineers in other disciplines such as geotechnical and civil, geophysics and tectonophysics.

We hope the manual will serve as a useful reference tool for engineers requiring vital information for designing large-scale hydraulic fracture stimulation treatment for enhanced recovery. We believe that there is room for improvement and development of more optimized techniques. Hence, we would gladly welcome written comments and/or field data for analysis and incorporation in future updates of this manual.

Selim S. Hannan, Ph. D., P. Eng.
Ben I. Nzekwu, Ph. D., P. Eng.
Calgary, Alberta

ABOUT THE AUTHORS

Selim S. Hannan received his M.Sc. degree in petroleum engineering-geology from Moscow Gubkin Institute of Petro-Chemical and Gas Industry (formerly USSR). His Ph.D. degree was obtained from the University of Toronto, where he specialized in rock mechanics, rock physics, and computer modeling.

Currently, Selim is a consultant with the Alberta Oil Sands Technology and Research Authority (AOSTRA) working primarily with hydraulic fracturing, mini-frac testing, geotechnical, geomechanical, and reservoir simulation studies. His interest is diversified in areas of hydraulic fracturing and reservoir stimulation, numerical simulation, enhanced oil recovery, reservoir geology and geophysics, hydrocarbon exploration, high pressure experimental studies, horizontal well applications, joint venture exploration and development project with the Commonwealth of Independent States, and research and development.

He has taught courses through the Adult and Continuing Education departments of the University of Calgary, Mount Royal College, and the Calgary Board of Education. Currently, through the Continuing Education division of the University of Calgary, he offers a course called "Petroleum Geomechanics" for petroleum industry professionals.

Selim is a member of APEGGA, CIM, and the Canadian Society of Exploration Geophysicists.

Ben I. Nzekwu is currently a Staff Reservoir Engineer with the Alberta Oil Sands Technology and Research Authority (AOSTRA), where he is involved in the evaluation and analysis of various horizontal well applications in both oil sands, heavy oil, and conventional oil reservoirs. Previously, he worked in the Oil Sands Department of BP Resources Canada Ltd. in the design, implementation, and analysis of thermal recovery projects.

He holds a B.Sc. degree in petroleum engineering from the University of Ibadan (Nigeria) and a Ph.D. in chemical engineering (with specialization in petroleum reservoir engineering) from the University of Calgary. His current interests include numerical simulation, horizontal well applications, thermal recovery process mechanisms, and the role of geomechanics in oil recovery. He previously worked for Gulf Oil (Nigeria) Ltd. offshore Nigeria and held teaching and research positions at the universities of Ibadan and Calgary. Dr. Nzekwu is also an instructor in a CIM course on Practical Aspects of Horizontal Well Applications. He is a member of the CIM, the SPE, and APEGGA.

SUMMARY

Mini-frac tests are conducted primarily to obtain an estimate of the minimum principal *in-situ* stress within a reservoir prior to any large scale hydraulic fracturing operation. They help to optimize fracturing operations and avoid undesirable effects by preventing fracture propagation into the bounding layers. The maximum injection pressure that can be used to avoid fracturing of the formation during injection processes such as waterflood, as well as the information on the geomechanical state of the formation, can be obtained from mini-frac test results.

Mini-frac tests can be used to estimate the following:

- Formation breakdown pressure
- Fracture re-opening pressure
- Fracture extension pressure
- Minimum *in-situ* stress/closure stress
- Tensile strength of the undisturbed formation
- Formation transmissibility
- Wellbore storage effects
- Skin factor
- Leak-off parameters

Of the various methods of *in-situ* stress determination, the mini-frac test is the simplest and most versatile, especially for deep wellbores. This method can be used in both porous and non-porous formations, and the procedures for field tests in both types of formation are similar.

The magnitude of the minimum *in-situ* stress can be predicted directly from mini-frac tests within certain error bounds, whether the minimum stress is vertical or horizontal. If the predicted minimum *in-situ* stress is horizontal, the magnitudes of all three principal stresses can be obtained — the horizontal stresses from the mini-frac test results and the theory, and the vertical or overburden stress from the depth, and average density of the formation. Only when the predicted minimum stress is vertical, the horizontal stresses may remain undetermined, unless the horizontal to vertical stress ratio is known. When the fracture azimuth or the direction of the minimum and maximum horizontal stresses need to be known, a borehole televiewer or an impression packer must be used wherever possible, otherwise the mini-frac field test should be supplemented with a wellbore breakout study or other *in-situ* stress measurement techniques and regional data.

If an *in-situ* stress regime in a certain area is assumed to be close to isotropic, then to obtain a true representation of the minimum *in-situ* stress, the fluid injection rate must be chosen carefully to avoid an alteration of the virgin stress regime — one option is to start with as low an injection rate as possible.

In recent years, several techniques have been proposed for *in-situ* stress determination, but our scientific understanding of the mini-frac method has been most advanced. The differential stress analysis (DSA) and the anelastic strain recovery (ASR) methods, which depend largely on core recovery, cannot be used where core recovery is poor, for example, in tar sands. But in consolidated formations, where core recovery is not a problem, ASA and DSA methods may be viewed sometime as alternatives to the mini-frac test if appropriate assumptions are made.

INTRODUCTION

In the Petroleum Industry, micro-frac and mini-frac tests are widely used primarily for the determination of the magnitude and orientation of *in-situ* stresses. The *in-situ* stress measurement tests which use low injection rates and volumes are regarded as micro-frac tests, to distinguish them from mini-frac tests, which use higher injection rates and volumes. However, the range of injection rate and volume for micro-frac and mini-frac tests has not been clearly defined. Survey of literature shows that most micro-frac tests have been conducted at injection rates of 0.002 to 0.1 m^3/min (2 to 100 L/min) during a short injection time of 3 to 20 minutes. On the other hand, most mini-frac tests have been conducted at injection rates of 0.03 to 10 m^3/min and the injection volume has varied over a wide range of 5 to 80 m^3. The injection rates used in mini-frac tests are sometimes as high as that used in hydraulic fracturing tests, and the injection volume used constitutes 30 to 50% of the main frac job size. An overlap in the injection rates of micro- and mini-frac tests is sometime seen.

Except for the injection rate and volume, the theory and practices of micro-frac and mini-frac tests are very similar. Of the two terms, the term mini-frac is most widely used in the petroleum industry. For convenience, we will adhere to the term "mini-frac" in all our discussions of the subject of micro-frac and mini-frac.

The determination of minimum *in-situ* stress is important in the analysis of wellbore stability and prediction of fracture geometry and orientation in hydraulic fracturing operation. *In-situ* stress data are essential for planning waterflood and underground waste disposal programs, monitoring surface heave and subsidence, evaluating the geomechanical state of uncemented sands like oil sands, understanding the geological setting of a basin or region, and predicting the earthquake activities and tectonic evolution of a basin or region.

If horizontal stress data can be obtained for a basin, then the tectonic history of the basin (*e.g.*, its formation in a stable cratonic belt or in a tectonically active continental margin belt) can be known. A consistent regional trend in horizontal stress orientation can sometimes also reveal the principal direction of the tectonic forces. *In-situ* stress data are widely used in mining, civil, and geological engineering projects also.

Mini-frac tests are important in many other ways:

- Mini-frac tests help understand failure of the formation under injection. The failure can be shear or tensile, depending on the injection condition.
- Mini-frac test results help optimize hydraulic fracturing operations for interwell communication and permeability enhancement in a tight reservoir.
- Mini-frac test results help fracture designs to prevent fracture propagation into bounding layers.
- Many reservoir engineering parameters, such as formation transmissibility, wellbore storage effects, and skin factor, can be obtained from pressure decline analysis of a mini-frac test if reservoir engineering analyses are employed to analyze mini-frac test data. Determination of these parameters requires that the pressure fall-off of the first cycle of the mini-frac test following the breakdown is recorded over a long period of time until the pressure stabilizes to about the original reservoir pressure.
- Mini-frac tests can be used to monitor the stress alteration that occurs due to steam stimulation of the reservoir. It can also be used to monitor alteration of stress states due to the fluid recovery from a reservoir.

- Several problems like borehole instability and shearing of casing can be averted if the axis of a horizontal well is kept parallel to one of the horizontal stresses. When used in conjunction with other methods such as DSA and ASR, or with tools such as an impression packer or a borehole televiewer, mini-frac tests can sometimes determine orientation of the horizontal stresses to help design drilling of the horizontal wells.

The theory and practice of mini-frac tests for *in-situ* stress determination have been a topic of discussion in a number of articles (Hubbert and Willis, 1957; Fairhurst, 1964; Haimson and Fairhurst, 1967; Bredehoeft *et al.*, 1976; Abou-Sayed *et al.*, 1978; Gronseth and Detournay, 1979; Nolte, 1979; Rosepillar, 1979; Dusseault, 1980a; McLennan and Roegiers, 1981; Hassan, 1982; Ratigan, 1982; Hickman and Zoback, 1983; Kry and Gronseth, 1983; Warpinski *et al.*, 1985; Soliman *et al.*, 1987; Brown, 1989; Cheung and Haimson, 1989; De Bree and Walters, 1989; Detournay *et al.*, 1989; Ikeda and Tsukahara, 1989; Jones and Sargeant, 1989; Kuriyagawa *et al.*, 1989; Meyer and Hagel, 1989; Proskin *et al.*, 1990; Boone *et al.*, 1991; Haimson and Zhao, 1991; Kim and Abbas, 1991). However, none of these articles provides a comprehensive overview of the subject matter.

OBJECTIVES OF THE MANUAL

Mini-frac tests and other *in-situ* stress measurement techniques were discussed in several publications. However, no single publication addresses all aspects of mini-frac tests and recent advances in *in-situ* stress measurement. This manual compiles various aspects of mini-frac testing and *in-situ* stress measurement techniques for easy accessibility by the users. It is mainly directed towards the use of petroleum industry professionals. However, many aspects of the manual can be used by researchers as well as the engineers working in other disciplines.

The objectives of this manual are to describe:

(a) the state of the art of "mini-frac tests;"

(b) emphasize their importance;

(c) discuss possible differences of the tests in porous and non-porous formations;

(d) recommend procedures for field testing, analysis, and interpretation;

(e) indicate the limitations of the technique; and

(f) compare mini-frac tests with the other *in-situ* stress measurement techniques.

Keywords: Micro-frac, mini-frac, hydraulic fracturing, formation breakdown, fracture re-opening pressure, instantaneous shut-in pressure, fracture extension or propagation pressure, fracture closure pressure, leak-off.

CHAPTER 1

STRESS ALTERATION CAUSED BY BOREHOLE PRESENCE

1 STRESS ALTERATION CAUSED BY BOREHOLE PRESENCE

1.1 ELASTIC ANALYSIS

1.1.1 For vertical uncased borehole

The presence of a wellbore alters the pre-existing stress field in the rock. This stress alteration can be approximately calculated by assuming that the rock is elastic, the borehole smooth and cylindrical, and the borehole axis vertical and parallel with one of the pre-existing regional principal stresses. The calculation is based on the solution in elastic theory for the stresses in an infinite plate containing a circular hole with its axis perpendicular to the plate derived first by Kirsch (1898) and later provided by Timoshenko (1934), and Hubbert and Willis (1957).

Expressed in polar coordinates with the center of the hole as the origin, the plane stress components at a point θ, r, or exterior to the hole in a plate with an otherwise uniform uniaxial stress, σ_x, are given by:

$$(1\text{–}1)\quad \sigma_r = \frac{\sigma_x}{2}\left[1 - \frac{r_w^2}{r^2}\right] + \frac{\sigma_x}{2}\left[1 + 3\frac{r_w^4}{r^4} - 4\frac{r_w^2}{r^2}\right]\cos 2\theta$$

$$(1\text{–}2)\quad \sigma_\theta = \frac{\sigma_x}{2}\left[1 + \frac{r_w^2}{r^2}\right] - \frac{\sigma_x}{2}\left[1 + 3\frac{r_w^4}{r^4}\right]\cos 2\theta$$

where σ_r – radial stress,
σ_θ – circumferential stress,
r_w – radius of the hole and
θ – parallel with the axis of the compressive stress, σ_x.

Similar solution for a regional principal stress, σ_y, at right angles to σ_x, in which θ + 90° is used for the angular coordinate should be added on to the equation to give the complete horizontal component of the stress in the vicinity of the borehole. The stresses calculated here are the effective stresses carried by the rock in addition to a hydrostatic fluid pressure, p_w, existing within the wellbore, as well as in the rock.

The values of the horizontal stresses across the principal planes in the vicinity of the borehole have been shown for various relative values of the σ_y/σ_x ratio (Figure 1–1 and 1–2). In every case, the stress concentrations are local and these stresses rapidly approach the undisturbed regional stresses within a few hole diameters. The principle of superposition of the two parts of the stress field is illustrated in Figure 1–1 for the case in which σ_y/σ_x is 1.0. For σ_x alone, the circumferential stress at the walls of the hole ranges from a minimum value of $-\sigma_x$ (tensile) across the plane parallel to the σ_x axis to a maximum of $+3\sigma_x$ across the plane normal to the σ_x-axis. When the two stresses are superposed, the stress field has radial symmetry and the circumferential stress at the walls of the hole is $+2\sigma_x$. The resultant stress fields for other ratios are shown in Figure 1–2. In the extreme case, when $\sigma_y/\sigma_x = 3$, the circumferential stress at the walls of the hole ranges from a minimum of zero to a maximum of $+8\sigma_x$.

The vertical component of the stress is also distorted in the vicinity of the borehole. The initial vertical stress is equal to the effective pressure of the overburden. The

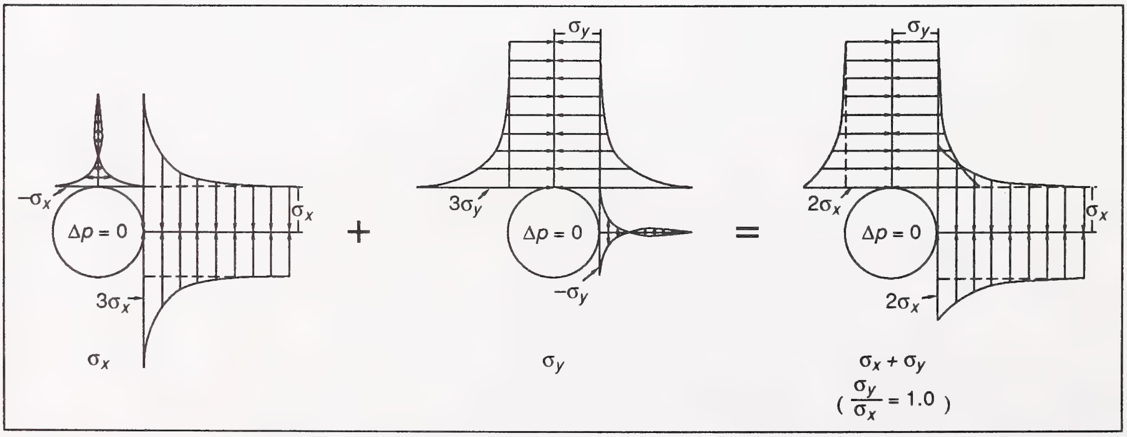

Figure 1–1. Superposition of stress states about a wellbore as a result of two horizontal stresses of equal magnitude (after Hubbert and Willis, 1957).

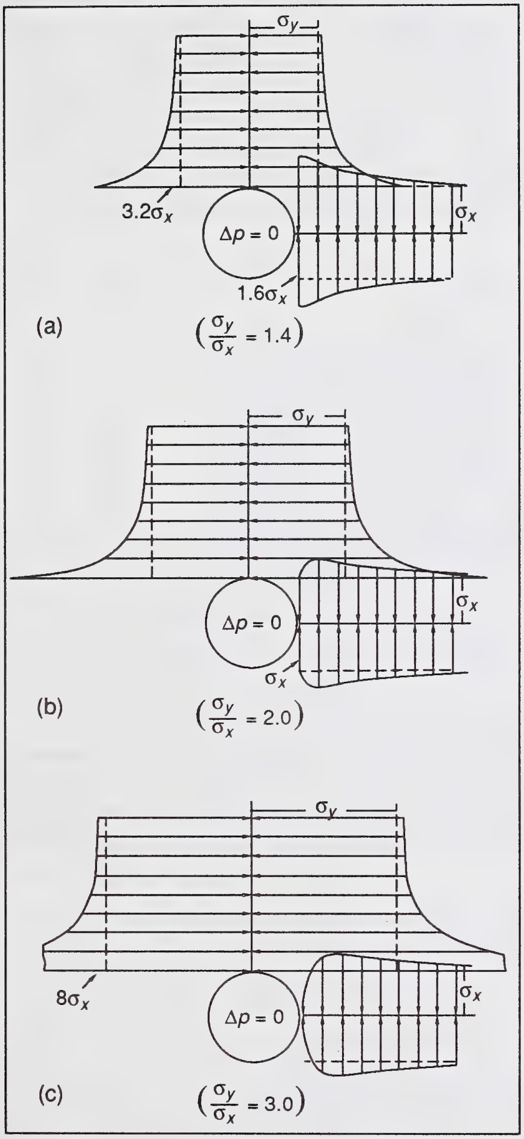

Figure 1–2. *Stress states about a borehole for regional stress ratios of σ_y/σ_x of 1.4, 2.0, and 3.0 (after Hubbert and Willis, 1957).*

distortion in the vertical stress is a function of the values of the regional horizontal stresses σ_x and σ_y. However, the magnitude of this distortion is small in comparison to the concentrations of the horizontal stresses and it rapidly disappears with distance away from the wellbore.

1.1.2 FOR INCLINED BOREHOLE

A schematic for an inclined borehole is shown in Figure 1–3. The stress resulting from the *in situ* stress and the internal borehole pressure p_w is given by the following:

$$\text{(1–3)}\quad \sigma_r = \frac{1}{2}(\sigma_x + \sigma_y)\left(1 - \frac{r_w^2}{r^2}\right) + \frac{1}{2}(\sigma_x - \sigma_y)\left(1 - 4\frac{r_w^2}{r^2} + 3\frac{r_w^4}{r^4}\right)\cos(2\theta) + \tau_{yx}\left(1 - 4\frac{r_w^2}{r^2} + 3\frac{r_w^4}{r^4}\right)\sin(2\theta) + \frac{r_w^2}{r^2}P_w$$

$$\text{(1–4)}\quad \sigma_\theta = \frac{1}{2}(\sigma_x + \sigma_y)\left(1 + \frac{r_w^2}{r^2}\right) - \frac{1}{2}(\sigma_x - \sigma_y)\left(1 + 3\frac{r_w^4}{r^4}\right)\cos(2\theta) - \tau_{xy}\left(1 + 3\frac{r_w^4}{r^4}\right)\sin(2\theta) - \frac{r_w^2}{r^2}P_w$$

$$\text{(1–5)}\quad \sigma_z = \sigma_z - 2\nu(\sigma_x - \sigma_y)\frac{r_w^2}{r^2}\cos(2\theta) - 4\nu\tau_{xy}\frac{r_w^2}{r^2}\sin(2\theta)$$

$$\text{(1–6)}\quad \tau_{r\theta} = \left[-\frac{1}{2}(\sigma_x - \sigma_y)\sin(2\theta) + \tau_{xy}\cos(2\theta)\right]\left(1 + 2\frac{r_w^2}{r^2} - 3\frac{r_w^4}{r^4}\right)$$

$$\text{(1–7)}\quad \tau_{rz} = \left[\tau_{xz}\cos\theta + \tau_{yz}\sin\theta\right]\left(1 - \frac{r_w^2}{r^2}\right)$$

$$\text{(1–8)}\quad \tau_{\theta z} = \left[-\tau_{xz}\sin\theta + \tau_{yz}\cos\theta\right]\left(1 + \frac{r_w^2}{r^2}\right)$$

At the borehole wall ($r = r_w$), these expressions simplify to the following:

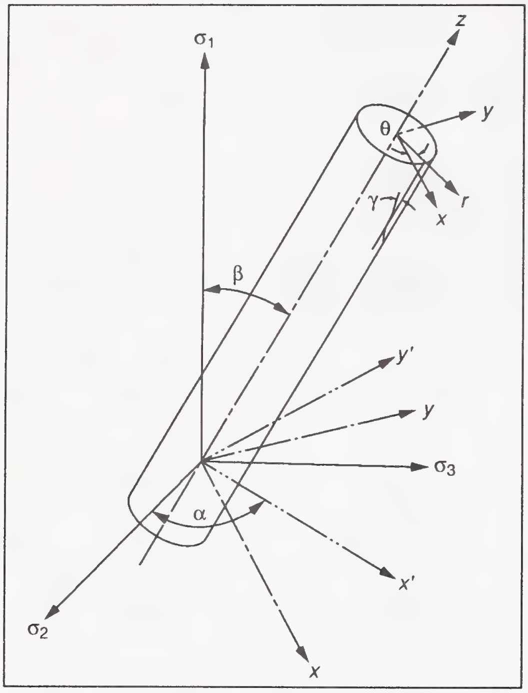

Figure 1–3. Parameters used for an inclined borehole geometry (after McLennan et al., 1989).

(1–9) $\sigma_r = P_w$

(1–10) $\sigma_\theta = \left(\sigma_x + \sigma_y - P_w\right) - 2\left(\sigma_x - \sigma_y\right)\cos(2\theta)$
$- 4\,\tau_{xy}\sin(2\theta)$

(1–11) $\sigma_z = \sigma_z - 2\nu\left(\sigma_x - \sigma_y\right)\cos(2\theta)$
$- 4\nu\,\tau_{xy}\sin(2\theta)$

(1–12) $\tau_{r\theta} = \tau_{rz} = 0$

(1–13) $\tau_{\theta z} = 2\left(-\tau_{xz}\sin\theta + \tau_{yz}\cos\theta\right)$

The major difference with a borehole (vertical or horizontal) drilled parallel to a principal axis is that one of the shear components, $\tau_{\theta z}$, remains finite at the borehole wall. The magnitude of this shear component will affect the overall stability of the borehole.

1.2 PLASTIC ANALYSIS

Certain rocks, particularly weak sedimentary rocks, at greater depths, do not respond elastically to the stress field associated with the introduction of a wellbore (McLennan *et al.*, 1989). These rocks tend to deform plastically with permanent deformation and without brittle failure. A plastic region will develop around the borehole (Figure 1–4), in which the stress distribution will be modified (Gnirk and Johnson, 1964; Gnirk, 1972).

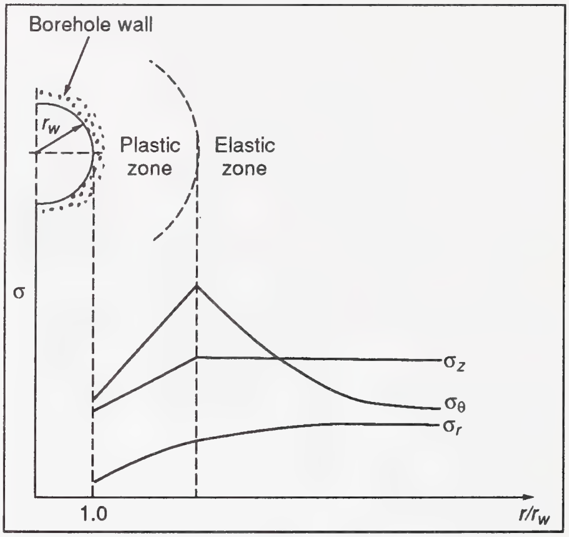

Figure 1–4. Zones of plastic and elastic deformation around a circular borehole (after McLennan et al., 1989).

Depending on the relative values of σ_r, σ_θ, and σ_z, Shi (1988) examined the following cases:

- Plastic failure mechanism
- Non-linear effects
- Time dependent effects

Considering various drilling mud weights and two limiting values for Poisson's ratio, Shi proposed seven different modes of failure (shown as zone I through VII in Figure 1–5).

Not all of the regions in the figure occur simultaneously. Their existence depends on the *in-situ* stress regime and the failure characteristics of the particular formation. Shi's analysis was done for a vertical uncased hole but the methodology can be extended to the general case of an inclined borehole.

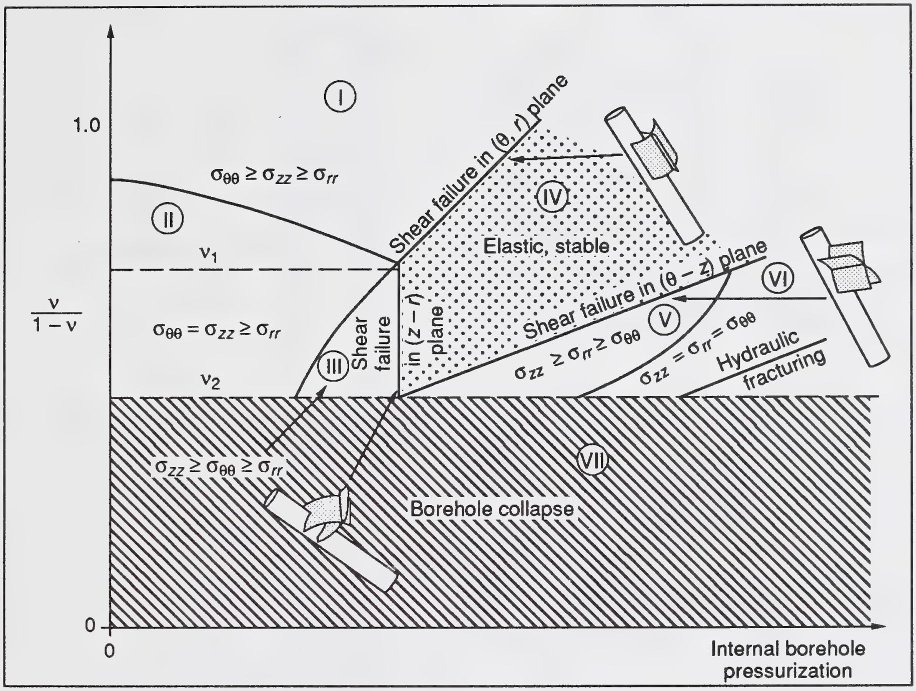
1.0
0
0
$\frac{\nu}{1-\nu}$
I
$\sigma_{\theta\theta} \geq \sigma_{zz} \geq \sigma_{rr}$
II
ν_1
$\sigma_{\theta\theta} = \sigma_{zz} \geq \sigma_{rr}$
ν_2
III
Shear failure
in (z − r) plane
Shear failure in (θ, r) plane
IV
Elastic, stable
Shear failure in (θ − z) plane
V
VI
$\sigma_{zz} \geq \sigma_{rr} \geq \sigma_{\theta\theta}$
$\sigma_{zz} = \sigma_{rr} = \sigma_{\theta\theta}$
Hydraulic fracturing
$\sigma_{zz} \geq \sigma_{\theta\theta} \geq \sigma_{rr}$
VII
Borehole collapse
Internal borehole pressurization

Figure 1–5. Mechanisms of plastic deformation occurring in a borehole (after Shi, 1988).

The introduction of non-linear effects, such as stress-dependent elastic constants, can cause buckling of the borehole wall (McLennan *et al.*, 1989). For certain parameter combinations, failure can occur at a finite distance from the borehole wall (Santarelli *et al.*, 1986; Guenot, 1988).

The stresses around a borehole can also be impacted by time-dependent material response like visco-elastic or visco-plastic behavior. Such an effect occurs largely following the drilling of the well. Fully coupled mathematical analysis indicated that the transient changes in the pore pressure field around the wellbore (due to poro-elastic effect and fluid permeation) modify the *in-situ* stress regime. Such transient effects can lead to failure away from the borehole wall. Detail analysis of the stress alteration due to the poro-elastic and time dependent effects is provided by Detournay and Cheng (1988).

1.3 EFFECT OF PRESSURE APPLIED TO AN UNCASED HOLE DURING MINI-FRAC TEST

The application within the borehole of a fluid pressure in excess of the original fluid pressure produces additional stresses. Lame solution for the stresses in a thick walled elastic cylinder, offered by Timoshenko (1934), formed the basis for derivation of stresses induced by the injection of a fluid that is non-penetrating. In this derivation, Hubbert and Willis (1957) assumed the outer radius of the wellbore to be very large and the pressure at the outer boundary of the cylindrical wellbore to be equal to zero. With a further assumption of uniform pressure along the entire length of the borehole, Hubbert and Willis (1957) obtained the following solutions for radial, circumferential, and vertical stresses:

$$(1\text{–}14)\quad \sigma_r = +\Delta p \frac{r_w^2}{r^2}$$

$$(1\text{–}15)\quad \sigma_\theta = -\Delta p \frac{r_w^2}{r^2}$$

$$(1\text{–}16)\quad \sigma_z = 0$$

In these equations:

Δp = increase in fluid pressure in the wellbore over the original pressure

r_w = hole radius, and

r = distance from the center of the hole

In reality, during a mini-frac test, the test interval is packed off. The injection fluid induces a uniform pressure over the packed-off interval. This pressure tends to force the packers away from the pressurized interval, but any such movement of the packers is prohibited by frictional forces that arise at the contact between the packers and the wall of the borehole. These frictional forces are modeled by a uniform band of shear stress over the interval of the hole occupied by the packers (Kehle, 1964). The shear force balances the force applied to the packer by the fracturing fluid pressure (Figure 1–6).

Kehle's (1964) analysis indicated that at either end of the packed-off interval the fracturing fluid injection induces a stress with which a horizontal fracture could be formed. However, over most parts of the pressurized interval, along the borehole wall (where $r = r_w$), the σ_θ was equal to the Δp, the pressure in excess of the original reservoir pressure. Thus for the pressurized interval, Kehle's analysis agrees closely to that of Hubbert and Willis (1957), where a uniform pressure was assumed over the entire length of the borehole.

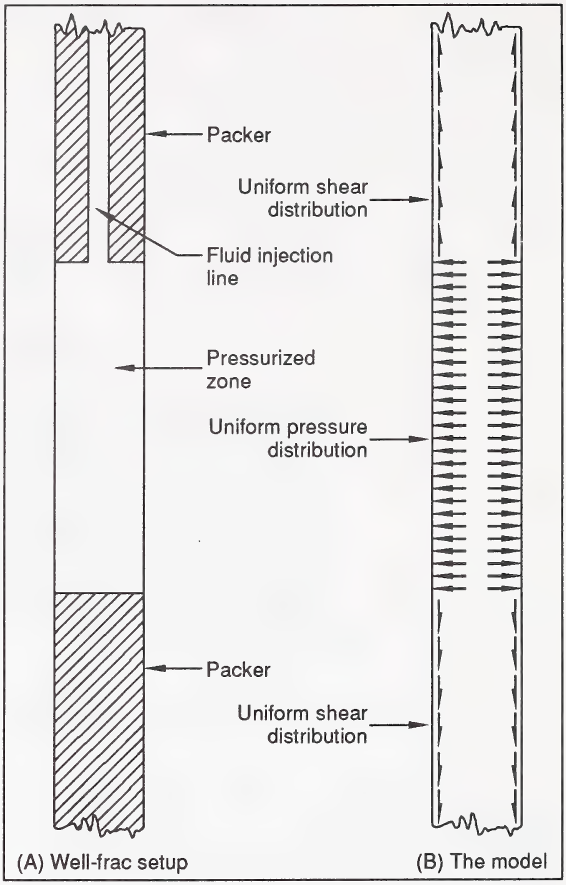
Packer
Uniform shear distribution
Fluid injection line
Pressurized zone
Uniform pressure distribution
Packer
Uniform shear distribution
(A) Well-frac setup
(B) The model

Figure 1–6*. Schematic diagram of the interval pressurized during mini-frac tests and the accompanying stresses (after Kehle, 1964).*

CHAPTER 2

THEORY OF FRACTURING

2 THEORY OF FRACTURING

2.1 DIFFERENCES BETWEEN MINI-FRAC AND HYDRAULIC FRACTURING STIMULATION TREATMENT (HFST)

While mini-frac tests are used to determine the magnitude and orientation of *in-situ* principal stresses and to help design large scale hydraulic fracturing operations, the hydraulic fracturing, as a means of stimulation, is used to establish deeper fluid communication within the reservoir and large wide channels for enhanced fluid flow from the formation to the wellbore.

While mini-frac tests require a small fluid volume, HFST requires injection of a large volume of fluid.

Highly viscous fluids, or fluids with proppant carrying capacity, are commonly used in HFST. Their use is not common in mini-frac tests. Sometimes, when mini-frac tests are designed to estimate leak-off parameters, fluids with proppant carrying capacity are used.

Although in the petroleum industry mini-frac is understood as a method of *in-situ* stress measurement to distinguish it from large scale hydraulic fracturing operations, in civil engineering, geological engineering, rock mechanics, and geophysics literature, no such distinction is made. In these literature, all *in-situ* stress measurements that involve fracturing of rock, independent of injection rate and volume, are broadly known as hydraulic fracturing techniques. Thus, some of the discussions of *in-situ* stress measurement included in this manual are applicable to micro- and mini-frac testing, as well as hydraulic fracturing.

2.2 THEORY AND EXPERIMENTAL OBSERVATIONS

The theory governing mini-frac test analysis is similar to that enunciated first by Hubbert and Willis (1957) on hydraulic fracturing theory. The *in-situ* stresses are resolved into three principal stress components (Figure 2–1). In general, these three components are unequal and the tensile type fracture produced is perpendicular to the axis of the least principal stress. At a constant injection rate, the pressure increases rapidly unless the injection rate is very low or the formation is very permeable. When the applied pressure produces stress which exceeds the failure envelope (usually the hoop stress), the formation breakdown is initiated. Once formation breakdown occurs, the pressure is applied to the walls of the fracture as fluid injection continues. The stress concentration in the vicinity of the wellbore is reduced. The pressure required to hold the fracture open is then equal to the component of the undisturbed stress field normal to the plane of the fracture. A pressure slightly greater than this can extend the fracture.

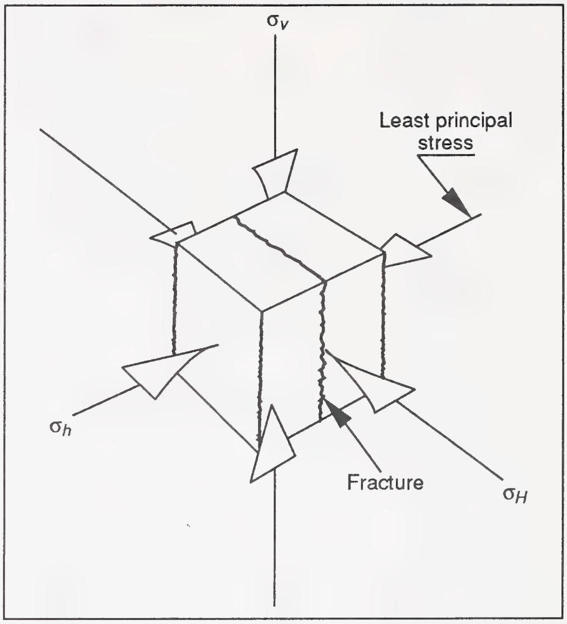

Figure 2–1. Schematic showing resolution of in-situ stress into three mutually perpendicular principal stress components and fracture growth perpendicular to the least principal stress.

The minimum injection pressure required to keep a fracture open and extend it, is slightly greater than the original undisturbed *in-situ* stress normal to the plane of the fracture. This is the basis for obtaining the minimum *in-situ* stress from the instantaneous shut-in pressure (ISIP) (Kehle, 1964; Haimson, 1972; Zoback *et al.*, 1977; Gronseth and Detournay, 1979; Gronseth and Kry, 1983). Thus, usually ISIP is a good indicator of *in-situ* stress provided (i) it can be ascertained reliably from pressure–time curves, (ii) fluid is of low viscosity, and (iii) poro- and thermo-elastic effects are small.

2.2.1 Growth of a fracture

An idealized representation of the pressure–time relationship of a mini-frac test is shown in Figure 2–2. On fluid injection, initially the pressure increases until breakdown. The fracture often initiates as a micro-scale fracture and continues propagating until the breakdown pressure is

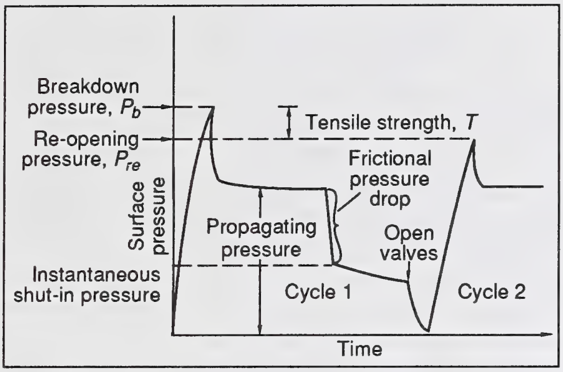

Figure 2–2. *Schematic representation of the stages in the growth of a mini-frac (from Roegiers, 1989).*

reached (McLennan *et al.*, 1989). After breakdown, the fracture continues to propagate provided injection continues. Because of energy dissipation by fracturing, the pressure declines to a point and remains almost constant if a constant injection rate is maintained. In Figure 2–2, this pressure is shown as the propagating pressure and is also regarded as the fracture extension pressure. If the pressure is recorded at the surface, then the rapid pressure drop seen after shut-in is due to the friction in the wellbore and in the perforations in case of a perforated well. The point from where the pressure begins to drop less rapidly is regarded as instantaneous shut-in pressure (ISIP).

At shut-in, the fluid pressure within the fracture is still greater than the least principal stress. This excess pressure is dissipated on propagation of a fracture after shut-in or fluid leak-off from the fracture into the formation. The rate of decrease of pressure within the fracture will depend on the rate of fluid loss to the formation and the current fracture stiffness. The ISIP corresponds to a state of quasi-static equilibrium between the minimum principal stress acting to close the fracture and the pressure in the fracture to hold it open. Hence the ISIP is often also called the closure stress. Once the fracture closes, there should be a logarithmic type pressure decay which is characteristic of pseudo-radial flow.

2.2.1.1 Fracture initiation in uncased hole

McLennan *et al.* (1989) indicated that regardless of the orientation and azimuth of the wellbore, there will be a tendency for the fracture to initiate along the wellbore in uncased hole completions. The fracture will later reorient to a more favourable direction of propagation. This is supported by the work of Daneshy (1973a) and Strubhar *et al.*'s (1975). However, exceptions to the above were also observed. For example, mean stress values acting in a plane perpendicular to the borehole axis can be large enough to induce longitudinal stresses (generated by Poisson's effect) adequately large to cause failure perpendicular to the wellbore trajectory. This was documented theoretically by Ljunggren *et al.* (1988) and experimentally by Bjarnason *et al.* (1988).

2.2.1.2 Fracture initiation in perforated cased hole

In a perforated cased hole, fracture initiation takes place from a point or spherical cavity (McLennan *et al.*, 1989). Orientation of the fracture was least affected by perforations. Instead it was governed by the *in-situ* stress condition (Daneshy, 1973b). Thus it seems, to ensure fracture propagation perpendicular to the least principal stress, the casing should be perforated at a single point or within a small longitudinal interval. Perforation of a long interval may produce fractures similar to that observed in uncased holes.

A more detailed experimental investigation of the effect of perforations on fracture initiation was later conducted by Behrmann and Elbel (1991) in a large triaxial stress frame that simulated downhole conditions. Like Daneshy (1973b), they also found the breakdown pressure to be affected by perforation arrangement. From a series of tests performed with balanced and underbalanced perforations at various orientations to the minimum stress, they concluded that the following factors could affect fracture initiation from a perforated completions:

1. Pore pressure build-up before fracture initiation.
2. Pressurization of the annulus.
3. Perforation orientation with respect to the plane perpendicular to the minimum horizontal stress, which in most cases was the minimum principal stress.

Behrmann and Elbel (1991) found the fracture to initiate at the base of perforations and at the intersection of the plane normal to the minimum far-field stress that passes through the wellbore axis and the wellbore surface. Their results suggested that the site of fracture initiation depended on the perforation orientation with respect to the plane normal to the minimum far-field stress and pore-pressure build-up which in turn depended on reservoir and fracture fluid properties, fracture-fluid injection rate, and wellbore and perforation permeability damage.

These authors found fracture initiation to be different on opposite sides of the fracture even in homogeneous formations. Even though the fracture did not initiate normal to the minimum horizontal stress, all fractures reoriented into the plane normal to the minimum horizontal stress within one wellbore diameter. It is now known that the reorientation rate is a function of the rate of propagation of the fracture, the homogeneity of the medium, and anisotropy of the stress field (Christianson *et al.*, 1988). Multiple fracture initiations were also evident; however, only the primary single fracture propagated beyond one wellbore diameter.

2.2.1.3 Location and orientation of a fracture in a deviated wellbore

Yew *et al.* (1989) developed a mathematical procedure for predicting location and initial orientation of a fracture in a deviated wellbore. The angular position of initiation of a fracture can be obtained by differentiating the magnitude of maximum principal stress $\sigma_m(\theta)$ with respect to the cylindrical coordinate, where, $\sigma_m(\theta)$ has been defined as:

$$(2\text{–}1)\quad \sigma_m(\theta) = \frac{\sigma_z + \sigma_\theta}{2} \sqrt{\left(\frac{\sigma_\theta - \sigma_z}{2}\right)^2 + \sigma_{\theta z}^2}$$

They suggest that the initial orientation of the fracture, γ, can be obtained from the following equation:

$$(2\text{–}2)\quad \gamma = \frac{1}{2}\tan^{-1}\left(\frac{2\,\sigma_{\theta z}}{\sigma_\theta - \sigma_z}\right)$$

In the above two equations:

$$(2\text{–}3)\quad \sigma_\theta = P + \sigma_{xx}\,(1 - 2\cos 2\theta) + \sigma_{yy}\,(1 + 2\cos 2\theta) - 4\,\sigma_{xy}\sin 2\theta$$

$$(2\text{–}4)\quad \sigma_z = \sigma_{zz} + \nu\left[2\left(\sigma_{xx} - \sigma_{yy}\right)\cos 2\theta + 4\,\sigma_{xy}\sin 2\theta\right]$$

$$(2\text{–}5)\quad \sigma_{\theta z} = -\,2\sigma_{xz}\sin\theta + 2\sigma_{yz}\cos\theta$$

where – *P* is the wellbore pressure

– ν is the Poisson's ratio of the rock medium and

– σ_{xx}, σ_{yy}, and σ_{zz} are the corresponding *in-situ* stress components in the (x, y, z) coordinate system.

– σ_{xy}, σ_{xz}, and σ_{yz} are the *in-situ* stress components in the *xy, xz, and yz* planes, respectively.

For a fracture initiated from a deviated wellbore, the following results were obtained.

In a deviated wellbore, there exists a zone, θ_t, around the wellbore surface, where the circumferential stress is tensile. For a deviated well, the mini-fracture produced on the well surface is at an angle (γ) with respect to the well axis. The initial fracture plane eventually turns perpendicular to the minimum *in-situ* stress. The turning occurs during the early stage of propagation. The turning rate is pressure dependent, with the higher rates being associated with lower pumping pressures. Spacing between the perforated holes becomes an important factor influencing the link-up of multiple mini-fractures. If the spacing between perforation holes is too large, then the fractures initiated from the top perforations may not link up with the bottom set of perforations. Otherwise, if the perforations are closely spaced, as the fractures grow they may coalesce and can form "S-shaped" fractures. Yew *et al.* (1989) suggest that the criterion for link up of two mini-fractures can be established by comparing the magnitude of stress intensity factors at fracture tips and the distribution of strain energy density around the periphery of fractures.

Hallam and Last (1990) conducted a laboratory experiment to examine the geometry of hydraulic fractures from open and cased boreholes with a deviation of up to 30° from the vertical. The study showed that the fractures which are initiated from deviated wellbores are usually rough and initiate as a set of parallel starter fractures, perpendicular to the minimum *in-situ* stress. For small deviations, these initial fractures link up to form a single fracture in good communication with the wellbore. For larger deviations, fractures may not coalesce. Thus what may look like a single non-planar fracture, in reality may consist of an array of slightly overlapping non-linking fractures.

The minimum *in-situ* stress obtained from a mini-frac test can either be the minimum horizontal principal stress ($\sigma_{h\min}$) if the fracture is vertical, or else the vertical or overburden stress (σ_v) if the fracture is horizontal. This interpretation depends on the knowledge of the fracture orientation, which in itself must be inferred from the test. The vertical or overburden stress (σ_v) can be estimated from the following formulation assuming no arching effect of the overburden:

$$(2\text{–}6)\quad \sigma_v = h\rho g$$

where h is the overburden thickness to the depth at which σ_v is measured, g is the acceleration due to gravity, and ρ is the average density of the rock-forming materials lying above the depth of measurement of σ_v. The average density can be estimated quite accurately from a density log. In reality, the sequence of rocks above a certain depth can be of varying lithology. Hence, the most appropriate density value is the one derived by averaging the densities of individual lithologic units. At shallow depths, the vertical stress (σ_v) often is the least principal stress, but at great depths often the minimum horizontal stress (σ_h) is the least principal stress. The important stages of fracture growth are discussed below.

2.2.1.4 Formation breakdown pressure (P_b)

As the pressure within the sealed-off interval is increased during a mini-frac test in an uncased well, the fracture initiates as soon as the circumferential stress overcomes the strength of the rock and the *in-situ* stress concentrations. When no fluid leak-off occurs, the formation breakdown pressure (P_b) for an open hole mini-frac test in a vertical wellbore is expressed as:

$$(2\text{–}7)\quad P_b = 3\sigma_h - \sigma_H - P_p + T \quad \text{with } \sigma_H \geq \sigma_h$$

where σ_h and σ_H are the two horizontal principal stresses; P_p, the formation pore pressure; and T, the tensile strength.

The equation provides an upper bound for breakdown pressure (Detournay *et al.*, 1986). However, if fluid penetration occurs prior to formation breakdown, then the expression for breakdown becomes more complex.

Formation breakdown pressure in case of fluid penetration is given by,

$$(2\text{–}8)\quad P_b = \frac{\left(3\sigma_h - \sigma_H - 2\eta P_p + T\right)}{2\,(1-\eta)}$$

where, η, the fluid efficiency is defined by

$$(2\text{–}9)\quad \eta = \frac{\alpha\,(1-2\,\nu)}{2\,(1-\nu)}$$

In Eq. (2–9), α is the poro-elastic constant and is defined as

$$(2\text{–}10)\quad \alpha = \frac{1 - C_s}{C_b}$$

where C_s is the matrix compressibility, C_b is the bulk compressibility of the material, and ν is the Poisson's ratio.

Eqs. (2–7) and (2–8) suggest that the breakdown pressure is independent of the borehole geometry. However, the magnitude of breakdown pressure is affected by the values of pre-existing regional stresses, borehole geometry, and by the ability of the fracturing fluid to penetrate into the rock mass.

Pore pressure, P_p, can be determined by downhole pressure gauges, piezometers, or measurement of surface pressure, after equilibrium is reached following shut-in of injection. It can be estimated from previous drill stem tests or pressure fall-off tests. If σ_h is determined from a mini-frac test, then σ_H can be obtained from either Eqs. (2–7) or (2–8), provided P_p and η are known and assuming smooth circular cylindrical geometry of the wellbore.

2.2.1.5 Fracture reopening pressure (P_{re})

Once the fracture is initiated, the tensile strength of the rock is reduced to zero. Thus, provided the injection rate is kept constant, the fracture reopening pressure (P_{re}), in absence of fluid penetration into the rock matrix, can be defined as:

$$(2\text{–}11)\quad P_{re} = 3\sigma_h - \sigma_H - P_p$$

In case of fluid penetration, P_{re} is given by:

$$(2\text{–}12)\quad P_{re} = \frac{\left(3\sigma_h - \sigma_H - 2\eta P_p\right)}{2\,(1-\eta)}$$

Eqs. (2–7) to (2–12) assume smooth, cylindrical borehole wall topography.

Incomplete formation breakdown. In theory, if a hydraulic fracture is induced in the first cycle, there should not be a large difference in the fracture reopening pressures of successive cycles. However, in reality, in some tests a significant difference in fracture reopening pressure is found to occur even between the second and third cycles. The most likely cause of this is incomplete formation breakdown occurring in the first cycle, if the well is shut-in immediately after the formation breakdown. In fact, breakdown is a phenomenon of fracture growth initiating in the near wellbore region. Thus when the formation is pressurized a few times during a mini-frac test, the fracture reopening pressure of the second or third pressurization cycle could be used to determine σ_h. This way it is possible to reduce the error that may result from use of data from an incomplete breakdown on the first cycle.

If the pressurization of the interval is carried over several cycles, the reopening pressure of the latest pressurization cycle may not offer the best option for accurate determination of minimum *in-situ* stress. Repeated pressurization could cause flexing of the fracture, dislodge materials at the wellbore, create large irregularities and holes, thereby never allowing the fracture to close completely on cessation of injection. In mini-frac tests of poorly consolidated tar sands, reopening pressure of later pressurization cycles were found to be greater than those of the earlier cycles, perhaps due to the large influence of back stress. Thus determination of minimum *in-situ* stress from reopening pressure should be done with caution.

2.3 FRACTURING IN THE ABSENCE OR PRESENCE OF FLUID PENETRATION INTO THE FORMATION (FOR VERTICAL FRACTURES AND VERTICAL WELLBORES)

2.3.1 In the absence of fluid penetration

Hickman and Zoback (1983) indicated that in the absence of fluid penetration, the results of a mini-frac test could be affected by three sets of conditions:

Set 1: The breakdown pressure is greater, but the reopening pressure is either greater than or equal to σ_h; that is, $P_b > P_{re} \geq \sigma_h$. From Eq. (2–11), it is found that this condition is applicable when

$$(2\text{–}13)\quad \frac{\sigma_H + P_p}{\sigma_h} \leq 2$$

Set 2: The breakdown pressure is greater than σ_h, which is greater than the fracture reopening pressure (P_{re}); that is $P_b > \sigma_h > P_{re}$. From Eqs. (2–7) and (2–11), it can be shown that this situation holds when

$$(2\text{–}14)\quad \frac{\sigma_H + P_p}{\sigma_h} > 2 > \frac{\sigma_H + P_p - T}{\sigma_h}$$

Set 3: The σ_h is greater than the fracture reopening pressure but equal to the breakdown pressure, that is $\sigma_h = P_b > P_{re}$. By rearranging Eq. (2–7), it can be shown that this condition will apply when

$$(2\text{–}15)\quad \frac{\sigma_H + P_p - T}{\sigma_h} = 2$$

Eqs. (2–13), (2–14), and (2–15) show that a set 1-type hydraulic fracture would occur where the *in-situ* stress difference is low. The set 2- and 3-type hydraulic fractures are common to cases exhibiting high horizontal stress differences (*i.e.*, $\sigma_H >> \sigma_h$).

2.3.2 In the presence of fluid penetration

Three similar sets of conditions can also be expected in the case of fluid penetration into the rock:

Set 1: From Eq. (2–12), it is found that set 1 conditions, as described in the previous section, would be encountered when

$$(2\text{–}16)\quad \frac{\sigma_H + 2\eta P_p}{\sigma_h} \leq 1 + 2\eta$$

Set 2: From Eqs. (2–8) and (2–12), it can be shown that the conditions similar to those described in the earlier section would be obtained when

$$(2\text{–}17)\quad \frac{\sigma_H + 2\eta P_p}{\sigma_h} > 1 + 2\eta > \frac{\sigma_H + 2\eta P_p - T}{\sigma_h}$$

Set 3: Rearranging Eq. (2–8) demonstrates that the conditions outlined in the previous section will apply when

$$(2\text{–}18)\quad \frac{\sigma_H + 2\eta P_p - T}{\sigma_h} = 1 + 2\eta$$

2.4 FRACTURING OF CEMENTED ROCKS AND POROUS UNCEMENTED TAR SANDS

The theory of a mini-frac test which assumes linear elastic theory was first applied to cemented sandstones. There had been some concerns in applying this theory to porous, uncemented tar sands. The reasons for concern are as follows:

1. While the stress–strain relationship of most cemented sandstones is linear and largely elastic, for tar sands this relationship is non-linear and to a certain extent non-elastic.
2. While cemented sandstones have high cohesive and often high tensile strengths, tar sands have very low cohesive and tensile strengths. Hence, tar sands fail more easily than cemented sandstones.
3. Due to very low cohesive and tensile strength, both the tensile and shear failure in tar sands seem to occur in close succession. Preliminary studies suggest that the type of failure that precedes depends upon the injection rate and can also depend on fluid type (low or high viscosity, hot or cold). At low injection rates, when leak-off into the formation dominates, if a hot injection fluid is used, shear failure can occur and tensile failure may not occur, but at high injection rates when the chances of leak-off are reduced, the tensile failure could occur first followed by a possibility of shear failure. Saltuklaroglu (1991) reported the occurrence of shear failure in poorly consolidated tar sands with the use of cold water at low injection rates. In cemented sandstone reservoirs, the fracture growth occurs primarily by tensile parting.
4. If a hot injection fluid is used to fracture a tar sand formation, the thermal heating of viscous bitumen can accelerate build-up of pore pressure, contributing towards a rapid reduction of the shearing resistance. In using a hot injection fluid, thermally induced stress build-up occurs in both consolidated sandstones and poorly consolidated tar sands, but pore pressure build-up could be significant in tar sands.

Because of these differences in the behaviour of cemented sandstones and tar sands, the following factors are important for the mini-frac test in tar sands, :

- Even when the failure is purely tensile, in calculating the maximum horizontal stress from the minimum *in-situ* stress, Eqs. (2–8) and (2–12) should be used to account for significant leak-off.
- At low injection rates, if the failure appears to be primarily by shearing, the ISIP may not represent the true minimum *in-situ* stress magnitude.
- While in cemented consolidated sandstones there could be a large difference between the formation breakdown pressure, fracture extension pressure, and closure pressure, in poorly consolidated tar sands, because of a low tensile strength, the difference between the breakdown pressure, fracture propagation pressure, and closure pressure could be very small. Such a result may be observed if a pressure measurement is taken downhole. The possibility of such an occurrence is greater when the test is conducted in an uncased hole and the friction effect is less. In cased hole tests, such an effect may not be observed because of the perforation friction effect.

CHAPTER 3

MINI-FRAC
FIELD TESTING
PROCEDURE

3 MINI-FRAC FIELD TESTING PROCEDURE

3.1 CHOICE OF INJECTION FLUID AND RATE

Mini-frac tests are usually conducted to measure the minimum *in-situ* stress, but with some modification to testing procedures, the data can provide pertinent reservoir engineering parameters. The main objective of the test should be properly set before such a test is conducted. If the mini-frac test is carried out solely for the determination of the minimum *in-situ* stress, then it is best to use cold water as the fracturing fluid. The use of hot water or steam is not recommended because the thermal stresses induced by the hot water or steam injection can alter the magnitude of the original *in-situ* stresses. In tar sands, hot fluid can cause large leak-off and pore pressure build-up. Because of their low tensile and cohesive strength and poorly cemented nature, fracturing of tar sands does not require a rapid injection rate. However, for tensile parting of the formation, the injection rate must exceed the rate of leak-off into the formation. A large injection pressure is often required to fracture a well-consolidated formation. If the fluid leak-off is low and the compliance of the well tubulars and equipment meet required criteria, the well-consolidated formations can be fractured even at low rates.

3.2 MINI-FRAC TESTS IN UNCASED AND CASED HOLES

Most often mini-frac tests are performed in uncased holes by isolating the mini-frac interval below a packer or with a straddle packer assembly and pressurizing the interval until it fails. These tests, which often only require low pumping rates and volumes, can be conducted prior to the use of the well for any other purpose. In uncased wells, borehole televiewers or impression packers can be used to determine the azimuth of the induced fracture.

If borehole stability poses a problem, as is sometimes the case for uncased wells in unconsolidated sands, the mini-frac tests are conducted in cased wells through perforations. Perforations in cased wells are usually performed across the fluid-saturated interval. Hence, to overcome the fluid loss during the mini-frac test through a perforated cased well, a larger injection rate and/or volume often is required.

Mini-frac tests performed by Warpinski (1989) in a marine sandstone at similar depths in two wells (an uncased well and a perforated cased well) gave very similar values of ISIP. The wells were spaced 65 m apart.

Fracture orientation at the wellbore can be affected by large stress concentration. Esso Canada reported results of micro-frac (low rate and low volume tests) stress determinations in uncased and cased wells perforated with helical patterns (20° phasing), line patterns (0° phasing), and using casing guns with 120° phasing (Kry and Gronseth, 1983). Kry and Gronseth suggest that a helical perforation pattern helps achieve an appropriate orientation of the fracture at the wellbore. Pressurization and initiation of the fracture can occur outside of the stress concentration region around the wellbore if penetration of the perforation is deep enough. In cased hole tests, a more accurate estimate of the minimum *in-situ* stress is obtained when the induced fracture extends more than two to three borehole diameters from the well.

Once the interval for a mini-frac test is chosen, a preliminary test to determine the permeability effect is conducted by raising the pressure in the interval by 1–2 MPa above the existing pore pressure and monitoring the pressure decay after shut-in. The magnitude of the permeability will determine the minimum rate necessary for a mini-frac test.

3.2.1 Field test procedures

Mini-frac tests are best conducted in a well where the axis of the well is parallel to one of the principal stresses. Thus, in theory, mini-frac tests can be conducted in both vertical and horizontal wells, if the axis of the wells are parallel to the vertical or one of the horizontal stresses. However, most mini-frac tests reported in the literature were conducted in vertical wells and the information obtained from vertical wells is used to design the location of horizontal wells. Mini-frac tests normally are not performed in inclined wells. Experiments have shown that when the inclination (θ) of the well from the minimum horizontal stress is different from 0 or 90°, then the induced fractures can be non-planar or S-shaped (Rabba, 1989). However, at low values of θ (below 15°), the ISIP values observed were not too different from those obtained when θ was zero. Twenty separate *in-situ* stress measurements were obtained by Gronseth (1988) in deviated, perforated cased wells at the same depth in poorly consolidated tar sands. The results of the measurements are presented in Table 3–1. Despite well inclinations up to 48°, the minimum *in-situ* stress values varied between 9.5 MPa and 12 MPa. The variation does not appear to be systematic.

Table 3–1. Results of 20 in-situ *measurements conducted by ESSO in deviated, perforated cased holes at a 454 m depth (after Gronseth, 1988).*

Well number	Well inc. deg.	Well direction	H_{min} MPa	Vertical MPa	Total vol. inj. m^3	Comments
1	42.5	N4°W	11.9	9.5	2.19	Roll over*
2	48.0	N13°E	12.0	9.5	2.38	
3	32.0	N22°E	10.1	9.5	1.64	
4	40.0	N56°E	9.5	9.5	1.78	Hor. Frac.
5	39.0	N70°E	11.4	9.5	1.33	
6	33.25	N7°W	11.4	9.5	1.44	
7	25.0	N20°W	11.4	9.5	1.76	Roll over
8	14.0	N44°E	11.1	9.5	1.89	Roll over
9	32.0	S88°E	10.2	9.5	2.57	
10	42.5	S75°E	9.9	9.5	1.54	
11	31.0	N90°W	11.1	9.5	1.39	
12	17.75	S86°W	10.4	9.5	1.22	
13	25.30	S6°W	10.3	9.5	1.11	Roll over
14	25.0	S29°E	10.7	9.5	1.60	
15	36.50	S37°E	10.2	9.5	1.58	Roll over
16	43.0	S70°W	10.2	9.5	1.44	Roll over
17	41.0	S60°W	10.2	9.5	2.52	Roll over
18	38.75	S36°Y	10.5	9.5	1.73	Roll over
19	38.75	S12°W	9.7	9.5	1.57	
20	39.50	S14°E	11.4	9.5	1.17	

* Changeover of minimum *in-situ* stress orientation.

Most often the mini-frac tests are conducted to assess the minimum *in-situ* stress of the virgin formation before the development of a reservoir. Thus, an exploration well or any other newly drilled well, can be used to conduct mini-frac tests before its use for production. Sometimes an estimate of the changes in the *in-situ* stress regime is desired after a reservoir has been produced for a certain length of time. In these cases, the tests can be performed in an observation well drilled in close proximity to the injection or production well.

3.2.1.1 Equipment required to conduct a mini-frac test

The following tools are often required to conduct a mini-frac test:

1. Tool string (open or cased hole as required).
2. Bottomhole or straddle packer assembly.
3. Downhole gauges, quartz surface read-out gauges.
4. Data acquisition system with computer and X–Y display and plotter.
5. Flow-back manifold with magnetic or turbine flow meters, high pressure needle valves.
6. Surface pressure transducers.
7. Operations communication system.
8. Injection system capable of steady flow delivery at rates ranging from 2 to 100 L/min for micro-fracs and up to 3 m^3/min for mini-fracs.

Mini-frac tests can be conducted in either an open hole or a cased hole. Before conducting a mini-frac test one must first decide the purpose of the test, *i.e.*, if the test is for the determination of minimum *in-situ* stress alone or will include evaluation of the reservoir parameters like transmissibility and permeability.

3.2.1.2 Uncased hole testing procedures

Typical testing equipment and well configuration used in an uncased hole mini-frac test are schematically shown in Figure 3–1. The procedures for conducting mini-frac tests in a vertical well are as follows:

1. Lower inflatable packers and set them at the top and bottom of the testing interval. If more than one intervals is to be tested, then straddle packers should be used.

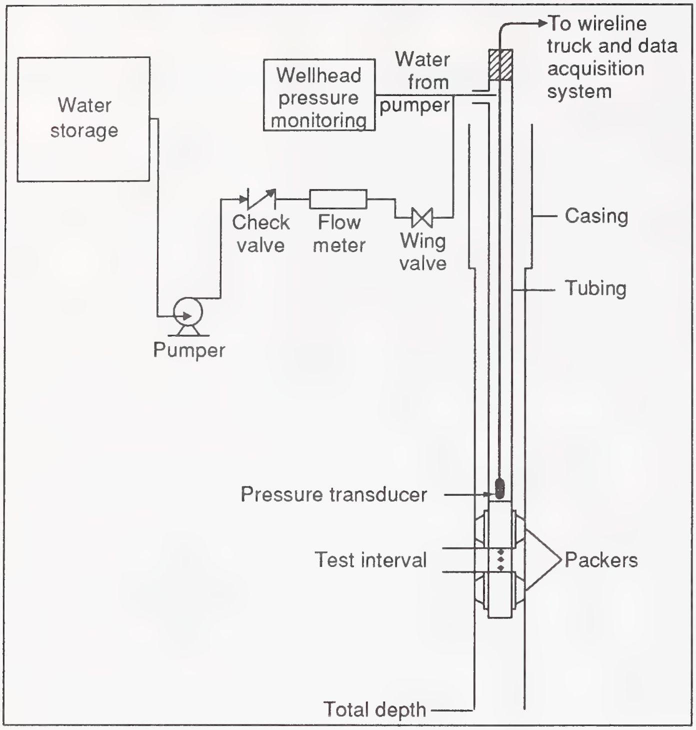

Figure 3–1. Schematic diagram showing open-hole mini-frac testing equipment and well configuration.

2. To monitor pressure behaviour during injection and pressure decline, install the bottomhole pressure gauges through a wireline unit. This will allow accurate data collection since most bottomhole pressure gauges have higher pressure sensitivity and are less affected by wellbore effects than surface pressure gauges.
3. Mount the surface pressure monitoring equipment to the wellhead.
4. Begin monitoring the bottomhole pressure with pressure gauges placed at the bottom of the interval. Constant monitoring of bottomhole pressure is required to identify the time for pressure stabilization. Stabilization of pressure in a tar sands setting could take an unduly long time if a bottomhole shut-in tool is not used.
5. Install the frac pumper and necessary facilities to inject sufficient volume of clean water.
6. Pressure test the lines from the pumper to the wellhead not exceeding the manufacturer's specifications.
7. Fill up the wellbore with fresh water. Record the volume of water required to fill up the wellbore.
8. Ensure proper functioning of bottomhole, wellhead, and casing pressure recorders. Set the recorders to print the pressure readings every two to three seconds.
9. Start pumping continuously at a constant rate for two to three minutes. The choice of the pumping rate would depend on the reservoir rock type. For example, because of low cohesive and tensile strengths, a high pumping rate would not be required for breakdown of poorly consolidated tar sands, whereas the breakdown of tight formations would require a high injection rate. The injection into a poorly consolidated tar sands could start at a low rate of 0.01 m^3/min, whereas for tight sandstones and carbonate reservoirs, the injection rate could start at 0.08 m^3/min.
10. Inject fluid for few minutes (3–4 min) until the pressure stabilizes, then terminate the injection and shut-in the wing valve at the surface.
11. Monitor the bottomhole pressure during injection and look for any evidence of formation breakdown. The breakdown can be identified by a rapid fall after a continuous increase in the pressure. If no breakdown has occurred, increase the rate to about twice the rate used earlier and maintain that constant rate until the pressure stabilizes. Before increasing the rate, let the pressure from the earlier rate stabilize. The injection rate can further be increased to 0.12, 0.24, 0.48, 0.64, and 0.96 m^3/min until the breakdown.
12. Monitor the bottomhole pressure carefully for any sign of formation breakdown. If the occurrence of breakdown is evident, then continue pumping for two to three more minutes before discontinuing injection. Prolonged injection is discouraged to avoid fracture propagation into the bounding layers. Record the bottomhole pressure for at least 40 minutes after the breakdown. During this period, the bottomhole pressure should stabilize. If the pressure does not stabilize, then continue recording until it

does. If absolute permeability is to be determined, then sufficient time should be allowed for pressure fall-off before the test is repeated. The pressure should initially be recorded frequently (every two to three seconds) until the closure of the fracture. Afterward, the pressure can be recorded at longer intervals (2 – 3 min).

13. Record the total injection time and volume.
14. Repeat steps 11 to 13 two more times. If the formation breakdown has already occurred, the injection rate need not be increased in the second and third cycles. To open up an induced fracture, the same injection rate can be maintained. Also during the same injection cycle, the injection rate should not be increased and the two successive injection cycles must be separated by at least 40 minutes to allow pressure stabilization.
15. (a) If the mini-frac test is conducted for various intervals, it is best to carry out the test first at the deepest interval and then gradually move to the upper intervals. However, the test can also be started at the shallowest interval and gradually moved to lower intervals, but probably with some difficulty. If more than one interval is to be tested, it is then preferable to isolate the test intervals with bridge plugs.

    (b) To test a new interval, first deflate the straddle packers, then set the bottom packer along the bottom of the new interval and repeat the procedures outlined in steps 11 to 14.
16. After the pressure from the last test has stabilized, the wireline unit, as well as the frac pumpers and the inflatable packer, can be removed.

3.2.1.3 Cased hole testing procedures

Except for a few differences, cased hole mini-frac test procedures are very similar to uncased hole tests. The procedures for conducting mini-frac tests in a cased hole are summarized below:

1. Perforate the interval/intervals to be tested.
2. Set standard or straddle packers as required. If more than one interval is to be tested, straddle packers should be used. To separate the test interval from other intervals, besides the packers, bridge plugs may also be used.
3. Mount the surface pressure monitoring equipment to the wellhead.
4. Begin monitoring the bottomhole pressure with pressure gauges placed at the bottom of the interval. Constant monitoring of bottomhole pressure is required to identify the time for pressure stabilization. Stabilization of pressure in an tar sands setting could take an unduly long time if a bottomhole shut-in tool is not used.
5. Fill up the annulus with fresh water and record the volume of water required to fill up the wellbore. This way, while a static fluid column is maintained in the annulus, fluid injection during a mini-frac test can be conducted through the tubing. When packers are not used, the fluid can be pumped down the annulus and the bottomhole pressure can be monitored while a static fluid column is maintained in the tubing.
6. Reset packer if necessary.
7. Conduct injectivity and falling head tests, if required, to establish the injection rate necessary for a mini-frac test.
8. Follow steps 9 to 16 as described in the section on uncased hole testing procedures.

3.2.1.4 Variations due to reservoir types

Although certain injection rates have been suggested for use in mini-frac testing of tight formations, the injection rates required for breakdown would vary from one reservoir setting to another. Gronseth and Kry (1987), and Jones and Sargeant (1989) advocate use of as low an injection rate as possible (1 – 50 L/min). Gronseth and Kry (1987) further suggest that the injection volume should also be minimum (about 0.5 to 2 m^3) to eliminate wellbore effects.

CHAPTER 4

ANALYSIS AND INTERPRETATION PROCEDURES OF THE RESULTS

4 ANALYSIS AND INTERPRETATION PROCEDURES OF THE RESULTS

4.1 PROCEDURE FOR *IN-SITU* STRESS MEASUREMENT

4.1.1 Conventional procedure

The data of a mini-frac test can be analyzed in various ways to provide information on the *in-situ* stress regime. The bottomhole pressure should be plotted against the injection rate for the entire injection period, and against the time for both the injection and shut-in period. If several mini-frac tests are conducted at the same interval at variable injection rates, then the pressure *versus* the injection rate and time plot should be made for all the tests. The following information can be obtained from these plots.

4.1.1.1 Formation breakdown pressure (P_b)

The formation breakdown is identified on a pressure–time plot by a steady increase in pressure immediately followed by a sharp drop in pressure (Figure 2–2). The point where a rapid fall in pressure begins is regarded as the fracture initiation pressure and is considered as formation breakdown pressure. The formation breakdown pressure may vary depending on the lithology, the *in-situ* stress regime, the fluid saturation of the test interval, and the depth of formation. Scott (1990) found the formation breakdown in gypstone to depend on the injection rate; the breakdown pressure being greater for the higher injection rate.

4.1.1.2 Fracture reopening pressure (P_{re})

Once the fluid injection is discontinued, in most cases, almost a complete closure of the fracture takes place. If the injection is resumed again, the originally formed fracture reopens. The pressure at which a fracture reopens is usually lower than the formation breakdown pressure. In theory, the fracture reopening pressure should be lower than the formation breakdown pressure by the magnitude of the tensile strength of the intact rock. But in a few cases, the fracture reopening pressure is found to decrease with repeated injection cycles with a tendency of the reopening pressure to level off in later cycles. This would most likely happen when a complete breakdown was not obtained in the first cycle. Even if a complete breakdown occurred in the first cycle, a slight decrease in fracture reopening pressure could be observed if the fluid diffusion from the wellbore to the surrounding rock became significant.

4.1.1.3 Instantaneous Shut-In Pressure (ISIP), fracture closure, and minimum *in-situ* stress from pressure–time curves

Fracture propagation continues for sometime following the termination of fluid injection. Fracture geometry evolution following the termination of fluid injection can occur due to the following mechanisms:

(a) the fracture propagation;

(b) the fluid leak-off into the pores, vugs, cavities, and micro-cracks within the formation by diffusion; and

(c) the residual strain and creep effect.

The early part of the closure is affected mostly by the first two mechanisms, whereas the latter part is dominated by the third mechanism.

ISIP obtained from multiple pressurization of a zone does not always remain constant from cycle to cycle. Usually the ISIP of the first pressurization cycle has been found to be significantly higher than the magnitude of the stresses acting perpendicular to the fracture plane. To eliminate the uncertainty in the determination of ISIP, Gronseth and Kry (1983) suggest that the ISIP should be obtained as the inflection point in the pressure–time record following the shut-in. The method proposed by Gronseth and Kry is graphically represented in Figure 4–1 in terms of two pressure–time records. Line t_1 is the tangent to the pressure– time record immediately following shut-in. The pressure at which the pressure–time record deviates from the tangent line is the ISIP. When this departure cannot be identified clearly, they suggest that a second line t_2 drawn tangent to the pressure–time record at a slightly greater time can be used to determine the inflection point. In the second case, the ISIP can be obtained from the intersection of two tangents.

Gronseth and Kry (1983) suggest that the minimum ISIP obtained after several pressurization cycles is the best estimate of the minimum *in-situ* stress.

Sometimes a steep decline in the surface pressure is observed immediately after the shut-in. Such a decline is partly due to the frictional pressure drop resulting from shut-in of injection and partly due to the fluid pressure gradient trying to reach an equilibrium and, to some degree, the fracture propagation even after shut-in.

At ISIP, the fracture has the maximum width, but on fracture propagation after shut-in, the fluid leak-off is accelerated. This in turn has an effect on the rate of fracture closure. Thus when the fracture propagates after shut-in,

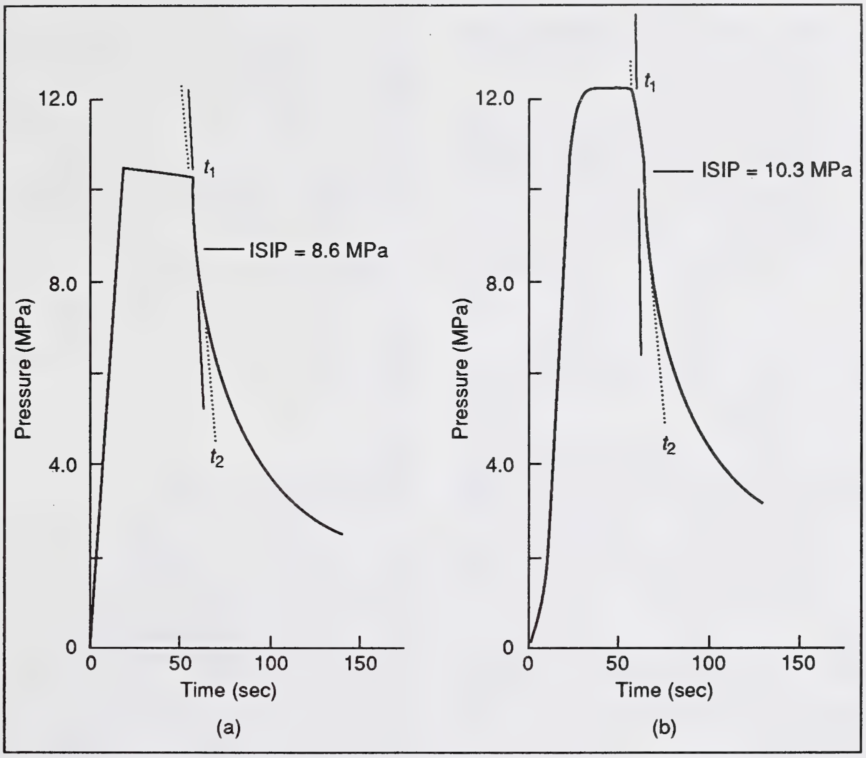

Figure 4–1. *Method of determining instantaneous shut-in pressure using tangent lines to the fall-off curve of a pressure–time record (after Gronseth and Kry, 1983).*

the ISIP can be higher than the closure or *in-situ* stress. If the fracture propagation following the shut-in is negligible, the ISIP can be taken as an indicator of fracture closure.

McLennan and Roegiers (1981) indicated that the ISIP could be higher than the true minimum *in-situ* stress by as much as 20%. ISIP can also be affected by the fracture orientation. They found a higher closure stress in excess of the minimum stress for a slightly inclined fracture (2°). The effect could be more pronounced if the fracture inclination was higher.

Thus a determination of the minimum *in-situ* stress from fracturing is not as simple as it seems from the theory. It is sometimes difficult to obtain an accurate estimate of the minimum *in-situ* stress from a mini-frac test (when the fluid leak-off rate is too large). Hence, Gronseth and Kry (1983) and Hickman and Zoback (1983) suggest that the field mini-frac tests should be carried out with repeated pressurization cycles of progressively longer duration and pumping at a constant flow rate throughout a test. The stable ISIP reached after repeated pressurization cycles should be used as a measure of the minimum *in-situ* stress.

4.1.2 Reservoir engineering procedure

4.1.2.1 Understanding regimes in the presence of a fracture

If it assumed that a finite conductivity fracture is initiated by mini-frac tests and, if the effect of gravity is ignored, then the regimes that might be expected before the pressure transient reaches the reservoir boundaries are as follows (Gringarten and Ramey, 1974; Cinco–Ley and Samaniego, 1978; Poon, 1986):

(a) *Wellbore storage and skin effect*. This effect is usually identified by a unit slope straight line in a log–log plot of the pressure–time data. It usually dominates the early transient data from the beginning of the test and sometimes can mask flow characteristics that follow.

(b) *Fracture linear flow regime*. This regime is indicative of flow along the length of the fracture. Provided there is no wellbore storage effect, this regime is recognized by the half slope straight line in a log–log plot of pressure–time data as shown in Figure 4–3. Sometime this regime is not identified because of wellbore storage effects.

(c) Bi-linear flow regime. This regime occurs when the fluid flow along the fracture length and the leak-off rate are equally important. It is identified by a smaller slope straight line in a log–log plot.

(d) Formation linear flow regime. This regime is dominated by a higher leak-off rate than the flow along the fracture and usually occurs after bi-linear flow regime. Like fracture linear flow, it is recognized by a half slope straight line in a log–log plot of pressure *versus* time.

(e) Pseudo-radial flow. If the boundary effects are not felt, the fluid flow pattern around a fracture becomes almost radial. It is identified by a semi-log straight line and the slope of the semi-log straight line is used to estimate the permeability — thickness product of the reservoir.

These regimes are shown schematically in Figures 4–2 and 4–3. The reservoir engineering procedures employed for *in-situ* stress determination require a good understanding of these regimes.

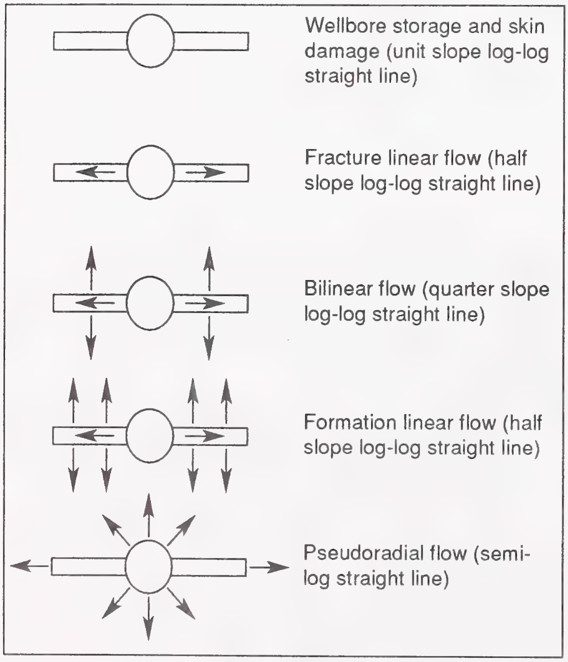
Wellbore storage and skin damage (unit slope log-log straight line)
Fracture linear flow (half slope log-log straight line)
Bilinear flow (quarter slope log-log straight line)
Formation linear flow (half slope log-log straight line)
Pseudoradial flow (semi-log straight line)

Figure 4–2. Flow regimes that are expected in a well with a finite conductivity fracture (after Poon, 1986).

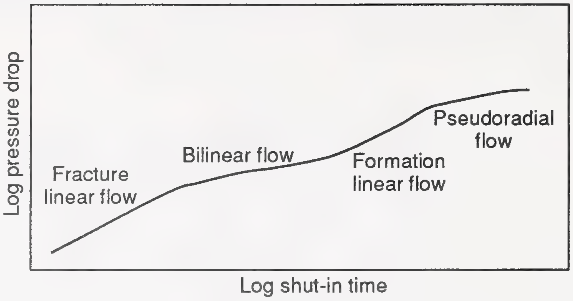

Figure 4–3. Schematic plot of mini-frac pressure fall-off data showing various flow regimes. Note data are plotted on a log–log scale.

4.1.2.2 Methods of analysis

Estimation of the minimum *in-situ* stress from ISIP or closure stress of a pressure–time curve is the most commonly used method. However, in recent years other methods have been proposed. The values predicted by these methods often are close. Any of these methods can be used to compare minimum *in-situ* stress measurement from ISIP or closure stress. Other methods of minimum *in-situ* stress determination using variants of pressure–time data analysis are as follows:

(a) Pressure *versus* square root of shut-in time.

(b) Tandem square root or linear flow plot.

(c) Pressure decay rate.

(d) Log pressure *versus* shut-in time.

(e) Log *dp versus* log *dt*.

(f) Pump-in/flow-back test.

(g) Pressure *versus* flow rate.

(h) Fracture reopening test.

(i) Horner plot.

Pressure* versus *square root of time since shut-in. This method was proposed originally by Nolte (1982). This reservoir engineering method assumes that after fluid injection into the formation is stopped, the pressure decline due to fluid leak-off should be linear as long as the fracture remains open. The method is often used in conjunction with the log–log plot of pressure–time data. On the log–log plot, the fracture linear flow regime is identified by its characteristic half slope. The log–log plot indicates if the closure stress has been identified accurately on a pressure *versus* square root of time plot. A plot of pressure *versus* the square root of time since shut-in is usually a declining straight line, but once the fracture closes there would be a deviation from the straight line (Figure 4–4). The point of first deviation in slope from a straight line is taken as the closure stress or the minimum *in-situ* stress.

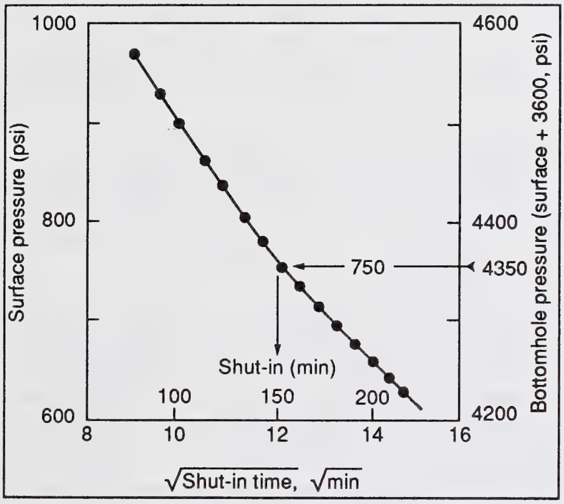

***Figure 4–4.** Interpretation of closure pressure from the change in slope of pressure versus square root of shut-in time. Plot indicates a surface pressure of 750 psi (from Nolte, 1986).*

The other variants of pressure *versus* shut-in time plot used are:

P *versus* $\sqrt{t}$

P *versus* $\sqrt{t - t_s}$

P *versus* $\sqrt{t - 0.5t_s}$

P *versus* Nolte G-function

In the above cases,

t = time from the start of injection

t_s = time at shut-in

All of the above cases take into account the fact that the leak-off rate follows the law

$$q = \frac{C}{\sqrt{t - t_o}}$$

where t_o is the time the element of the fracture was first exposed to leak-off. Often these plots can be ambiguous.

All variants of pressure *versus* square root of shut-in time method work well with consolidated formations, where formation compressibility is not pressure dependent. In unconsolidated formations where the compressibility is pressure dependent, these methods may not work well. Details on the application of these methods are not covered in this manual.

Tandem square root or linear flow plot. In linear flow plots, the bottomhole or surface pressure is plotted against $sqrt(T_{inj} + dt) - sqrt(dt)$ and the closure or minimum *in-situ* stress is calculated from the slope of the linear segment of the plot corresponding to small time since shut-in. This type of plot superimposes pressure for the linear flow during injection on the one during fall-off. The fundamental assumption is that until the occurrence of fracture closure, the flow inside a fracture is linear. Soon after fracture closure, the flow becomes non-linear. Determination of the minimum *in-situ* stress from the slope of the linear portion of the plot is shown in Figure 4–5.

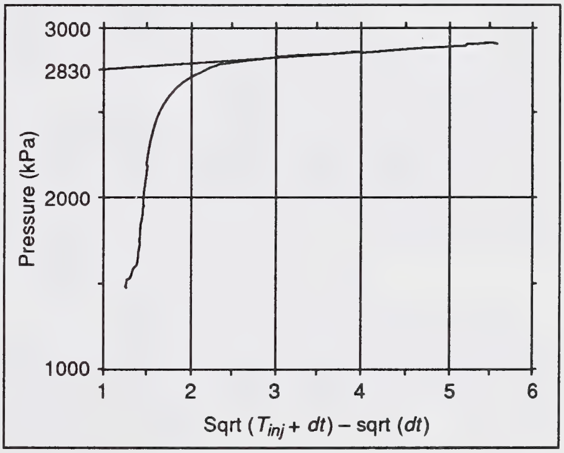

***Figure 4–5.** A linear plot used to predict minimum in-situ stress value in a mudstone interval. Change in slope following shut-in of the injection corresponds to a minimum in-situ stress value of 2830 kPa.*

Log pressure* versus *time since shut-in. Often either the log of the difference of the pressure since shut-in and the reservoir pressure, or the log of the bottomhole pressure, is plotted against the time since shut-in. This type of plot is based on an exponential leak-off after the closure. Thus the inflection point on the slope of a curve is taken to be equal to the ISIP or the minimum *in-situ* stress (Figure 4–6).

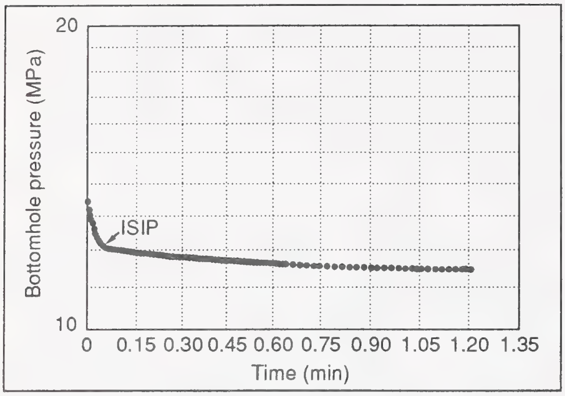

Figure 4–6. On a semi-log plot of pressure versus shut-in time such as this, ISIP is the inflection point corresponding to the change in slope (from Warpinski, 1989).

Log* dP versus *log* dt *plot. This plot is based on an exponential leak-off after the closure. The plot is often used in reservoir engineering to estimate the duration of wellbore storage. The end of wellbore storage is followed by linear or bi-linear flow in the fracture as long as the fracture remains open. When the fracture begins to close, the *dP versus dt* curve deviates from a straight line. The *dP* value corresponding to this deviation from a straight line denotes the closure of the fracture. Once *dP* is known, the ISIP or the minimum *in-situ* stress can be obtained (Figure 4–7).

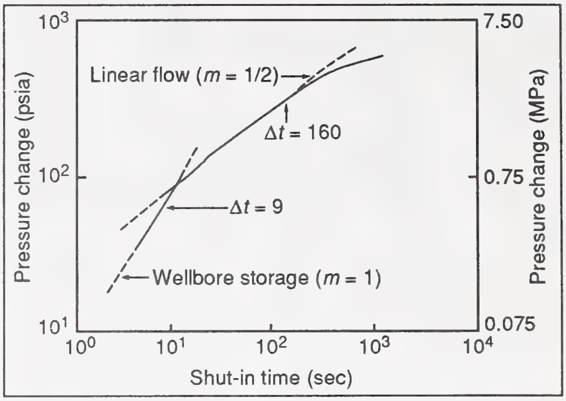

Figure 4–7. On a log dP versus log dt plot, closure pressure corresponds to a value where fracture linear flow deviates from a straight line. In this plot, pressure corresponding to a Δt value of 160 seconds is the closure pressure (from Whitehead et al., 1989).

Pressure decay rate. The pressure decay following the cessation of fluid injection is caused by an extension of the fracture as well as the leak-off of the injected fluid from the fracture into the surrounding rock. As these processes continue, the pressure eventually reaches a value which is equal to the far field stress normal to the fracture causing the fracture to close.

The pressure decay rate method is based on the assumption that the pressure decay consists of two distinct stages — a stage of linear flow when the fracture is still open and the other stage of radial flow following the fracture closure. The pressure change per unit time (*dP*/*dt*) plotted against pressure (*P*) thus results in a bi-linear curve representing the opened and closed fracture pressure regime. The point of intersection of two linear curves is considered to be the closure stress or the minimum *in-situ* stress (Figure 4–8). The type of bi-linear curve seen for poorly consolidated sands is shown later in Figure 6–13.

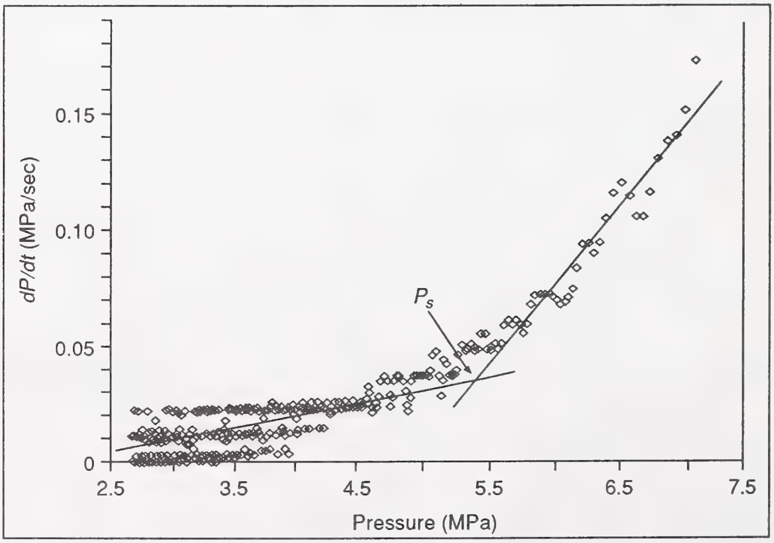

Figure 4–8. Shut-in pressure determination using bi-linear pressure-decay rate method. Shut-in pressure is shown as P_s where bi-linear curves intersect (from Lee and Haimson, 1989).

Pump-in/flow-back test. In low permeability formations, where the fracture closure time following a pump shut-in is usually long, the pump-in/flow-back test can be used as a time-saving alternative method. In this type of test, the pressure decline after shut-in and after the start of backflow shows a distinct inflection point corresponding to the fracture closure (Figure 4–9). However, the success of obtaining a distinct inflection point depends very much upon the flow-back rate. The test may have to be repeated two or three times using differential flow-back rates to achieve a distinct closure pressure. It is essential to keep the flow-back rate constant each time the test is conducted.

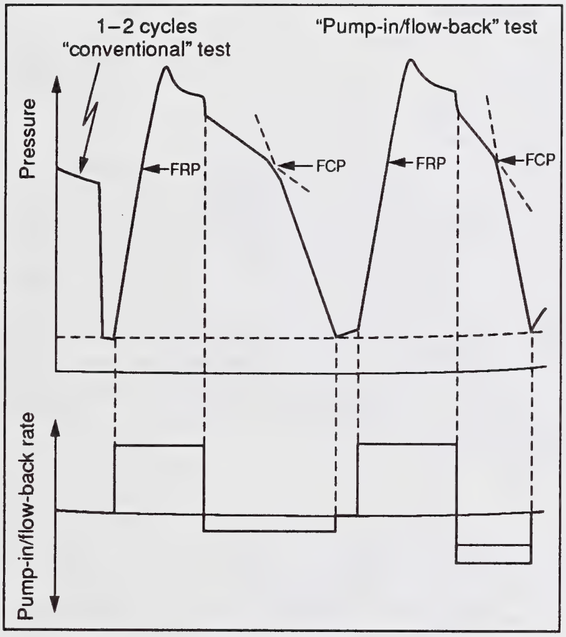

Figure 4–9. *Profile of first two pump-in/flow-back test cycles following the first cycle of the formation breakdown (not shown here). FRP and FCP denote fracture reopening pressure and fracture closing pressure, respectively (from De Bree and Walters, 1989).*

Pressure versus injection rate. The method requires repeated pressurization of the test interval at multiple injection rates and hence is a long process. The test is very similar to a step rate test. The pressurization of the test interval usually starts at a very low injection rate until the pressure stabilizes. The injection rate is then increased to a new constant level and maintained until a constant bottomhole pressure is observed. This process is continued at several successively increasing injection rates (about 6 to 8) allowing the bottomhole pressure to stabilize at each rate before using a higher rate. Finally, the maximum pressure attained at each rate *versus* the injection rate data are plotted on a normal scale. The plot normally exhibits two dominant slopes (Figure 4–10).

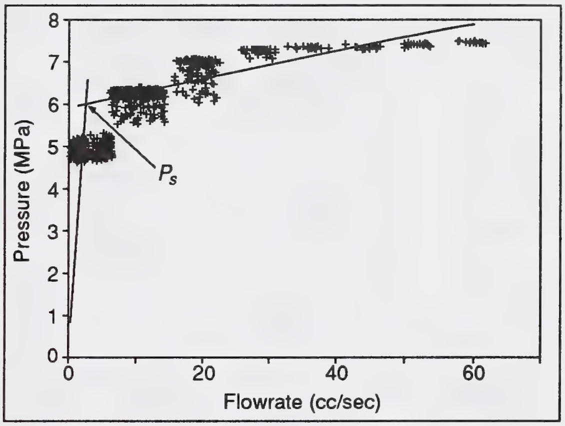

Figure 4–10. *On a pressure versus flow rate plot, closure or minimum in-situ stress is obtained as the intersection point (P_s on the plot) where steeper pre-fracture closure curve intersects with a post-fracture curve (from Lee and Haimson, 1989).*

The interpretation of the plot is based on the rational that below a certain pressure (noted as P_s in the figure) the fracture remains closed and the slope of pressure *versus* injection rate curve is considerably steeper than that observed after the reopening of the fracture. The point P_s where the change in slope occurs is considered to be the fracture closure or minimum *in-situ* stress.

Since the rates used are discrete, there could be a transition zone between two successive rates where fracturing could occur. Whenever such a transition zone occurs, the selection of P_s may be questionable if the change in the slope is not abrupt.

The method has been found very successful for determination of minimum *in-situ* stress in consolidated rock types. In tar sands applications, the method has not provided encouraging results; however, further studies are required to establish usefulness of the method in tar sands.

Fracture reopening test. Minimum *in-situ* stress can be estimated from fracture reopening tests. On subsequent fluid injection at a constant rate following the initial breakdown of a formation, the slope of the pressure *versus* time curve should be constant until the fracture reopens. Deviation from the straight line would occur when the fracture reopens (Figure 4–11). The point of deviation is considered as the reopening pressure and is in theory the upper limit of minimum *in-situ* stress (Whitehead *et al.*, 1989).

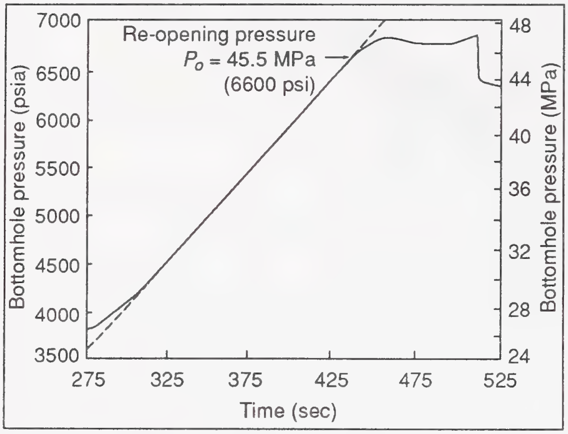

Figure 4–11. In a plot of fracture re-opening method, closure or minimum in-situ stress is identified as the deviation of pressure versus injection time curve from a straight line. In this plot, minimum in-situ stress equals 45.5 MPa (from Whitehead et al., 1989).

Fracture reopening test results like pump-in/flowback test results can be misleading if the injection rate used for fracture reopening far exceeds the rate used originally for breakdown.

Horner plot. The Horner plot is a plot of pressure against log $(T_{inj} + dt)/dt$, where T_{inj} is the total injection time and dt is the time since shut-in. The plot was originally used in reservoir engineering for a pressure decline analysis. Authors like McLennan and Roegiers (1981) have suggested that when the pressure fall-off data are plotted on a Horner plot, a change in slope can occur where the fracture closes. The Horner method assumes that until the fracture has closed completely and the pressure transient effects are controlled by radial flow, a straight line will be observed on the Horner plot; prior to the fracture closure the relationship is believed to deviate from a straight line. The point of deviation is considered to correspond with the *in-situ* stress acting across the fracture. A typical example showing the *in-situ* stress determination from the slope of a Horner plot is shown in Figure 4–12. McLennan and Roegiers also indicated that the following situations can be observed when Horner plots are used to determine the minimum *in-situ* stress.

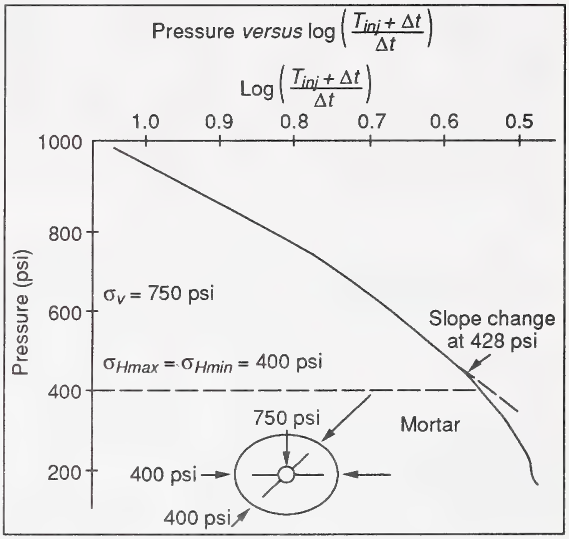

Figure 4–12. Determination of in-situ minimum stress from the slope of a Horner plot. Here the maximum stress is vertical (750 psi). The two horizontal stresses are equal (400 psi). The change in slope of Horner plot corresponds to an in-situ stress value of 428 psi (from McLennan and Roegiers, 1981).

- In certain cases, inflection points of a Horner plot may represent the stresses acting across the fracture rather than the current principal stress. Similar results were suggested earlier by Mizuta and Kobayashi (1980).
- If the fractures are inclined, the minimum *in-situ* stress can be overestimated. This can be significantly large if the difference between the vertical and the horizontal stresses is large. This is shown in Figure 4–13 for a fracture inclined at 2°. While the applied stress was 225 psi, the inflection point on the Horner plot gave a value of 290 psi.
- It may be possible to determine more than one *in-situ* stress value from multiple points on the Horner plot. Multiple points may represent the presence of a quasi-orthogonal fracture system (Figure 4–14).

The deviation from a straight line expected to be seen at the closure of a fracture may be masked in cases of

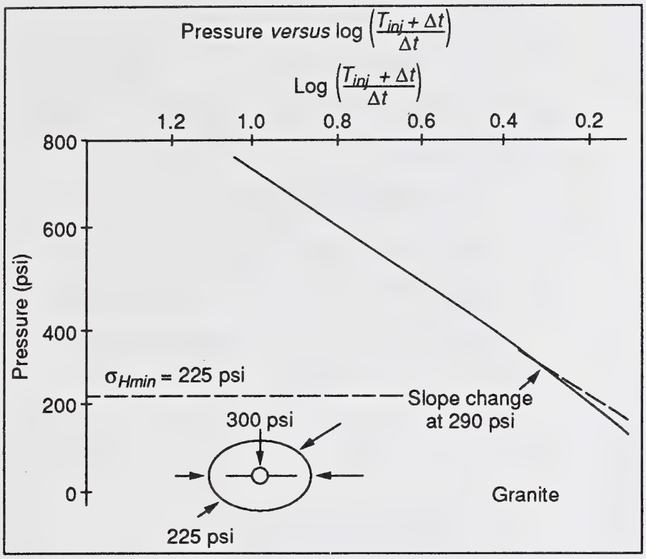

Figure 4–13. Plot showing the effect of fracture inclination on in-situ stress value. While minimum in-situ stress is 225 psi, for a 2° inclination of the fracture Horner plot's inflection point corresponds to a higher minimum in-situ stress value of 290 psi (after McLennan and Roegiers, 1981).

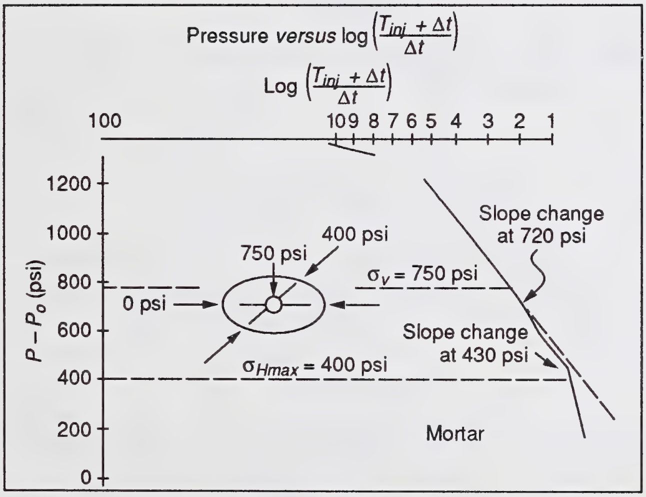

Figure 4–14. Presence of two inflection points on the slope of the Horner plot. Inflection points represent stress magnitudes corresponding to quasi-orthogonal fracture system (after McLennan and Roegiers, 1981).

high wellbore storage. The method can also be used for minimum *in-situ* stress determination in tar sands provided wellbore storage effect is minimal.

4.2 PROCEDURE FOR OBTAINING RESERVOIR PARAMETERS

4.2.1 Determination of reservoir parameters from mini-frac test data

Reservoir parameters like absolute permeability, transmissibility, skin effect, and wellbore storage can be obtained from a mini-frac test analysis, although it is not a standard practice. Normally in mini-frac tests, fluid injection is repeated in multiple cycles without allowance for large time intervals between two cycles. Under these circumstances, mini-frac tests are not suitable for measurement of absolute permeability and may not provide representative values, unless the following procedures are adopted.

1. After the formation breakdown, pressure fall-off should be monitored for a considerable length of time until pressure stabilizes to about the original reservoir pressure. The fluid injection into the test interval should be resumed only after such a pressure stabilization. This way the aforementioned reservoir parameters can be obtained from the first fluid injection cycle. In later cycles of fluid injection, the time interval between two tests does not have to be long once reservoir parameters have been determined from the first cycle.

2. In tar sands, stabilization of pressure following fluid injection during the first cycle of a mini-frac test might take an unduly long time. To reduce the pressure stabilization time, bottomhole shut-in tools are recommended.

3. To select the appropriate linear flow regime for Horner analysis, sometimes log–log derivative plots may have to be used, as in Figure 4–3.

4.2.1.1 Formation transmissibility and absolute permeability

Formation transmissibility and absolute permeability can be obtained from standard Horner analysis similar to that used in the pressure build-up test analysis. The analysis consists of a semi-log plot of bottomhole or surface pressure *versus* $(T_{inj} + dt)/dt$. If slope "*m*" of the straight line portion of the plot is known, then the transmissibility of the formation, kh/μ, can be determined from the following equation proposed by Horner (1951):

$$\frac{kh}{\mu} = \frac{CqB}{m} \tag{4–1}$$

where k = the effective permeability
h = the effective reservoir flow thickness
μ = the reservoir fluid viscosity
q = the fluid injection rate
B = the formation volume factor
C = a constant

The Horner plot is most often used when $T_{inj} < T_{injss}$. T_{injss} represents the time to the beginning of pseudo-steady-state flow. The Horner plot can also be used to analyze the data when $T_{inj} > T_{injss}$. Analysis using the Horner plot requires more time. The Miller–Dyes–Hutchinson (MDH) plot is used whenever $T_{inj} > T_{injss}$, because it is easier to plot and is less time consuming. In the MDH plot, the pressure drop data are plotted against shut-in time data on a semi-log scale. From the slope, m, the transmissibility of the formation is estimated using Eq. (4–1). Once the transmissibility is calculated, the absolute permeability can be obtained if the thickness "h" and the viscosity "μ" are known. The slope of the Horner plot shown in Figure 4–15 is used in Appendix A in a sample calculation of transmissibility of a tar sands formation.

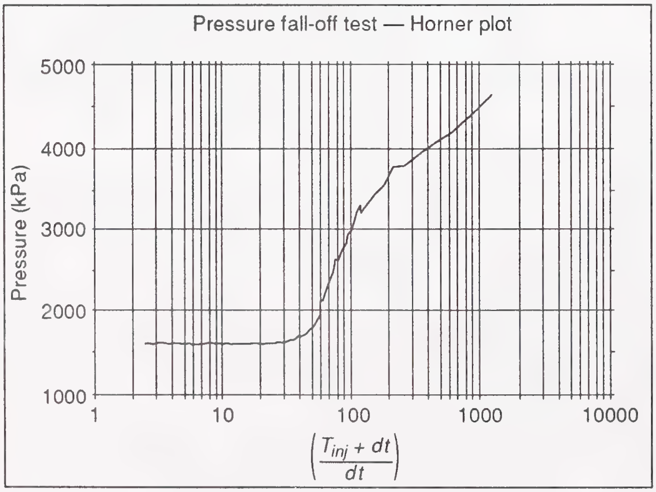

Figure 4–15. Pressure fall-off data of a mini-frac test can be plotted on a Horner plot to derive formation transmissibility. Calculation of transmissibility using the slope of this plot is presented in Appendix A.

4.2.1.2 Skin effect

The formation damage that occurs near the wellbore is regarded as the skin effect. The skin damage in a thin radius around the wellbore can be caused by a combination of several factors:

1. the mud filtrate near the wellbore,
2. the cement bond, and
3. limited perforation density through the casing.

Skin damage can be estimated from the skin factor "S" defined by Everdingen (1953) and Hurst (1953) as:

$$S = 1.151\left[\frac{\left(P_{wf} - P_1\right)}{m} - \log\left(\frac{k}{\left(\phi\mu C_t R_w^2\right)}\right) + c\right] \tag{4–2}$$

where P_{wf} = the flowing pressure
P_1 = the pressure at $(t_{inj} + dt)/dt$ equal to 1 from the Horner plot
m = the slope of a Horner plot
R_w = the wellbore radius
C_t = the total compressibility of a formation
ϕ = the porosity of a formation
c = a constant

If the slope "m" is known from Horner plot, then the skin factor "S" can be estimated from Eq. (4–2). The skin factor "S" is used to evaluate the wellbore quality resulting from a stimulation treatment. While a positive "S" value denotes damage, a negative value denotes improvement. An improvement in the wellbore condition can be caused either by an improved permeability in the vicinity of the wellbore by acidizing and other well treatments or by hydraulically induced horizontal and vertical fractures. The value of S can vary from about –5 for a hydraulically fractured well to $+\infty$ for a well that is too badly damaged to produce (Earlougher, 1977). The determination of the skin effect is important to assess the need for workover or to evaluate the benefits of a workover for enhanced production. The procedure for estimating the skin factor from a Horner plot using Eq. (4–2) is shown in Appendix A.

4.2.1.3 Wellbore storage

To estimate the duration of wellbore storage and skin effect, a plot of pressure differentials, *dp*, against the shut-in time, *dt*, should be constructed on log–log scale. The end of wellbore storage is marked by deviation from the unit slope straight line. The time at which the deviation occurs corresponds to the total duration of wellbore storage. A plot of Δp *versus* Δt showing the method of calculating wellbore storage is presented in Figure 4–16. In this figure, the end of wellbore storage corresponds to a Δt value of two hours. A large duration of wellbore storage is undesirable, because the longer the duration of the wellbore storage, the greater is its effect on the fracture linear flow. Thus, the fracture linear flow regime may never be seen if the duration is large.

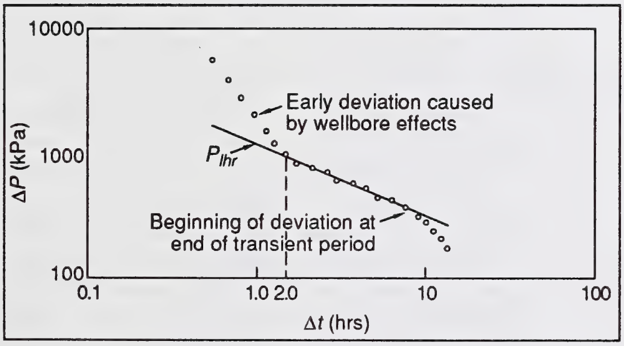

Figure 4–16. *Log–log plot of pressure differentials versus shut-in time data can help identify the end of wellbore storage effect. The end of wellbore storage effect is followed usually by a linear flow within the fracture.*

During mini-frac tests in tar sands, the wellbore can be affected by the following additional factors: dilation, local shear failure, and presence of gas in liquid. The use of bottomhole shut-in tools during mini-frac tests in tar sands has been found very useful in reducing the wellbore storage effect.

4.3 PROCEDURE FOR OBTAINING FLUID LEAK-OFF PARAMETERS

The pressure-time curve of a mini-frac test to estimate fluid leak-off parameters. leak-off coefficient, fluid efficiency can be used, as well as fracture geometry. The leak-off coefficient can be used in a fracture simulator to predict fracture growth as a function of injection rate and time. Leak-off parameters also help determine the fluid loss additive required for the main fracturing treatment. In fact correct modeling of fluid leak-off is critical to optimize the fracture treatment design and identify the fracture closure. An estimate of fluid leak-off coefficient will be valid if the following assumptions are true:

1. Total fluid loss of the formation occurs in the form of matrix leak-off.
2. Total fluid leak-off occurs along the net fracture height interval.
3. The fracturing fluid does not degrade with time and temperature.
4. The created fracture closes completely after the fluid injection is stopped.
5. Fluid compressibility and expansion effects due to temperature are neglected.

Nolte (1979) uses the following equation to estimate the leak-off coefficient, *C*.

$$(4\text{–}3)\quad C = \frac{P^* H^2 \beta_s}{E' H_p \sqrt{t_o}}$$

where P^* = type curve matching pressure
H = gross fracture height
H_p = fluid loss height
β_s = ratio of the average and wellbore pressure at shut-in
t_o = injection time
E' = plane strain modulus and is expressed as $E' = E/(1-\nu^2)$

where E = elastic modulus
ν = Poisson's ratio

Nolte's method is a curve matching technique, in which pressure difference from shut-in time is plotted against a dimensionless shut-in time (δ) defined as:

$$(4\text{–}4)\quad \delta = \frac{\Delta t}{T_{inj}}$$

where Δt = time since shut-in, and
T_{inj} = total injection time

The parameter P^* of Eq. (4–3) is obtained by matching the pressure decline data after shut-in with type curves provided by Nolte (Figure 4–17). An example calculation of fluid leak-off coefficient using Nolte's method is provided in Appendix A. Once P^* has been determined, the following other parameters can also be obtained:

(a) fluid efficiency,

(b) closure time, and

(c) fracture width and length or radius,

provided the gross height is assumed either to be constant (Perkins–Kern and Christianovich–Zheltov models) or to be related to the fracture length by special relationships (penny and ellipsoidal models) (Ripley, 1992).

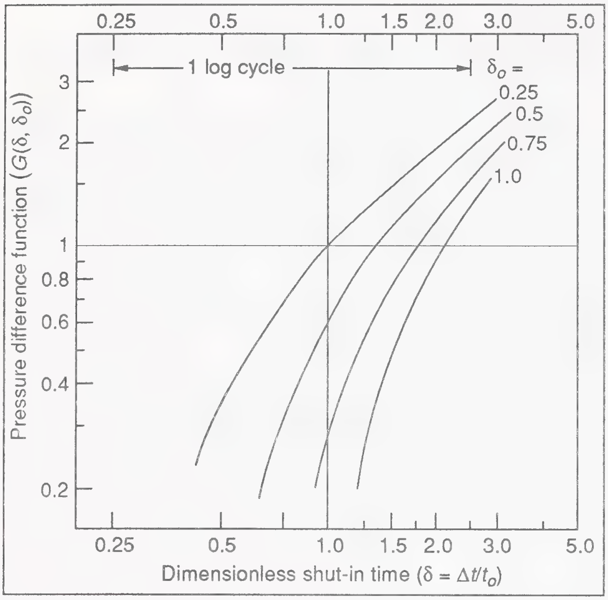

Figure 4–17. Nolte's type curve matching master curve (after Nolte, 1979).

In Nolte's method, the calculated closure time often does not agree with the field observed value. In an alternative method, called the energy balance method, proposed by Lee (1986), the rheological properties of the fracturing fluid are taken into account and the fluid leak-off calculation is evaluated from the beginning of pumping to field observed closure time.

The method uses an energy balance equation to solve the fracture geometry. The power law coefficient n' and K' of a viscous fluid are used to determine the fracture geometry. Since the rheological properties of the fracture fluid are important in the analysis, good quality control practices during the mini-frac tests are required to provide the correct information.

The energy balance method uses the type curve procedure utilizing field measured closure pressure and closure time. In the type curve procedure, the pressure decline data is matched to type curves, similar to that described by Nolte, to determine P^*. The closure time is calculated from the type curves. If this calculated time differs considerably from the observed closure time, the reliability of this analysis is questionable. Lee suggests that direct measurement of pressure *versus* time can be more accurate. Thus the type curve procedure should only be used in cases where closure cannot be determined accurately. Fluid efficiency is determined analytically from field measured closure time. Further details on the energy balance method are provided by Lee (1986, 1987).

Sometimes the knowledge of the reservoir porosity and permeability helps to determine if the fluid leak-off is matrix controlled. If the calculated leak-off is much greater than predicted values, then the fracture height selected in the design estimates can be overestimated, otherwise the high leak-off could be due to the presence of fractures or fissures. At low effective stresses in tar sands reservoirs, geomechanical effects lead to enhanced injectivity around the fractures.

CHAPTER 5

FACTORS AFFECTING MINI-FRAC TEST RESULTS

5 FACTORS AFFECTING MINI-FRAC TEST RESULTS

Factors affecting the results of mini-frac tests depend to some degree on whether the tests are performed in cased or uncased wells. The factors can be classified under four groups:

(a) Geological

(b) Operational

(c) Fracture growth pattern

(d) Mode of analysis

5.1 RESERVOIR/GEOLOGIC FACTORS

5.1.1 Reservoir lithology/geomechanical behaviour of the rock

Warpinski *et al.* (1985) found the breakdown and reopening pressures to be higher in sandstones than in shale. Mini-frac tests conducted in a 30-m deep interval of the McMurray Formation showed the breakdown, reopening, and extension pressures to be the largest in tar sands, intermediate in interbedded sand and mudstone, and the least in mudstone (Figure 5–1). In all cases, the injection rate was nearly the same. These variations are perhaps caused by a difference in the lithological as well as the geomechanical properties.

Compilation of worldwide hydraulic fracturing data suggests that the stress magnitude is affected by rock lithology (Bush and Meyer, 1988). Lithologic factors affecting *in-situ* stress magnitudes are believed to be the grain size, shape, orientation, strength, and type of matrix materials. These factors in turn determine the rock's ability to retain residual stresses and respond to applied stress. During its long geologic history, a rock is affected by tectonic and gravimetric loading and by thermal, chemical, and mechanical processes. Besides pore pressure, the other mechanical processes and properties affecting the state of stresses are slip, fracture, elastic properties, and visco-plastic flow (Bush and Meyer, 1988).

The current mechanical properties of the formation may provide rough estimates of subsurface horizontal stresses. However, they are inadequate to explain the variation in horizontal stresses observed in adjacent lithological units/formations. The temperature, creep, and changes in material properties and stress occurring during burial have a significant influence on the present state of stress observed in rocks (Prats, 1981).

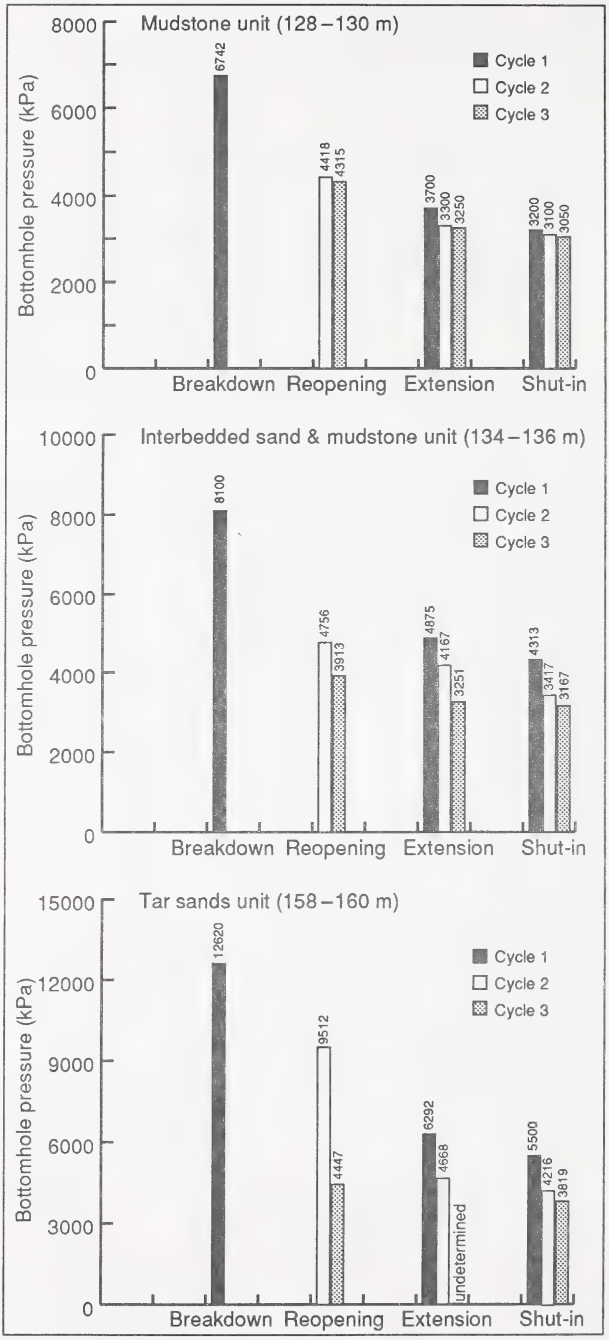

Figure 5–1. A bar graph showing variations in breakdown, reopening, extension, and shut-in pressures for three different lithological intervals. Extension and shut-in are shown for the three cycles, and reopening for the second and third cycles (see also Table 6–1).

5.1.2 Time dependent rock deformation

In weak, friable rocks where a large part of the deformation is non-elastic, complete fracture closure may occur over a considerable period of time after shut-in. For rocks which are non-porous and deformation is predominantly elastic, the fracture closure following the shut-in is expected to be instantaneous for a micro-frac, but not for the larger mini-frac.

5.1.3 Presence of natural fractures, joints, and cracks

Natural fractures may either be in an incipient (closed) state or open; much of which depends on the depth of occurrence and rock type. If the natural fractures are open, they may serve as an escape route for the injected fracturing fluid, thereby reducing the efficiency of the fluid to fracture. But in cases where fractures are in an incipient state, the pressure of the injected fluid may cause those incipient fractures to reopen instead of allowing new fractures to initiate. Thus in a pressure–time plot, the breakdown pressure can be lower than expected for an unfractured rock. This would explain the lack of a distinct peak on the pressure record in the first injection cycle.

On the other hand, if the state of the natural fractures is such that the fractures act as conduit for fluid flow, then the fracture growth is a compromise between overcoming a stress field and/or overcoming entrance losses into pre-existing fractures of preferential permeability (Roegiers *et al.*, 1982; Layne and Siriwardane, 1988). Thus it is possible to inflate or extend these natural fractures even if they are not aligned perpendicular to the minimum *in-situ* stress direction. In those cases where pre-existing fractures are not aligned perpendicular to the minimum *in-situ* stress direction, accurate determination of the minimum *in-situ* stress can be difficult.

5.1.4 Effect of overpressure or depleted reservoir pressure

In the U.S. Gulf Coast region, Breckels and Eekelen (1981) have observed that underpressured formations generally have lower horizontal total stress than normally pressured or over-pressured formations. Salz (1977) found an exponential decrease in fracture propagation pressure with reduction in reservoir pore pressure even in the tight sandstone reservoir of the Vicksburg Formation of south Texas. These examples suggest that the total stresses in poro-elastic media depend on pore pressure. Thus by delaying the fracturing of the reservoir until the reservoir pressure is lowered to a sufficiently low level, fracture containment within the productive interval can be achieved.

Hagoort (1981) has suggested that whenever lowering of the reservoir pressure occurs with negligible areal strains, the change in total horizontal stress ($\Delta\sigma_h$) is related to the change in reservoir pressure (ΔP):

$$(5\text{–}1)\quad \Delta\sigma_h = \frac{1-2\nu}{1-\nu}\ \alpha\,\Delta P$$

This equation shows that the reduction in reservoir pressure can result in a reduction of the total horizontal stress in the reservoir, and subsequently, in a lower fracturing pressure.

5.1.5 Fluid saturation of the test interval

If the mini-frac test is performed in a high permeability interval, much of the injected fluid can be lost to the high permeable flow path. This will reduce the effectiveness of the injected fluid to fracturing. It is not clear yet how fluid saturation of a test interval will affect the formation breakdown. However, it seems that large injection volumes and high injection rates are required to fracture a fluid saturated interval.

5.1.6 Influence of poro-elastic effects

Whenever poro-elastic effects are important, significant back stresses can be generated. If the back stresses are significantly high, both the closure stress and the instantaneous shut-in pressure, ISIP, can be higher than in cases where poro-elastic effects are absent (Boone *et al.*, 1991). This can lead to an overestimation of the minimum *in-situ* stress, if closure stress is used for the minimum *in-situ* stress determination.

5.2 OPERATIONAL FACTORS

5.2.1 Property of the fracturing fluid

Conventional fracturing theory, which has been developed based on the results of tests on well-consolidated, low porosity rocks does not predict the dependence of formation breakdown on viscosity of the fluid. However, observation of fracture growth in porous rocks provides an indication of the dependence of formation breakdown pressure on the viscosity of the fracturing fluid — higher breakdown pressure for a high viscosity fracturing fluid than for a low viscosity fluid, like water. The reason for this is not fully understood; it is possible that the low penetration ability of the more viscous fluid results in a large compressive stress leading to a large breakdown pressure, whereas if a low viscosity fluid like water, which has a high penetration ability, is used, the build-up of a large compressive stress is minimized because the leak-off causes pore pressure build-up. Consequently, the breakdown pressure is minimized with low viscosity fluid. Systematic study is required to confirm the results.

5.2.2 Effect of injection rate

Eqs. (2–7) and (2–8), described in Section 2.2.1.4, do not indicate dependence of breakdown pressure on injection rates; however, for the same fluid injected into similar reservoirs, the breakdown pressure was observed to be higher at higher fluid injection rates. This was supported by the laboratory fracturing tests conducted by Morgenstern *et al.* (1992) on gypstone (low permeability quartzose sand cemented with gypsum). Their study repeatedly suggested high breakdown pressure at high injection rates and a low breakdown pressure at low rates. The effect appears to be similar to that of a viscous fluid. A rapid injection rate prevents fluid penetration into the formation, causes a large stress concentration, thereby giving rise to a large formation breakdown pressure.

In addition, in the tests with gypstone, Morgenstern *et al.* also found that high injection rates produced a rapid fracture propagation and a high fracture efficiency. The low injection rates decreased fracture efficiency and the speed of fracture propagation.

5.2.3 Repeated pressure cycling

If the shut-in of a well occurs immediately after the formation breakdown, then the breakdown may remain incomplete. Consequently, the tensile stress may not be released completely, thereby causing a large discrepancy in the fracture reopening pressures between cycles. Test procedures described in Chapter 3 are designed to avoid such problems.

5.2.4 Data gathering procedures

It is very important to have a sophisticated data gathering system so that the formation breakdown and shut-in pressure responses can be monitored closely at small time intervals — preferably at two to three second intervals. This is because rapid changes have been observed over short time intervals.

5.3 FRACTURE GROWTH PATTERN

5.3.1 Continuation of fracture growth after shut-in

Fractures have been reported to propagate for sometime even after the pumping has stopped (Enever and Wooltorton, 1982; Hickman and Zoback, 1983; Gronseth and Kry, 1983). This causes a slight decrease in ISIP. A decrease in ISIP with an increase in injection volume has also been reported by Hickman and Zoback for eight hydraulic fractures in a Monticello well near Columbia, South Carolina. Kry (1992) suggests that this type of decrease in ISIP is perhaps due to the progressive propagation and growth of the fracture away from the region of large stress concentration occurring around the wellbore.

5.3.2 Effect of stress in the bounding layers

If the mini-frac test interval is short and bounded by low and high stress intervals at its top and bottom, respectively, then by using a large injection rate, the fracture may grow asymmetrically into the bounding intervals with larger growth occurring in the low stress interval. The pressure–time plot for such a case may show a lower ISIP value, because of low stress magnitude in the upper interval.

Shoji *et al.* (1985) have indicated that fracture toughness of the reservoir rock can affect the fracture size. Thiercelin *et al.* (1989) have shown that the fracture geometry can be significantly affected by contrasts in fracture toughness. Bounding layers with fracture toughness higher than that of the pay zone can act to effectively contain a fracture between the layers, and a pay zone layer with fracture toughness higher than bounding layers can lead to fracture growth in the bounding layers. As indicated earlier, fracture growth in the bounding layers can affect the ISIP value.

5.3.3 Fracture growth in the damaged or near wellbore region

Due to stress concentration, damage, cracking, weakness, and anisotropy in the vicinity of a perforated interval or wellbore, the fracture may not grow truly perpendicular to the minimum principal stress. Sometimes, the fracturing fluids fracture the cement outside the casing and go into the other zones. Fracture growth non-perpendicular to the minimum *in-situ* stress may appear on a pressure–time curve as an increase in ISIP.

5.3.4 Multiple fracture growth

As the injection rate in most micro-frac tests is usually low, the possibility of multiple fracture growth is quite low. However, if the injection rate is large enough and continues for some time after the formation breakdown, or if the injection is carried out in multiple cycles, then an offset in the ratio of the stress magnitude may cause a reversal in fracture growth orientation and even growth of multiple fractures. The effect of high injection rate causing growth of multiple fractures has been reported by Roegiers (1991). While multiple fractures grow as a change in stress regime, their growth in turn may perturb the local stress regime. The effect of this on a pressure–time curve can be quite complex. Warpinski (1991) maintains that any complex multiple fracturing may lead to overpressuring.

5.3.5 Frictional pressure drop during injection through perforation

As the fluid is injected through a narrow perforation interval at a rapid rate, the turbulent flow of the fluid may give rise to high frictional forces. Consequently, on a pressure–time curve, the ISIP value could be higher than its true value. Thus ISIP or closure stress should be corrected for the frictional pressure drop. This correction can be calculated if both surface and bottomhole pressure measurement devices have been used.

5.3.6 Fracture tip geometry

Most fractures are assumed to have a narrow tip where a large stress concentration occurs. The high stress concentration that occurs at the tip of the fracture can be explained best in terms of stress intensity factor concept developed in linear elastic fracture mechanics. Fracture mechanics assume that pre-existing defects always pervade a continuum and induce high stress concentration in their vicinity and become the nucleus of crack initiation and/or propagation. Irwin (1957) demonstrated that the stress concentration varies inversely as the square root of the distance ($r^{1/2}$) from the crack tip (Figure 5–2) as:

$$(5\text{–}2)\quad \sigma_{ij} = \frac{K_I}{\sqrt{2\pi r}\, f_{ij}(\theta)}$$

where, K_I is referred to as the stress intensity factor for the opening mode of deformation of the rock and $f_{ij}(\theta)$ represents a bounded function depending only on the angle θ referenced to the plane of the fracture.

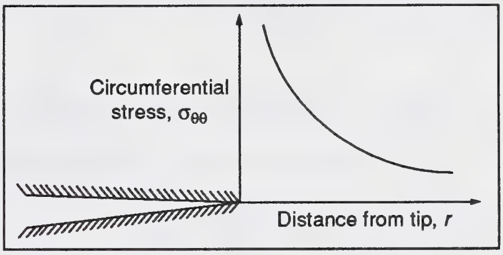

Figure 5–2. *Stress concentration near the tip of a crack (after Roegiers et al., 1989).*

The fracture will propagate when K_I reaches a critical value, called the critical stress intensity factor, K_{IC}, or fracture toughness. Fracture toughness being a measure of the resistance of the rock to crack propagation and being affected by the loading parameters and the geometry of the fracture can affect the ISIP value.

5.3.7 Fracture surface topography

The theory of fracture growth by the tensile failure mechanism assumes the topography of a fracture surface as "mated." Thus it is believed that when the injection pump is shut off, the mated fracture closes completely and a sudden stiffening in the fracture compliance characteristics would be expected. In reality, any mismatch in the fracture surface topography caused by grain crushing, breakage, dissolution, or slight shearing may result in an uneven closure of the fracture. Such results are most likely to be observed in tar sands. The fracture closure may be gradual, accordingly, the fracture would be more compliant and its stiffening effect more gradual. A sharp drop in the pressure seen on complete closure may not be discernible. Thus an accurate estimate of closure can be difficult.

5.4 MODE OF ANALYSIS

The analysis of mini-frac test results for prediction of *in-situ* stress should not be limited to ISIP only, because *in-situ* stress can be estimated incorrectly if estimation is based only on ISIP. In recent years several other interpretation techniques for *in-situ* stress measurement have been developed. Some of these methods have been discussed in an earlier section and the results of the *in-situ* stress determined by these methods are given in Table 6–1. Other methods of minimum *in-situ* stress determination are presented in Chapter 7. A difference of up to 10% between the results of various methods listed in Table 6–1 is not unusual.

5.5 LIMITATIONS OF THE MINI-FRAC TESTS

Mini-frac tests should ideally be run in vertical or horizontal wells, where the axis of the well is parallel to one of the *in-situ* stresses. This makes the interpretation of the test results theoretically sound. Tests conducted in deviated wells may require specialized interpretation.

In the petroleum industry, mini-frac is the most widely used method for the determination of the minimum *in-situ* stress. In comparing the estimate of minimum stress by different methods (Table 6–1), ISIP was found to be higher than most other methods by about 10%, suggesting that the minimum *in-situ* stress can sometime be overestimated if it is determined from ISIP. Thus when the reliability of ISIP measurements are in doubt, other methods of analysis should be used for *in-situ* stress determination.

CHAPTER 6

CASE STUDIES

6 CASE STUDIES

Chapter 4 discussed the procedures for analysis and interpretation of the mini-frac test results. While the procedures and techniques described will apply to both conventional and non-conventional (heavy oil and tar sands) reservoirs, the case studies discussed in this chapter refer to tar sands reservoirs. The examples show how the mini-frac field test results were interpreted to acquire information on the *in-situ* stress and other reservoir parameters.

6.1 CASE 1

The mini-frac tests were conducted in three separate lithological units of Athabasca tar sands deposits in a depth interval of 128 – 160 m. The units consisted of mudstone (128 – 130 m), interbedded sand and mudstone (134 – 136 m) and tar sands (158 – 160 m) (Figure 6–1). At each interval three tests were conducted. Although most mini-frac tests in tar sands are performed through cased well perforations, these tests were performed in an uncased well. For the two upper units, the injection rate was kept the same throughout the test, whereas in some tests of the lower tar sands unit, the injection rate was increased three times during a single test. A summary of the test results in all intervals is shown in Table 6–1. The pressure–time data of all tests of each lithologic unit are presented in Figures 6–2 to 6–10.

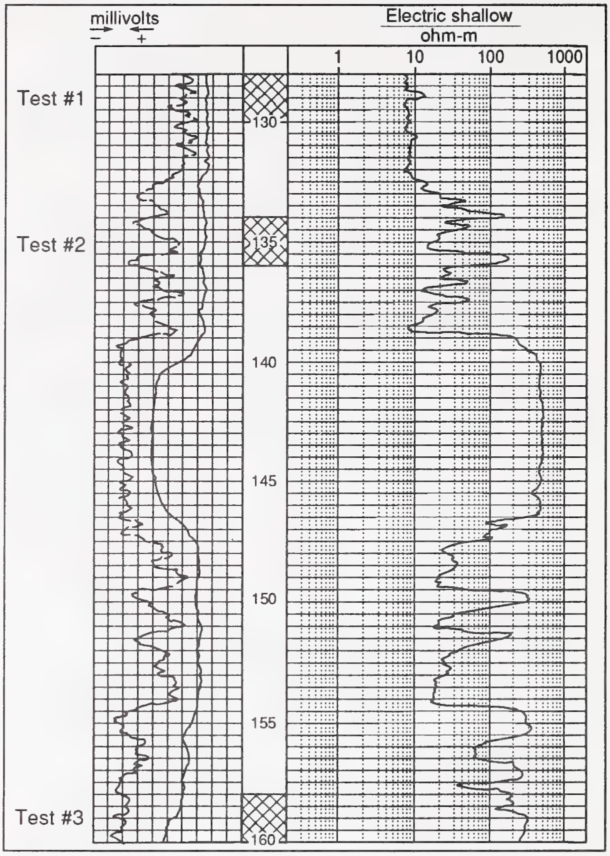

Figure 6–1. SP and resistivity log response of the mini-frac test intervals. Test intervals are shown with hatched lines.

The breakdown pressure was the largest in the rich tar sands interval and the least in mudstone. In all lithologic units, the fracture reopening pressure was considerably lower than the breakdown pressure. In all cases, the ISIP and the minimum closure stress were determined. The ISIP represented the "upper value" of the closure stress. In two units, except the mudstone, there was a significant difference between the ISIP and the estimated minimum closure stress. The ISIP of the second cycle should not be significantly different from the reopening pressure of the third cycle. However, the difference was large. In fact, the reopening pressure decreased as the number of cycles increased. The reason for such a large discrepancy was not well understood. However, it seems the higher injection rates used in successive cycles following growth of the fracture could have influenced the *in-situ* stress ratio, and the fracture reopening pressures of later cycles.

Five methods are used here to determine the minimum *in-situ* stress from mini-frac test #1B performed in a mudstone interval. These methods are:

1. Pressure–time plot
2. Horner plot
3. Tandem square root plot
4. *P versus* square root of time since shut-in
5. Pressure decay rate

The results of these methods are presented in Table 6–1. The derivation of ISIP from a pressure–time curve is shown in Figure 6–2. The tandem square root plot used to obtain closure or minimum *in-situ* stress is shown in Figure 4–5. The log–log plot of the pressure differentials *versus* the shut-in time could not be used to identify the fracture closure stress because of a strong wellbore storage effect. Plots of other methods used for test #1B are shown in Figures 6–11 to 6–13. The value predicted by the tandem square root method was consistently lower. However, the minimum stresses predicted by all methods were within ±10% of each other.

Table 6–1. Summary of mini-frac tests conducted in the McMurray Formation of the Athabasca tar sands.

		Test #1 A	Test #1 B	Test #1C	Test #2A	Test #2B	Test #2C	Test #3A	Test #3B	Test #3C
Depth			128 – 130 m			134 – 136 m			158 – 160 m	
Average injection rate	(L/m)	4.0	20.0	53.0	3.0	22.0	50.0	3.0 7.0 10.0	20.0	29.0 39.0 52.8
	(m^3/d)	5.8	28.8	74.6	4.3	31.7	72.0	4.3 10.0 14.4	28.8	41.8 56.2 76.0
Cumulative fluid injection (m^3)		0.122	0.620	1.610	0.15	0.55	1.52	0.44	0.90	2.38
Injection time, t_{inj} from the start (min)		21.8	31.0	29.5	38.6	25.6	19.4	51.0 66.1 86.4	23.0	21.4 41.0 60.8
Breakdown pressure (kPa)		6742	–	–	8100	–	–	8670, 12620	–	–
Fracture reopening pressure (kPa)		–	4418	4315	–	4756	3913	–	9512	4447
Fracture extension or propagating pressure (kPa)		3700	3300	3250	4875	4167 – 4292	3251	6292	4668	undetermined
ISIP (kPa)		3100	3100	3050	4313	3417	3167	4360	4216	3819
Minimum closure stress estimated from tandem square root plot (kPa)		3067	2893	2917	–	2980	–	3786	3853	3713
Minimum closure stress estimated from Horner plots (kPa)		2935	2879	2950	–	–	–	3779	3838	3710
Closure stress estimated from BHP *versus* square root of shut-in time plot (kPa)		2620	2794	2540	3214	2980	–	3980	3833	–

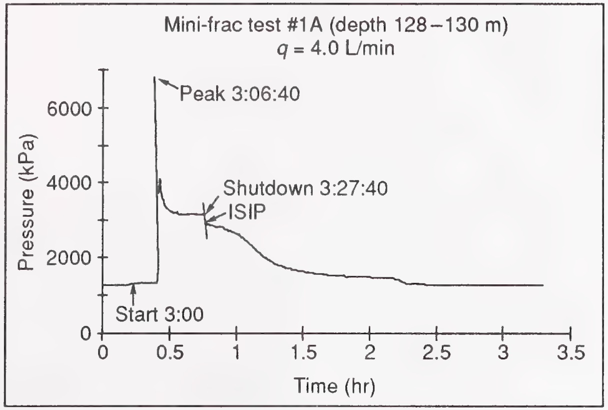

Figure 6–2. The first cycle of a mini-frac test in a mudstone unit.

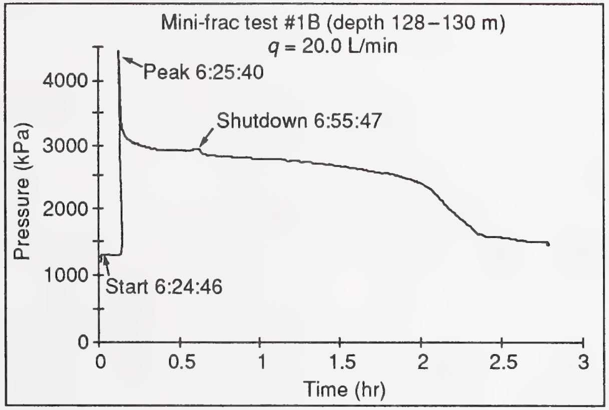

Figure 6–3. The second cycle of a mini-frac test in the same mudstone unit.

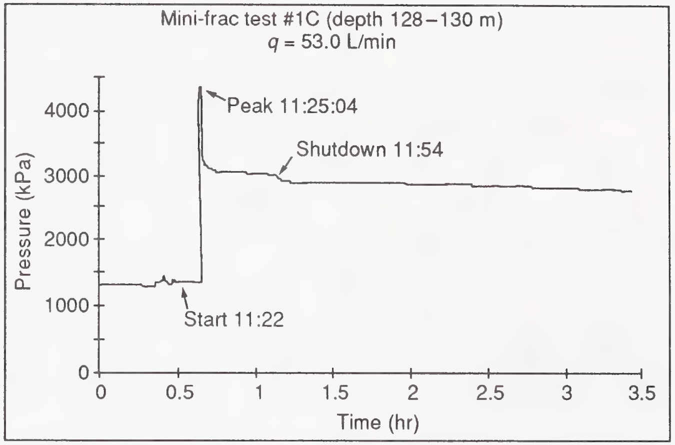

Figure 6–4. The third cycle of a mini-frac test in the same mudstone unit.

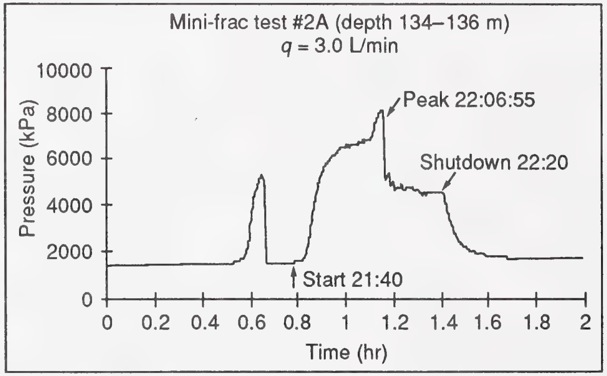

Figure 6–5. The first cycle of a mini-frac test in an interbedded sand and mudstone unit.

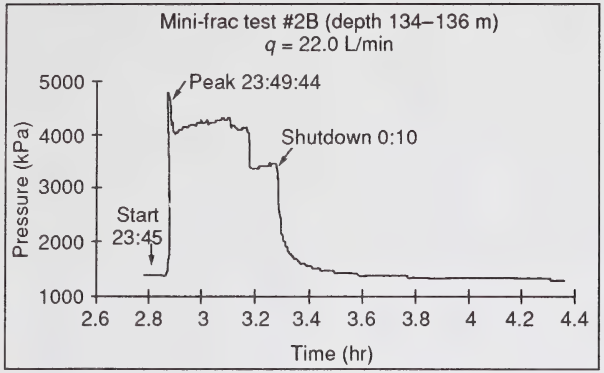

Figure 6–6. *The second cycle of a mini-frac test in the same interbedded sand and mudstone unit.*

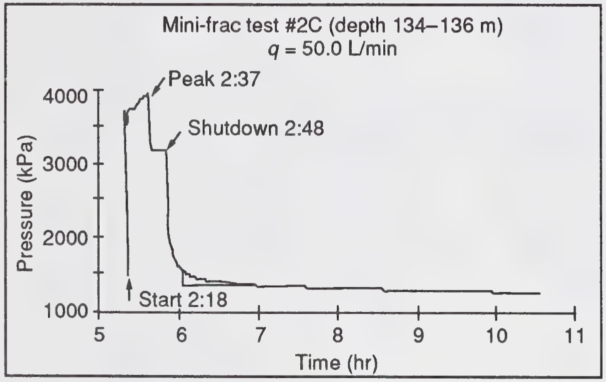

Figure 6–7. *The third cycle of a mini-frac test in the same interbedded sand and mudstone unit.*

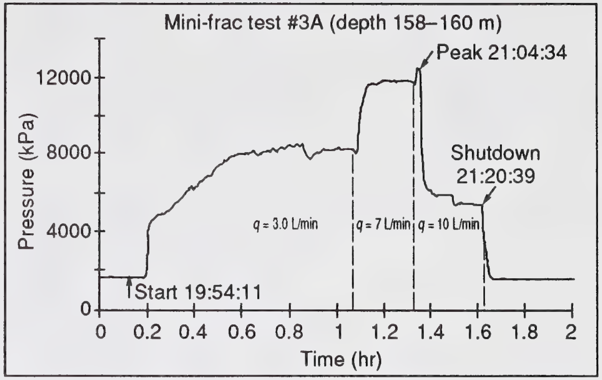

Figure 6–8. *The first cycle of a mini-frac test in a tar sands interval.*

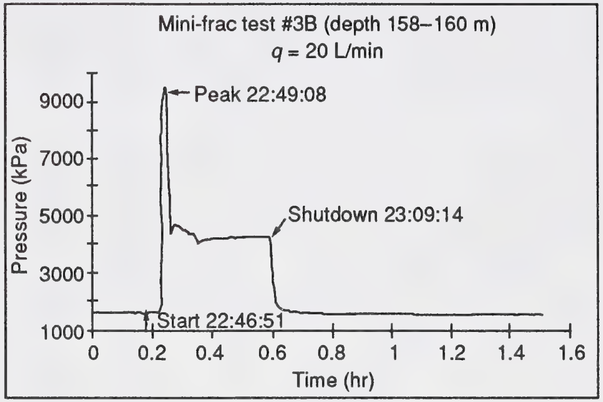

Figure 6–9. *The second cycle of a mini-frac test in the same tar sands interval.*

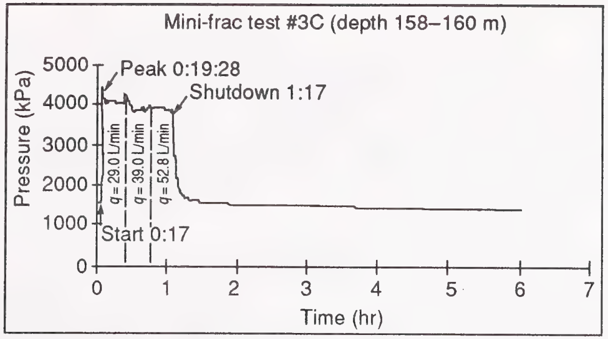

Figure 6–10. *The third cycle of a mini-frac test in the same tar sands interval.*

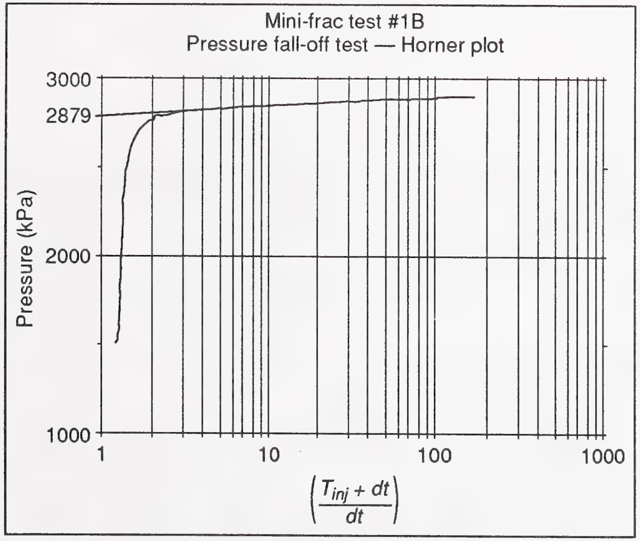

Figure 6–11. *The plot derived from the data of a mini-frac test performed in a mudstone interval predicts minimum in-situ stress of 2879 kPa.*

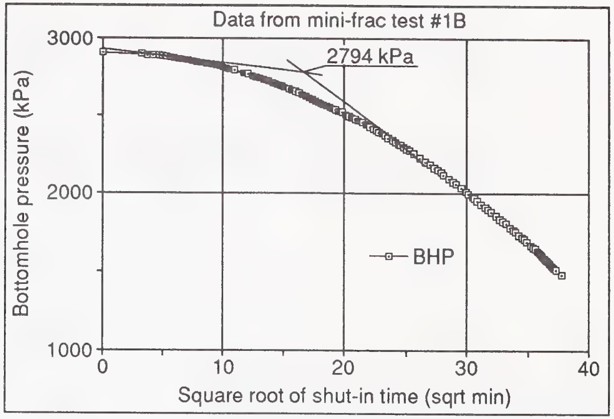

Figure 6–12. *The plot of mini-frac data on a pressure versus square root of shut-in time plot gives a value of 2794 kPa for fracture closure pressure. The test was performed in the same mudstone interval.*

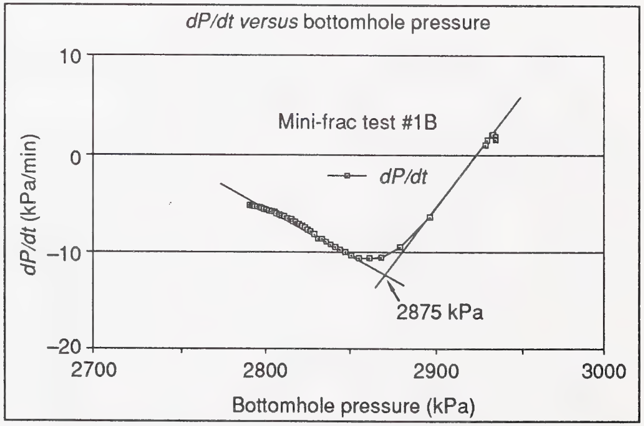

Figure 6–13. *The intersection of bi-linear curves of dP/dt versus bottomhole pressure plot predicts closure or minimum in-situ stress at 2875 kPa.*

Table 6–2. Reservoir engineering parameters estimated from mini-frac tests conducted in the McMurray Formation.

Depth interval (m)	128 – 130			134 – 136			158 – 160		
Lithology	Mudstone			Interbedded sand and mudstone			Oil sands		
	Test #1			Test #2			Test #3		
	#1A	#1B	#1C	#2A	#2B	#2C	#3A	#3B	#3C
Average injection rate (m^3/d)	5.8	28.8	51.8	54.3	31.7	72.0	9.6	28.8	58
Horner slope (kPa/cycle)	103	–	–	2048.3	979	506	505	2703	3797
Transmissibility (kh/μ(md·m/mPa·s))	121	–	–	5.0	70	300	41	23	33
Effective mobility (K/μ(md/mPa·s))	15.9	–	–	0.9	12.1	51.7	4.8	2.7	3.8
Effective permeability to water (K (md))	19.4	–	–	1.0	14.8	63.1	5.9	3.3	4.6
Skin factor	15.6	–	–	−3.7	−2.7	−1.47	5.1	−3.3	−3.9

The minimum stress predicted by various methods was compared with the overburden stress estimated with a pressure gradient of 22.6 kPa/m, which is recommended for the region. Based on the comparison, the minimum stress was considered to be vertical.

Horner plots were also used to predict the engineering parameter, such as the transmissibility, mobility, and the skin factor for all three lithological units. The results are shown in Table 6–2.

6.2 CASE 2

Proskin *et al.* (1990) reported the results of three cycles of a mini-frac test conducted in the Athabasca tar sands of the McMurray Formation at a depth of 237 m. The tests were conducted in a perforated cased well where the perforations were done across the fluid-saturated interval. The pressure–time plot of the three cycles of injection are shown in Figure 6–14. No clear breakdown was discernible at least in the first two cycles; however, the authors' analysis provided a breakdown pressure of 5300 kPa for the first cycle.

Case 1 test #3 (Table 6–1) and case 2 tests (Figure 6–14) were performed in the tar sands interval of the McMurray Formation; the depth of case 2 tests being 78 m below the depth of case 1 test #3. A higher fluid injection rate of 27.1 m^3/d was used in the case 2 test compared to 9.6 m^3/d in case 1 test #3. The formation breakdown pressure obtained at the higher injection rate was lower than the value obtained at the lower injection rate (5300 kPa compared to 9150 kPa). This observation suggests that the breakdown pressures for tests through perforated casing can be lower than the values of uncased well tests, if the injection occurs into a water-saturated interval.

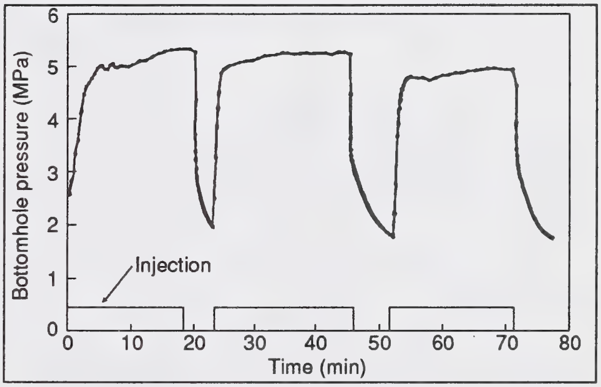

Figure 6–14. Pressure–time plot of a mini-frac test performed in an Alberta tar sands formation through a perforated well. In all three cycles, the injection rate was kept the same. Breakdown pressures cannot be identified clearly in any of the cycles (from Proskin et al., 1990).

6.3 CASE 3

Two mini-frac tests were conducted in the Wabiskaw Formation of the Athabasca deposit at a depth of 364 m. In both tests cold water was injected at a high injection rate of 185 m^3/d for about 10 minutes. Before the second test, the well was shut-in for three hours to allow the pressure from the first test to stabilize. The bottomhole pressure was monitored on a strip-chart recorder. Detailed recordings of the data were not achieved. The test results are presented in Table 6–3. Formation breakdown occurred within 30 seconds of the injection at 10,225 kPa and the reopening occurred at 8640 kPa. In both cycles, the closure stress was estimated to be about 8350 kPa.

The vertical stress for this depth was estimated as 8226 kPa using a pressure gradient of 22.6 kPa/m. The

Table 6–3. Summary of mini-frac tests conducted in the Wabiskaw Formation.

Test no.	Injection rate (m^3/d)	Injection time (min)	Breakdown pressure (kPa)	Fracture extension pressure (kPa)	Closure pressure (kPa)
1	185	10.0	10225	8740	8295
2	185	10.0	8640	8640	8400

vertical stress of 8226 kPa is close to the closure stress of 8350 kPa. This means the minimum stress at the reservoir depth could be vertical and suggests the possibility of obtaining a horizontal fracture. In the 350–450 m depth, stresses are believed to be isotropic. In an isotropic stress regime, the fracture orientation is no longer governed by the minimum *in-situ* stress. The orientation is more strongly influenced by the lithology and pre-existing weaknesses of the rock, and the fracture tends to move upward because less energy is required to do so. Thus, even if the fracture initiates as horizontal, it may eventually rotate to become vertical.

6.4 CASE 4

Three cycles of a mini-frac test were conducted in a perforated cased hole located in the Clearwater Formation of Cold Lake. The well was perforated over 1.73-m intervals at the bottom of a 10-m thick rich tar sands zone located at a 440-m depth. In all tests, cold water was injected at a high injection rate of 266 m^3/d for about 4.5 min. The pressure–time data were recorded on a strip chart recorder. Detailed recordings of the pressure–time data at breakdown and shut-in were not obtained. The well was shut-in for about an hour between the two tests. The breakdown pressure could not be recorded because it exceeded the maximum pressure range (11 MPa) of the strip chart recorder. The test results are shown in Table 6–4. The reopening pressures were significantly lower than the breakdown and decreased with cycles.

The closure stress increased (by about 200 kPa) from the first cycle to the third cycle. This increase in closure stress may have resulted from the effect of increased pore pressure within the test interval caused by repeated tests. This effect could be reduced if the shut-in time between the two tests was prolonged to allow complete pressure stabilization. The closure stress, on average, was lower than the ISIP by about 450 kPa. Using a pressure gradient of 22.6 kPa/m, the vertical stress at a 440-m depth was calculated as 9.9 MPa. The closure stress being lower than 9.9 MPa suggests that the minimum stress in the reservoir at this depth is horizontal. Consequently, at virgin reservoir conditions, vertical fractures are expected at this depth.

Dusseault (1980b) reported very small differences in the values of breakdown, fracture propagation, and shut-in

Table 6–4. Summary of mini-frac tests conducted in the Clearwater Formation of Cold Lake.

	Test #1	Test #2	Test #3
Injection volume (m^3)	0.72	0.55	0.73
Injection rate (m^3/d)	270	264	263
Injection time (sec)	230	180	240
Instantaneous shut-in pressure (kPa)	5995	5950	5907
Closure stress (kPa)	5375	5545	5585
Fracture closing time (sec)	200	240	365
Fracture extension pressure (kPa)	7200	6855	6640
Breakdown pressure (kPa)	11000	8235	7890
Formation pressure drop (kPa)	1205	905	733
Formation depth (m)	440	440	440
Closure stress gradient (kPa/m)	12.2	12.6	12.7
Fracture extension gradient (kPa/m)	16.4	15.6	15.1
Pore pressure (kPa)	3450		
Vertical stress (kPa)	9955		
Hydrostatic head (kPa)	3925		

All of the above mini-frac pressures have been converted from surface to bottomhole pressures.

pressures from a fracture test conducted in a tar sands reservoir at a slow injection rate. Such small differences suggest low tensile and cohesive strengths of tar sands. Such results are not observed when mini-frac tests are conducted at high injection rates. However, it is also true that at low injection rates, the pressure loss at the entry to the reservoir is low because of the low frictional losses and high at high injection rates because of high frictional losses. Hence, differences seen at low and high injection rates may also be due to this effect.

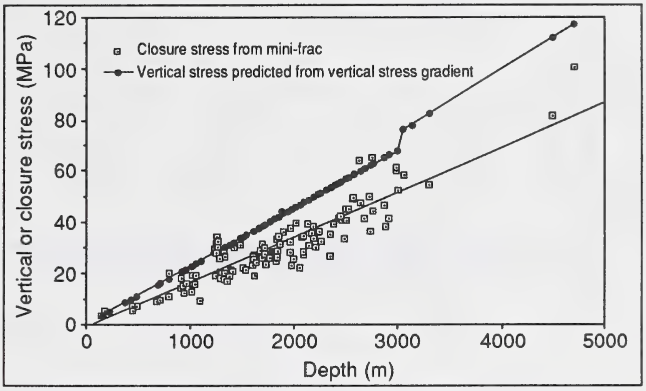

Figure 6–15. Variation of vertical and minimum in-situ stress in Alberta with depth.

6.5 ALBERTA MINI-FRAC DATA

The ISIPs and closure stresses derived from mini-frac tests conducted in various parts of Alberta are shown in Table 6–5. The data with "*" were obtained from Woodland and Bell (1989); those with "•" were contributed by the Petroleum Geomechanics Group of the Petroleum Society of CIM. The remaining data were from projects in which AOSTRA was involved. The data range from a 150- to 5000-m depth interval. For convenience, the data are presented in order of increasing depths. Most data were presented here as they became available to us. It is not known to us how the mini-frac tests were conducted and which methods were used to determine the closure stresses. Because of a lack of sufficient information, detailed analysis of the data could not be performed. The variability in the data is quite large; overall, the data show an increase in closure with depth.

The closure stresses are plotted against their depths (Figure 6–15). The data are least square fitted to a straight line. The vertical stresses are also shown. The vertical stresses were obtained with a stress gradient of 22.6 kPa/m (very similar value was used earlier by Dusseault, 1979, and Raisbeck and Currie, 1981) up to a depth of 3050 m, and a gradient of 24.9 kPa/m below 3050 m. Most of the data for the plot were obtained from a 900- to 3000-m depth interval. The data from other intervals are scarce. This makes the interpretation somewhat difficult. If the scatter in the data is ignored, then all closure stress data obtained below a depth of 150 m are found to lie beneath the vertical stress curve. In the 350–450-m depth interval, the stresses are believed to be isotropic (Dusseault, 1977). Otherwise, the minimum *in-situ* stresses below 450 m appear to be horizontal. Thus, in virgin reservoirs below 450 m, fractures are expected to be vertical.

Table 6–5. Mini-frac test results from various parts of Alberta.

Well name	Formation or lithology	Depth (m)	ISIP (MPa)	Closure stress (MPa)	Reservoir pressure (MPA)
AOSTRA 3-18-93-12W4	McMurray mudstone	129	3.1	2.9	–
AOSTRA 3-18-93-12W4	McMurray interbedded sand & mudstone	135	3.4	3.0	–
AOSTRA 15-7-93-12W4	McMurray tar sands	136	3.6	2.9	1.4
AOSTRA 3-18-93-12W4	McMurray tar sands	159	3.8	3.7	–
AOSTRA 15-7-93-12W4	McMurray limestone	169	–	4.7	1.8
Husky 1-16-95-7W4	McMurray tar sands	214	–	4.7	–
General American 4-30-81-19W4	Wabiskaw Formation	364	–	8.3	–
Bow Valley 1-14-65-2W4	Clearwater Formation C1 zone tar	425	–	7.1	–
Bow Valley 1-14-65-2W4	Clearwater Formation C2 zone	440	–	5.4	2.7
BP 11-1-65-5W4	Clearwater Formation tar sands	468	–	6.9	–
● North Can. Inglenook 4-16-28-23W4	Viking sandstone	682	14.5	9.0	–
● North Can. Inglenook 9-9-28-23W4	Viking sandstone	700	14.9	9.3	–
✖ Norcen Provost 11-5-39-3W4	Lloydminster sand	778	14.2	10.7	–
Home 10-22-84-18W6	Gething sandstone	793	20.0	19.5	–
✖ Dome Pembina a16-3-48-2W5	Belly River sandstone	908	15.4	14.0	7.0
● Monteta Tal Skiff 6-16-5-14W4	Sawtooth sandstone	910	20.8	18.3	–
● Dome *et al.* Pembina 10-3-48-2W5	Belly River sandstone	918	17.2	14.1	–
● Dome *et al.* Pembina 6-8-48-2W5	Belly River sandstone	932	17.1	15.2	–
✖ Dome Cessford 8-10-24-12W4	Basal Colorado sandstone	937	20.1	12.4	3.5
✖ Home a5-26-84-18W6	Gething sandstone	946	23.0	21.1	–
✖ Canterra Provost 8-30-34-6W4	Glauconite sandstone	950	21.2	16.0	–
● Anderson *et al.* 14-14-85-8W6	Cecil sandstone	950	19.5	17.0	9.7
✖ Dome Cessford 12-30-24-12W4	Glauconite sandstone	1004	17.7	12.7	5.6
✖ Dome Cessford 6-20-24-12W4	Basal quartz sandstone	1018	20.3	19.0	8.6
✖ Dome Pembina 14-11-47-3W5	Belly River sandstone	1025	17.0	15.7	7.0
● Dome *et al.* Cessford 14-19-24-12W4	Mannville sandstone	1041.5	20.9	15.8	7.3
● Anderson *et al.* Manyberry 6-35-4-5W4	Mannville sandstone	1055	21.6	19.0	5.5
✖ Shell Manyberries 5-28-5-5W4	Basal quartz sandstone	1100	10.0	9.0	–
✖ PCI Wapiti 8-23-67-8W6 (micro-frac)	Cardium sandstone	1236	–	29.8	–
✖ PCI Minhik 8-15-45-4W5	Basal Belly River sandstone	1238	24.8	20.2	9.0
✖ PCP 11-18-23-18W4	Glauconite sandstone	1240	20.9	–	–
✖ PCI Wapiti 8-23-67-8W6 (micro-frac)	Cardium sandstone	1241	–	31.1	–
✖ PCI Wapiti 8-23-67-8W6 (micro-frac)	Cardium sandstone	1248	–	32.2	–
✖ PCI Wapiti 8-23-67-8W6 (micro-frac)	Cardium sandstone	1254	–	34.1	–
✖ Esso Pembina 8-31-49-6W5	Cardium sandstone	1257	19.7	19.0	–
✖ PCI Wapiti 8-23-67-8W6 (micro-frac)	Cardium sandstone	1260	–	30.4	–
✖ PCI Wapiti 8-23-67-8W6 (micro-frac)	Cardium sandstone	1265	–	32.4	–
✖ Amoco Wapiti 13-7-67-7W6	Cardium sandstone	1278	28.0	25.8	–

Table 6–5. Cont'd....

Well name	Formation or lithology	Depth (m)	ISIP (MPa)	Closure stress (MPa)	Reservoir pressure (MPA)
✖ Esso Berrymore 10-33-49-5W5	Cardium sandstone	1295	21.8	20.0	–
✖ Gulf Golden Spike 8-9-51-27W4	Glauconite sandstone	1300	22.1	18.2	12.2
✖ PCI Steep Creek 4-31-66-7W6	Cardium sandstone	1323	30.4	28.2	10.5
✖ Esso Berrymore 4-5-50-6W5	Cardium sandstone	1327	19.3	18.0	–
✖ Amoco Wapiti 13-7-67-7W6	Cardium sandstone	1329	29.6	26.8	–
✖ Esso Berrymore 6-29c-49-6W5	Cardium sandstone	1329	20.8	20.0	–
✖ Gulf Leduc 8-24-49-26W4	Basal quartz sandstone	1337	21.5	20.4	10.7
✖ Gulf Butte 5-31-11-18W4	Shauvon sandstone	1346	19.1	18.4	11.4
✖ Esso Berrymore 10-33-49-5W5	Cardium sandstone	1361	21.0	17.0	–
✖ Mobil Pembina 16-3-48-2W5	Cardium sandstone	1381	21.1	18.6	–
✖ Gulf Holburn 6-36-50-28W4	Basal quartz sandstone	1393	22.7	21.2	10.9
✖ Gulf Chigwell 6-14-43-26W4	Basal Belly River sandstone	1415	22.0	20.7	7.5
● Anderson *et al.* 5-17-81-4W6	Dunvegan Limestone	1417	34.2	30.0	14.0
● Dome *et al.* Kidney 2-2-89-6W5	Wabamum sandstone	1493	34.6	31.0	–
✖ Suncor a14-8-39-3W5	Basal quartz sandstone	1510	24.3	22.1	–
✖ Suncor Chigwell 9-24-41-25W4	Glauconite sandstone	1545	25.6	21.3	11.7
✖ Chevron Mitsue 10-23-72-4W5	Gilwood sandstone	1612	26.9	23.0	–
✖ Chevron Mitsue 8-12-73-5W5	Gilwood sandstone	1614	28.8	26.5	–
✖ Gulf Westrose 6-11-46-28W4	Glauconite sandstone	1618	21.3	19.3	15.1
✖ Shell Pembina 15-12-48-9W5	Cardium sandstone	1620	–	24.5	–
✖ Chevron Mitsue 2-7-73-4W5	Gilwood sandstone	1621	29.2	27.0	–
✖ Chevron Mitsue 8-12-73-5W5	Gilwood sandstone	1635	28.2	24.0	–
✖ Chevron Mitsue 12-30-71-3W5	Gilwood sandstone	1663	35.3	27.0	–
✖ Chevron Mitsue 5-23-72-5W5	Gilwood sandstone	1675	32.5	28.7	–
✖ Chevron Mitsue 8-13-72-8W5	Gilwood sandstone	1686	30.8	26.0	–
✖ Amoco Nipisi 4-18-79-7W5	Gilwood sandstone	1702	34.1	31.5	16.0
✖ Amoco Nipisi 4-18-79-7W5	Gilwood sandstone	1706	35.4	30.2	14.0
● Dome Brazeau River 6-31-47-13W5	Belly River sandstone	1724	36.2	27.9	14.3
✖ Chevron Mitsue 2-17-78-3W5	Gilwood sandstone	1725	29.0	28.0	–
✖ Bumper Crystal 14-1-46-4W5	Viking sandstone	1734	30.5	23.5	–
✖ Chevron Mitsue 2-10-71-4W5	Gilwood sandstone	1769	32.6	26.2	–
● Simonette 2-6-63-25W5	Dunvegan sandstone	1792.3	36.9	–	13.2
✖ PCI Bigoray 16-28-52-8W5	Basal quartz sandstone	1799	29.1	28.3	–
● Simonette 12-31-62-25W5	Dunvegan sandstone	1803	37.0	–	13.2
● Simonette 2-1-63-26W5	Dunvegan sandstone	1805	35.1	–	13.5
✖ Gulf Kaybob 4-29-63-19W5	Gething sandstone	1815	30.4	27.8	14.3
✖ Gulf Wolf 12-23-51-13W5	Cardium sandstone	1820	32.9	28.9	17.1
✖ Gulf Wolf 12-23-51-13W5	Cardium sandstone	1831	31.6	29.0	7.4

Table 6–5. Cont'd....

Well name	Formation or lithology	Depth (m)	ISIP (MPa)	Closure stress (MPa)	Reservoir pressure (MPA)
● Simonette 2-2-63-26W5	Dunvegan sandstone	1831.5	36.2	25.0	–
● Progress 10-20-78-10W6	Montney sandstone	1837.5	39.4	–	18.2
✖ Cdn. Hunter Jayar 16-9-62-4W6	Cardium sandstone	1838	40.5	33.5	21.2
● Simonette 11-25-62-26W5	Dunvegan sandstone	1838.5	36.9	–	–
✖ Chevron Mitsue 10-26-71-5W5	Gilwood sandstone	1844	32.5	27.0	–
✖ Shell Simonette 6-1-63-26W5	Dunvegan sandstone	1845	30.7	29.0	–
● Dome *et al.* Gordondale 14-33-78-11W6	Cardium sandstone	1847	43.5	–	–
✖ Shell Simonette 12-6-63-26W5	Dunvegan sandstone	1850	–	26.3	–
✖ Shell Gordondale 11-26-78-11W6	Doig sandstone	1855	35.2	34.2	–
✖ Shell Braeburn 8-25-77-10W6	Halfway sandstone	1870	–	31.7	–
● Crozet *et al.* 6-26-36-28W4	Penhold sandstone	1891	43.4	–	12.5
✖ Cdn Hunter Jayar 7-36-61-4W6	Cardium sandstone	1893	49.0	43.1	23.0
✖ Canterra 8-4-110-8W6	Muskeg dolomite	1905	40.0	36.0	–
● Braeburn 14-6-77-10W6	Halfway sandstone	1909	33.4	–	17.5
● Tindastall 14-1-37-1W5	Glauconitic sandstone	1950.5	29.0	–	16.1
✖ Conoco Simonette 8-6-63-26W5	Dunvegan sandstone	1964	34.3	28.0	–
● Dome *et al.* 16-8-75-9W6	Charlie Lake dolomite	1965	44.7	–	–
✖ Chevron Marlboro 11-22-55-19W5	Cardium sandstone	1971	40.6	37.8	–
✖ Esso Brazeau 4-5-47-15W5	Belly R. "E" sandstone	1973	38.3	32.5	–
✖ Dome Brazeau 16-29c-45-12W5	Basal Belly River sandstone	1979	34.0	23.0	12.0
✖ Conoco Simonette 12-6-63-26W5	Dunvegan "B" sandstone	1991	28.0	–	–
● Can. Hunter 11-6-70-11W6	Elmworth conglomerate	2000	42.0	–	11.6
✖ Gulf Peco 5-8-47-15W5	Basal Belly River sandstone	2001	29.4	25.8	13.0
✖ Esso 11-12-71-13W6 (micro-frac)	Elmworth sandstone	2021	–	39.7	15.2
● Dome Union 10-8-61-18W5	Fox Creek sandstone	2044	36.4	–	–
✖ Gulf Peco 5-8-47-15W5	Basal Belly River sandstone	2074	29.2	22.1	11.3
✖ Shell Wembley 8-13-72-8W5	Halfway dolomitic sandstone	2085	38.2	34.2	–
✖ Shell Wembley 8-13-72-8W5	2^{ND} white specks	2097	37.3	34.5	22.0
✖ Norcen Garrington 14-17-35-3W5	Viking sandstone	2101	36.9	27.6	–
✖ Shell Garrington 8-16-35-3W5	Viking sandstone	2107	31.7	28.6	–
✖ PCP Garrington 11-25-36-5W5	2^{ND} white specks	2131	47.0	39.2	27.0
✖ Sulpetro Wapiti 11-20-68-9W6	Fahler "D"	2147	32.6	31.0	–
● Cranberry 8-10-96-3W6	Slave Point limestone	2179.5	54.3	36.0	12.7
✖ Dome Medicine River 8-28-38-3W5	L-Jurassic	2196	–	34.0	16.5
✖ Esso Columbia 14-32-46-16W5	Basal Belly River sandstone	2197	44.8	38.0	–
✖ Esso 10-16-69-11W6 (micro-frac)	Elmworth Shale	2220	–	30.0	–
✖ Esso 10-16-69-11W6 (micro-frac)	Elmworth sandstone	2241	–	36.0	–
✖ Gulf Sylvan Lake 12-21-37-3W5	Jurassic "A"	2253	42.1	36.4	13.0

Table 6–5. Cont'd....

Well name	Formation or lithology	Depth (m)	ISIP (MPa)	Closure stress (MPa)	Reservoir pressure (MPA)
✱Amoco Medicine R. 2-21-38-4W5	Glauconite sandstone	2270	37.1	32.5	18.8
✱Cdn. Hunter Ansel 7-9-52-20W5	Cardium sandstone	2312	42.7	–	–
✱Amoco Ricinus 4-15-34-8W5	Cardium sandstone	2357	39.2	26.5	–
✱Mont 6-5-30-4W5	Cardium sandstone	2357	40.0	34.9	–
✱PCP Garrington 14-1-37-5W5	Ostracod sandstone	2398	40.8	39.0	21.0
✱Cdn. Hunter Caroline 12-12-32-6W5	Cardium sandstone	2400	44.5	–	–
✱Cdn. Hunter Minehead 11-12-49-18W5	Cardium sandstone	2433	49.2	41.5	23.8
✱PCP Garrington 6-35-36-5W5	Ostracod sandstone	2463	46.6	42.2	–
✱Amoco Ricinus 1-10-34-8W5	Cardium sandstone	2468	–	40.5	–
✱Amoco Ricinus 16-3-34-8W5	Cardium sandstone	2492	37.9	33.9	–
✱Home Garrington 8-4-37-5W5	Ostracod sandstone	2505	50.3	45.0	21.3
✱PCP Garrington 6-23-36-5W5	Glauconite sandstone	2510	43.1	40.3	26.5
✱Esso Brazeau 16-29c-45-12W5	Viking sandstone	2528	46.8	45.0	–
●Can. Hunter Ricinus 11-20-34-7W5	Cardium sandstone	2564	48.1	–	26.9
✱Cdn. Hunter Sundre 6-20-33-5W5	Viking sandstone	2578	58.9	49.0	17.8
✱Home Sundre 14-9-33-5W5	Viking sandstone	2588	57.2	49.2	17.6
✱Amoco Ricinus 4-15-34-8W5	Cardium sandstone	2641	68.7	64.1	15.5
✱Gulf Mitchell 3-26-49-20W5	Cardium sandstone	2656	47.8	46.9	26.0
✱PCP Garrington 14-1-37-5W5	Ostracod sandstone	2689	45.9	41.5	–
✱Amoco 1-1-36-9W5	Cardium sandstone	2730	52.2	50.0	–
✱Gulf Garrington 8-17-36-6W5	Glauconite sandstone	2741	49.8	36.4	19.3
✱Amoco 12-18-36-8W5	Cardium sandstone	2742	48.9	38.0	–
●Stanford Cecilia 14-31-57-22W5	Mannville sandstone	2757	52.9	–	–
✱Amoco Caroline 8-27-34-7W5	Viking sandstone	2762	48.0	44.0	–
✱Shell Clearwater 8-29-13W5	Exshaw shale	2768	–	65.1	–
✱Home Caroline 8-9-35-7W5	Viking sandstone	2875	49.0	46.0	–
✱Gulf Ricinus 2-26-36-9W5	Cardium sandstone	2891	49.8	38.2	–
✱Gulf Crimson 3-5-38-8W5	Glauconite sandstone	2922	47.7	41.4	31.6
✱Dome Caroline 1-12-35-7W5	Basal quartz siltstone	2992	–	60.0	–
✱Dome Caroline 1-12-35-7W5 (micro-frac)	Basal quartz sandstone siltstone	2996	–	61.0	–
✱Gulf Strachan 6-14-38-9W5	Ostracod sandstone	3005	52.8	52.2	28.0
✱Cdn. Hunter 3-16-63-8W6	Red Deer Coal	3066	67.1	58.2	–
✱Cdn. Hunter 3-16-63-8W6	Cadomin sandstone	3140	64.3	–	–
✱Dome Strachan 13-8-37-9W5	Glauconite sandstone	3314	73.0	54.4	7.9
✱Shell Panther R. #2 11-8-30-10W5	Turner Valley dolomite	4500	91.8	81.6	–
✱Shell Panther R. #7 8-36-29-11W5	Turner Valley dolomite	4714	105.5	100.5	–

Note: data with ✱ were obtained from Woodland and Bell (1989); those with ● were obtained from Geomechanics Interest Group of the Petroleum Society of CIM; and the rest were from projects in which AOSTRA was involved.

CHAPTER 7

ADVANCES IN *IN-SITU* STRESS MEASUREMENTS

7 ADVANCES IN *IN-SITU* STRESS MEASUREMENTS

Other methods for *in-situ* stress measurement have been suggested in recent years in addition to the mini-frac test method. These methods include:

- Borehole ellipticity measurement
- Anelastic strain recovery technique
- Differential strain analysis
- Wave velocity anisotropy
- Borehole slotting technique
- Borehole holographic interferometry
- Overcoring technique

7.1 BOREHOLE ELLIPTICITY MEASUREMENT

The possibility of determining the orientation of horizontal stresses from wellbore breakout has been suggested by Gough and Bell (1982) and Zoback *et al.* (1985). The breakout is a phenomenon of spalling of borehole wall in the direction of minimum horizontal stress (when borehole axis is vertical). Where the horizontal stresses are anisotropic, the borehole elongation may parallel the minimum horizontal stress (σ_{hmin}). Thus, the maximum horizontal stress would be perpendicular to the borehole elongation. The elongation depends on the horizontal stress contrast. Where horizontal stresses are nearly isotropic, the borehole elongation will be insignificant.

Although breakout elongation has proven to be an effective tool for predicting orientation of minimum *in-situ* stress, the horizontal stress magnitudes cannot be estimated from breakout dimensions (Haimson, 1988). Uncertainties in estimation are great. Further research is needed to investigate its effectiveness for predicting stress magnitudes.

Breakout technique has been combined with the hydraulic fracturing technique to measure *in-situ* stress at Auburn, New York (Hickman *et al.*, 1985) and in the Red River fault zone, China (Springer *et al.*, 1987). Stress orientation derived from an impression packer was supported by breakout elongation.

Whenever only the orientation of the minimum *in-situ* stress needs to be known, instead of conducting expensive mini-frac tests, a borehole breakout study can be conducted. This information can be obtained while drilling an exploratory well. No additional drill hole is required for this purpose. The technique may not be applied successfully in a poorly consolidated formation where damage to the wellbore while drilling could be quite large; this may in turn obscure minimum horizontal stress direction.

If the detection of a hydraulic fracture on the impression packer is obscured, or several fractures are detected in the test interval, or if the reliability of the results need to be known, breakout can then provide useful information regarding the stress directions.

7.2 ANELASTIC STRAIN RECOVERY (ASR)

This method depends on the strain relaxation that a rock undergoes following the *in-situ* coring operation. The recovered strains are measured in multiple directions and the principal strain axes are determined. These principal strain directions are assumed to correspond to the principal axes of *in-situ* stresses. Because the strain recovery is partly elastic and partly non-elastic, use of the ASR method requires the assumption of a relationship between the non-elastic strain and the total strain. The relative magnitude of the strain recovery in the different direction is used as an indication of relative stress magnitudes, thereby the principal orientation of the horizontal stresses is obtained. The absolute magnitude of the horizontal stresses is usually derived from a relationship with the overburden stress, if the relationship is known.

Teufel and Warpinski (1984) used ASR to confirm stress magnitudes and directions obtained from two deep hydraulic fracturing tests in the Piceance Basin, Colorado, and found excellent agreement.

7.3 DIFFERENTIAL STRESS ANALYSIS (DSA)

This method relies on the assumption that the density and distribution of micro-cracks resulting from stressing of a rock are directly proportional to the stress reduction the core has sustained. Hence, if a micro-crack distribution ellipsoid can be constructed, the orientation of the principal stresses causing their growth can be ascertained.

In this method, the anisotropic strain resulting from the presence of pre-existing cracks must be isolated before a strain analysis is performed on the stressed sample. The

DSA technique should yield the orientation of principal stresses, but to obtain the actual stress magnitude, the elastic constants and the overburden stress magnitudes must be known.

Dey and Brown (1986) employed the DSA to measure stresses at large depths at Fenton Hill, New Mexico. They also used the hydraulic fracturing tests to determine the *in-situ* stress and found minimum horizontal stress calculated from DSA to be close to that predicted by the ISIP of the hydraulic fracturing test.

The ASR and DSA methods are based on the same fundamental principles, but the methods can provide different results depending on the geologic situations. For example, if a rock formation has undergone intensive fracturing episodes during its tectonic history, then the DSA will represent the sum of the present and the past stress effect on the rock, whereas the ASR will represent its present state of stress only.

7.4 WAVE VELOCITY ANISOTROPY

The velocity of propagation of compressional (V_p) as well as shear wave (V_s) is stress dependent. In homogeneous materials, compressional wave velocity (V_p) is greatest parallel to the direction of the maximum stress and the least in the direction of the minimum stress (Hannan and Stesky, 1983, 1985; Schmitt, 1992). The measurement of compressional wave velocity in a borehole environment is not a problem; however, the shear wave velocity measurement still poses some problem largely because of signal contamination. As the research and the technological improvement continue, wave velocity measurement in a borehole may be used in the near future as a tool to predict the *in-situ* stress regime at any depth.

7.5 COMPRESSIONAL TO SHEAR WAVE VELOCITY (V_p / V_s) ANISOTROPY

The V_p/V_s ratio is also found to increase with stress and this ratio has been found to increase for wave propagation through a fractured rock (Moos and Zoback, 1983; Hannan and Stesky, 1985). Thus, if the compressional and shear wave velocities can be monitored during the operation of a mini-frac test then from the V_p/V_s ratio the minimum and maximum horizontal stress directions can be ascertained. The success of V_p/V_s ratio method largely depends upon the quality of the reflected shear wave signal, because of the difficulty in detecting the signal.

7.6 SHEAR WAVE POLARIZATION

Due to the polarization of shear wave in two mutually perpendicular directions, velocity of propagation of shear wave in two directions varies. The shear wave travels faster in one direction than in the other. Thus shear wave polarization holds great potential for determination of the principal *in-situ* stress direction. The technique is being studied now by various geophysics groups (Kry, 1992).

7.7 WAVE ATTENUATION

Pros *et al.* (1962), Toksoz *et al.* (1979), and Winkler and Nur (1982) reported to have found that the relative changes in wave attenuation are greater than those of velocity measured in the same type of rocks under the same stress conditions and the wave attenuation is potentially a better parameter than wave velocity for measurement of *in-situ* stress.

Laboratory and borehole wave attenuation studies conducted by Sun and Peng (1989) supported the feasibility of using the ultrasonic wave attenuation for measuring *in-situ* stress with reasonable accuracy at least up to a depth of 900 m.

7.8 BOREHOLE SLOTTING TECHNIQUE

This technique was first described by Bock (1986). A probe containing a small diamond saw cuts three half-moon-shaped radial slots in the borehole wall at prescribed orientations. A strain gauge attached to the probe measures the strain relief to the surfaces resulting from the cutting operations. The strain values are used to determine the elastic constants and then to calculate the principal stresses. Such tests are easy and rapid to conduct, hence several measurements can be conducted in a short time span over a narrow segment of the borehole wall. Several such measurements can well verify the calculated stresses.

7.9 BOREHOLE HOLOGRAPHIC INTERFEROMETRY

The method was reported earlier by Bass *et al.* (1986). In this method, a small drill is used to induce a radial side-hole in the wall of the test hole. The displacement resulting from the stress relief caused by the drilling is recorded as an interference hologram. The derivation of the stress state from the measured displacements is similar to that employed in overcoring methods. The method seems to have a great potential in measuring *in-situ* stress, particularly at shallow depths.

7.10 OVERCORING TECHNIQUE

This is a strain relief technique where the stress is reduced completely to zero by overcoring operation. The displacement during overcoring is detected and the material properties such as Young's modulus and Poisson's ratio of the rock must be known accurately to calculate the stress state. The overcoring is found to be a reliable technique at shallow depths. At great depths, where the effect of temperature on the overcored materials and the strain gauges is uncertain, the method has not been very successful.

Haimson (1981,1982), Li *et al.* (1982), and Doe *et al.* (1982) made a detailed comparison of overcoring stress measurements to hydraulic fracturing stress measurements and found good agreement between the two results.

Comparison of multiple methods of* in-situ *stress measurement. There are several distinguishable features between the various methods of *in-situ* stress measurement. These include:

1. While ASR and DSA methods require availability of oriented cores from depth, other methods, such as mini-frac tests, wave velocity anisotropy, wave attenuation, and wellbore breakout do not require any core recovery.
2. The magnitude of the minimum *in-situ* stress can be inferred directly from a mini-frac test, whether the minimum stress is overburden or horizontal. In ASR and DSA methods, stresses in the horizontal planes cannot be measured directly. The knowledge of overburden stress and an assumption of elastic and non-elastic strain recovery are required to estimate the absolute magnitude. From wellbore breakout, the *in-situ* stress magnitude cannot be derived with a reasonable accuracy.
3. The mini-frac test allows us to ascertain if the minimum *in-situ* stress is horizontal or vertical. Unless the fracture azimuth is measured using a borehole televiewer, an impression packer, or a dipmeter, the actual orientation of the horizontal stresses remains unknown. The orientation of maximum and minimum horizontal stresses can be obtained from wellbore breakout, ASR, and DSA methods.
4. In lithologies with a large residual strain energy, the ASR and DSA methods may not determine the *in-situ* stress accurately. But in a mini-frac test, the strain energy is largely released on initiation of a fracture.
5. While the scope of overcoring and borehole holographic interferometric techniques is limited largely to shallow depths, the mini-frac like wave velocity and borehole slotting techniques can be used at both shallow and great depths.

Recommendations for future research work. Since the early sixties when Fairhurst (1964) first proposed use of hydraulic fracturing techniques for *in-situ* stress measurement, extensive laboratory, field, and simulation studies have been conducted in the area of hydraulic fracturing and mini-frac testing. The knowledge gained in the last three decades has been enormous and has helped advance our understanding. One such area in which our understanding has improved is the poro-elastic effect influencing *in-situ* stress determination.

The procedure of mini-frac field testing has been developed reasonably well. However, difficulties are mainly encountered in the interpretation of data, largely because of the uncertainty in the failure mechanisms near the wellbore region, fluid diffusivity, role of pre-existing natural fractures, and inherent inhomogeneities.

The theory of *in-situ* stress measurement technique developed on the tensile failure criterion and elastic fracture mechanics principle seems to be working well with cemented, low porosity sandstones and carbonates. The same principle has been used in tar sands, although the mechanism of fracture growth in such poorly consolidated materials is poorly understood. Careful research work in fracturing of tar sands and poro-elastic materials is required to identify the appropriate mechanisms of fracture growth and establish the dependence of fracture growth mechanisms on:

(a) fluid viscosity,
(b) temperature conditions, and
(c) injection rates.

In hydraulic fracturing and mini-frac testing of well-cemented and poorly cemented materials, there are common areas where future studies should be directed:

(a) The distance the fracture will propagate before rotating to become perpendicular to the minimum principal stress.

(b) The distance along the well the fracture will propagate before leaving the axis of the wellbore.

(c) The effect of the presence of natural fractures on fracture growth, orientation, and *in-situ* stress determination.

(d) If the fracture growth rate and degree of orientation can be controlled or overridden by controlling treatment rate, volume, viscosity, and the nature of the perforated interval.

(e) Analysis and interpretation of the pressure–time curve when the stress state is isotropic

In several cases, the validity of *in-situ* stress determination in tar sands has been confirmed by comparing the minimum *in-situ* stress determined by hydraulic fracturing and mini-frac testing with the overburden stress values obtained independently. Whenever possible, *in-situ* stress results obtained from the mini-frac testing should be compared with results obtained from other independent measures. This will ascertain the accuracy of horizontal as well as vertical stress determined from mini-frac testing and hydraulic fracturing operations.

REFERENCES

REFERENCES

Abou–Sayed, A.S. and Brechtel, C.E., 1978, *In situ* stress determination by hydrofracturing: a fracture mechanics approach, Journal of Geophys. Research, vol. 83, no. B6, pp. 2851 – 2862.

Bass, J., Schmitt, D.R., and Ahrens, T.J., 1986, Holographic *in-situ* stress measurements, Geophys. J. Roy. Astron. Soc., vol. 85, pp. 13–14.

Behrmann, L.A. and Elbel, J.L., 1991, Effect of perforations on fracture initiation, Journ. of Petrol. Tech., pp. 608–615.

Bell, J.S. and Babcock, E.A., 1986, The stress regime of the Western Canadian Basin and implications for hydrocarbon production, Bull. Can. Petroleum Geology, vol. 34, no. 3, pp. 364–378.

Bjarnason, B., Ljunggren, C., and Stephenson, O., 1988, New developments in hydrofracturing stress measurements at Lulea University of Technology, Proc. Second Int. Workshop on Hydraulic Fracturing Stress Measurements (HFSM 7.88), Minnesota University, 1, pp. 113–140.

Bock, H., 1986, *In-situ* validation of the borehole slotting stressmeter: in Rock Stress, pp. 261–270, Lulea: Centek.

Boone, T.J. Kry, P.R., Bharatha, S., and Gronseth, J.M., 1991, Poro-elastic effects related to stress determination by micro-frac tests in permeable rock, Proc. 32ND U.S. Symposium on Rock Mechanics — Rock Mechanics as a Multidisciplinary Science, pp. 25–34.

Breckels, I.M. and van Eekelen, H.A.M., 1981, Relationship Between Horizontal Stress and Depth in Sedimentary Basins, SPE 10336, Paper presented at the 56TH Annual Fall Technical Conference and Exhibition of the Society of Petroleum Engineers of AIME, held in San Antonio, Texas, Oct. 5 –7, 1981.

Bredehoeft, J.D., Wolff, R.G., Keys, W.S., and Schuter, E., 1976, Hydraulic fracturing to determine the regional *in-situ* stress field, Piceance Basin, Colorado, Geol. Soc. Am. Bull., 87, pp. 250–258.

Brown, D.W., 1989, The potential for large errors in the inferred minimum earth stress when using incomplete hydraulic fracturing results, Int. J. Rock Mech. Min. Sci. & Geomech. Abstr., vol. 26, no. 6, pp. 573–577.

Bush, D.D. and Meyer, B.S., 1988, *In-situ* stress magnitude dependency on lithology, *in* Proc. of the 29TH U.S. Symposium of Rock Mechanics: Key questions in rock mechanics. Cundall, P.A., Sterling, R.L., and Starfield, A.M, Eds.

Cheung, L.S. and Haimson, B.C., 1989, Laboratory study of hydraulic fracturing pressure data — how valid is their conventional interpretation, Int. J. Rock Mech. Min. Sci. & Geomech. Abstr., vol. 26, no. 6, pp. 594–604.

Christianson, M.C., Hart, R.D., and Schatz, J.F., Numerical analysis of multiple radial fracturing, Proc. 29TH U.S. Symp. on Rock mech., Univ. of Minnesota, P.A. Cundall, R.A. Sterling, and A.M. Starfield, Eds., pp. 441–451.

Cinco–Ley, H. and Samaniego, V.F., 1978, Transient pressure analysis for fractured wells, SPE 7490, paper presented at the 53RD Fall Technical Conference of SPE held in Houston, Texas, Oct. 1–3, 1978.

Daneshy, A.A., 1973a, A study of inclined hydraulic fractures, SPE paper 4062, paper presented at the SPE–AIME 47TH Annual Fall Meeting held in San Antonio, Texas, October 8–11, 1973, pp. 61–68.

Daneshy, A.A., 1973b, Experimental investigation of hydraulic fracturing through perforations, J. of Petrol. Tech., Oct. 1973, pp. 1201–1206.

De Bree, P. and Walters, J.V., 1989, Micro/mini-frac test procedures and interpretation for *in-situ* stress determination, Int. J. Rock Mech. Min. Sci & Geomech. Abstr., vol. 26, no. 6, pp. 515–521.

Detournay, E., McLennan, J.D., and Roegiers, J.C., 1986, Poro-elastic concepts explain some of the hydraulic fracturing mechanisms, Paper SPE 15262.

Detournay, E. and Cheng, H.D., 1988, Poroelastic response of a borehole in a non-hydrostatic stress field, Int. J. Rock Mech., Min. Sci. & Geomech. Abstr., 25 (3), pp. 171–182.

Detournay, E., Cheng, H.D., Roegiers, J.C., and McLennan, J.D., 1989, Poro-elasticity considerations in *in-situ* stress determination by hydraulic fracturing, Int. J. Rock Mech. Min. Sci & Geomech. Abstr., vol. 26, no. 6, pp. 507–513.

Dey, T.N. and Brown, D.W., 1986, Stress measurements using hydraulic fracturing and differential strain analysis, in Rock Stress, pp. 351–358, Lulea: Centek.

REFERENCES

Doe, T.W. and others, 1982, Determination of the state of stress at the Stripa Mine, Sweden, Proc. of the Workshop on Hydraulic Fracturing Stress Measurements, U.S. National Committee on Rock Mechanics, Washington, D.C.

Dusseault, M.B., 1977, Stress state and hydraulic fracturing in the Athabasca Oil Sands, Journal of Can. Petrol. Tech., July–Sept. 1977, pp. 19–27.

Dusseault, M.B., 1979, A conceptual geomechanical model for hydraulic fracture in the Athabasca oil sands, A University of Alberta report.

Dusseault, M.B., 1980a, The behaviour of hydraulically induced fractures in oil sands, Underground Rock Eng., CIM special vol. 22, pp. 36–40.

Dusseault, M.B., 1980b, The development of permeability in cohesionless bituminous sands, Tar Sands Permeability Enhancement: Proc. of a workshop held at Albuquerque, New Mexico, May 8–9, 1980, pp. 45–84.

Earlougher, R.C., 1977, Advances in Well Test Analysis, Soc. of Petroleum Engineers of AIME monograph 5, Dallas, USA, p. 264.

Economides, M.J. and Nolte, K.G. edited, Reservoir stimulation, second edition, pp. 19–10.

Enever, J.R. and Wooltorton, B.A., 1982, Experience with hydraulic fracturing as a means of estimating *in-situ* stress in Australian coal basin sediments, Proc. of the Workshop on Hydraulic Fracturing Stress Measurements, U.S. Nat. Comm. on Rock Mech., Washington, D.C.

Everdingen, V.A.F., 1953, The skin effect and its influence on the productive capacity of a well, Trans AIME, 198, pp. 171–176.

Fairhurst, C., 1964, Measurement of *in-situ* rock stresses, with particular reference to hydraulic fracturing, Rock Mechanics and Engineering Geology, 1964, pp. 129–147.

Gnirk, P.F. and Johnson, R., 1964, The deformational behaviour of a circular mine shaft situated in a viscoelastic medium under hydrostatic stress, Proc. Sixth Symp. on Rock Mech., University of Missouri, Rolla, pp. 231–259.

Gnirk, P.F. and Johnson, R., 1972, The mechanical behaviour of uncased wellbores situated in elastic/plastic media under hydrostatic stress, SPEJ, pp. 49–59.

Gough, D.I and Bell, J.S., 1982, Stress orientation from borehole wall fractures, Can J. Earth Sci., 19, pp. 1358–1370.

Gringarten, A.C. and Ramey, H.J., Jr., 1974, Unsteady state pressure distribution created by a well with a single horizontal fracture, partial penetration or flow restricted entry, SPEJ August 1974, Trans AIME, 257, pp. 413–426.

Gronseth, J.M. and Detournay, E.M., 1979, Improved stress determination procedures by hydraulic fracturing, final report to U.S. Geological Survey, Menlo Park, California, Contract no. 14–08–001– 16768.

Gronseth, J.M. and Kry, P.R., 1983, Instantaneous shut-in pressure and its relationship to the minimum *in-situ* stress, *in* Zoback, M.D. and Haimson, B.C., Eds., Hydraulic Fracturing Stress Measurements, Washington, D.C., National Academy Press.

Gronseth, J.M. and Kry, P.R., 1987, *In-situ* stresses and the Norman Wells expansion project, CIM 87–38–57, paper presented at the 38TH Annual Technical Meeting of the Petroleum Soc. of CIM held in Calgary, June 7–10, 1987.

Gronseth, J.M., 1988, Cased hole *in-situ* stress determinations from deviated wellbores in an unconsolidated formation: 2ND International Workshop on Hydraulic Fracturing Stress Measurements, Minneapolis, Minnesota, June 15–18.

Gronseth, J.M., PCEJ Hangingstone pilot: pre-steam injection stress test, interim report, 1990.

Guenot, A., 1988, Contraintes et ruptures autour des forages petroliers, Proc. Sixth Int. Soc. Rock Mech. Cong., Montreal, pp. 109–118.

Hagoort, J., 1981, Waterflood-induced Hydraulic Fracturing, thesis, Koninklijke/Shell Exploratie en Produktie Laboratorium, p. 227.

Haimson, B.C. and Fairhurst, C., 1967, Initiation and extension of hydraulic fractures in rock, Soc. of Petrol. Eng. J., vol. 7, pp. 310–318.

Haimson, B.C., 1972, Earthquake related stresses at Rangley, Colorado, New horizons in rock mechanics, proceedings of the 14TH Symposium, Am. Soc. of Civil Engineers, pp. 689–707.

Haimson, B.C., 1981, Confirmation of hydrofracturing results through comparisons with other stress measurements, Proc. of the 22ND U.S. Symposium on Rock Mechanics, P. 379–385.

Haimson, B.C., 1982, A comparative study of deep hydrofracturing and overcoming stress measurements at six locations with particular interest to the Nevada Test Site, Proc. of the Workshop on Hydraulic Fracturing Stress Measurements, U.S. Nat. Comm. on Rock Mech., Wash. D.C., in press.

Haimson, B.C. and Rummel, F., 1982, Hydrofracturing stress measurement in the IRDP drillhole at Reydarfjordur, Iceland, J. Geophys. Res.

Haimson, B.C., 1988, Status of *in-situ* stress determination methods, *in* Cundall *et al.*, Eds., Key questions in rock mechanics, Proc. of the 29TH U.S. Symposium of Rock Mechanics, pp. 75–84.

Haimson, B.C. and Zhongliang, Zhao, 1991, Effect of borehole size and pressurization rate on hydraulic fracturing breakdown pressure, Proc. of the 32ND U.S. Symposium on Rock Mechanics — Rock Mechanics as a Multidisciplinary Science, held at the University of Oklahoma, Norman, July 10–12, pp. 191–200.

Hallam, S.D. and Last, N.C., 1990, Geometry of Hydraulic Fractures from Modestly Deviated Wellbores, SPE 20656, paper presented at the 65TH Annual Technical Conference & Exhibition of SPE held in New Orleans, Louisiana, September 23–26.

Hannan, S.S. and Stesky, R.M., 1983, Compressional velocities in intact and fractured shales from Southern Ontario, Paper presented at the annual spring meeting of Am. Geophys. Union, Baltimore, USA, May 31–June 2.

Hannan, S.S. and Stesky, R.M., 1985, Compressional and shear velocities in fractured shales, Paper presented at the annual meeting of the Canadian Soc. of Exploration Geophysicists, Calgary, Canada, May.

Hassan, D., 1982, A method for predicting hydraulic fracture azimuth and the implications thereof to improve hydrocarbon recovery, Petrol Soc. of CIM, paper no. 82–33–19.

Hickman, S.H. and Zoback, M.D., 1983, The interpretation of hydraulic fracturing pressure–time data to *in-situ* stress determination: Proc. of a workshop on hydraulic fracturing stress measurements, National Academy Press, Washington D.C., pp. 44–54.

Hickman, S.H., Healy, J.H., and Zoback, M.D., 1985, *In-situ* stress, natural fracture distribution and borehole elongation in the Auburn geothermal well, New York, J. Geophys. Res., vol. 90, pp. 5497–5512.

Horner, D.R., 1951, Pressure build-up in wells, Proc. Third World Pet. Congress., E.J. Brill, Leiden.

Hubbert, M.K. and Willis, D.G., 1957, Mechanics of hydraulic fracturing, Trans. Soc. of Petroleum Engineers of AIME, vol. 210, pp. 153–168.

Hurst, W., 1953, Establishment of the skin effect and its implication to fluid flow into a wellbore, Pet. Eng. Oct., B–6.

Ikeda, R. and Tsukahara, H., 1989, Hydraulic fracturing technique: pore pressure effect and stress heterogeneity, Int. J. Rock Mech. Min. Sci. & Geomech. Abstr., vol. 26, no. 6, pp. 471–475.

Irwin, G.R., 1957, Analysis of stresses and strains near the end of a crack transversing in a plate, J. Appl. Mech., pp. 361–364.

Jones, C. and Sargeant, J.P., 1989, Obtaining the minimum horizontal stress from micro-frac test data: a new approach utilizing a derivative algorithm, SPE 18867, paper presented at the SPE Production Operations Symposium held in Oklahoma City, Oklahoma, March 13–14, 1989, pp. 381–388.

Kehle, R.O., 1964, The determination of tectonic stress through analysis of hydraulic well fracturing, J. Geophys. Res., vol. 69, pp. 259–273.

Kim, C.M. and Abbas, H.H., 1991, Hydraulic fracture initiation from horizontal wellbores: laboratory experiments, Proc. of the 32ND U.S. Symposium on Rock Mechanics — Rock mechanics as a multidisciplinary science, held at the University of Oklahoma, Norman, July 10–12, 1991, pp. 231–240.

Kirsch, G., 1898, Die Theorie der Elasitizitat und die Bedurfrisse der Festigkeitslehre: Zeitschr. Ver. Deutsch. Ingenieure, vol. 42, p. 797.

Kry, P.R. and Gronseth, J.M., 1983, *In-situ* stresses and hydraulic fracturing in deep basin, Journal of Can. Petrol. Tech., pp. 31–35.

Kry, P.R., 1992, Senior Research Advisor, Esso Canada Research Centre, Personal Communication.

Kuriyagawa, M., Kobayashi, H., Matsunaga, I., and others, 1989, Application of hydraulic fracturing to three dimensional *in-situ* stress measurement, Int. J. Rock Mech. Min. Sci. & Geomech. Abstr., vol. 26, no. 6, pp. 587–593.

REFERENCES

Layne, A.W., and Siriwardane, H.J., 1988, Insights into hydraulic fracturing of a horizontal well in a naturally fractured formation, Paper SPE 18255.

Lee, W.S., 1986, New method of mini-frac analysis offers greater accuracy and enhanced applicability, SPE 15941, Paper presented at the SPE Eastern Regional Meeting held in Columbus, Ohio, November 12–14.

Lee, W.S., 1987, Study of the effects of fluid rheology on mini-frac analysis, SPE 16916, Paper presented at the 62ND Annual Technical Conference and Exhibition of the SPE held in Dallas, Texas, September 27–30.

Lee, M.Y. and Haimson, B.C., 1989, Statistical evaluation of hydraulic fracturing stress measurement parameters, Int. J. Rock Mech. Min. Sci & Geomech. Abstr., vol. 26, no. 6, pp. 447–456.

Li, F.Q. and others, 1982, Experiments of *in-situ* stress measurements using the stress relieving and hydraulic fracturing techniques, Proc. of the Workshop on Hydraulic Fracturing Stress Measurements, U.S. Nat. Comm. of Rock Mech., Washington, D.C.

Ljunggren C., Amadei, B., and Stephenson, O., 1988, Use of the Hoek and Brown failure criterion to determine *in-situ* stress from hydraulic fracturing measurements, Proc. Conf. of Appl. Rock Eng. (CARE '88), Newcastle-upon-Tyne (January) pp. 133–142.

McLennan, J.D., and Roegiers, J.C., 1981, Do instantaneous shut-in pressures accurately represent the minimum principal stress?, USGS workshop on hydraulic fracturing stress measurement, Monterey, California.

McLennan, J.D., Roegiers, J.C., and Economides, M.J., 1989, Extended reach and horizontal wells, *in* Economides, M.J. and Nolte, K.G., Eds., Reservoir Stimulation, Prentice Hall, Englewood Cliffs, second edition.

Meyer, B.R., and Hagel, M.W., 1989, Simulated mini-frac analysis, Journal of Can. Petrol. Tech., vol. 28, no. 5, pp. 63–73.

Mizuta, Y. and Kobayashi, H., 1980, Improved stress determination procedures by hydraulic fracturing, Final report to the USGS, Grant no. USDI 14–08–0001–17775.

Moos, D. and Zoback, N.D., 1983, *In-situ* studies of velocity in fractured crystalline rocks, J. Geophys. Res., vol. 88, no. B3, pp. 2345–2358.

Morgenstern, N.R., Scott, J.D., Guo, F., and Wang, Y., 1992, Report produced at the large scale hydraulic fracturing workshop held at the University of Alberta, March 19.

Nolte, K.G., 1979, Determination of fracture parameters from fracturing pressure decline, Paper SPE 8341 presented at SPE–AIME 54TH Annual Fall Technical Conference and Exhibition, Las Vegas.

Nolte, K.G., 1982, Fracture design considerations based on pressure analysis — Paper SPE 10911 presented at the 1982 SPE Cotton Valley Symposium, Tyler, May 20.

Nolte, K.G., 1986, A general analysis of fracturing pressure decline with application to three models, SPE Formation Evaluation, pp. 571–583.

Poon, D., 1986, Analysis of pressure fall-off data during the hydraulic fracturing of the AMOCO GLISP H–3 well, AOSTRA internal report.

Prats, M., 1981, Effect of burial history on the subsurface horizontal stresses of formations having different material properties, Journal Soc. of Petrol. Engineers of AIME, pp. 658–662.

Pros, Z., Vanek, J., and Klima, K., 1962, The velocity of the elastic waves in diabase and graywacke under up to 4 kilobars, Geophysics and Geodesy, pp. 347–367.

Proskin, S.A., Scott, J.D., and Chhina H.S., 1990, Current practice in the interpretation of micro-frac tests in oil sands, SPE paper no. 20040, presented at the 60TH California Regional meeting held in Ventura, California, April 4–6.

Rabba, W.E., 1989, Experimental study of hydraulic fracture geometry initiated from horizontal wells, SPE 19720, paper presented at the 64TH Annual Technical Conference and Exhibition of the Soc. of Petrol. Eng., held in San Antonio, Texas, Oct 8–11, pp. 189–203.

Raisbeck, J.M. and Currie, J.B., 1981, A laboratory investigation of hydraulic fracturing in oil sands, *In situ*, 5(1), pp. 1–24.

Ratigan, J.L., 1982, A statistical fracture mechanics determination of the apparent tensile strength in hydraulic fracture, Proc. of the Workshop on Hydraulic Fracturing Stress Measurements, U.S. Nat. Comm. on Rock Mech., Washington D.C.

Ripley, H., 1992, Formerly of Halliburton Services, Personal communication.

Roegiers, J.C., McLennan, J.D., and Murphy D.L., 1982, Influence of pre-existing discontinuities on the hydraulic fracturing propagation process, First U.S./Japan Tech. Sem. on Hydraulic Fracturing, Tokyo, Japan (November).

Roegiers, J.C., 1989, Elements of rock mechanics, in Economides, M.J. and Nolte, K.G., Eds., Reservoir Stimulation, Prentice Hall, Englewood Cliffs, second edition.

Roegiers, J.C., 1991, Professor, Department of Petroleum and Geological Engineering, University of Oklahoma, USA, personal communication.

Rosepillar, M.J., 1979, Determination of principal stresses and confinement of hydraulic fractures in Cotton Valley, paper presented at the 54TH Annual Fall Technical Conference and Exhibition of the Soc. of Petrol. Engineers of AIME, Las Vegas, Nevada, Sept. 23–26.

Saltuklaroglu, M., 1991, Determination of fracture parameters during cyclic steaming in Cold Lake oil sands, Paper presented at the 5TH UNITAR International Conference on Heavy Crude and Tar Sands, pp. 47–61.

Salz, L.B., 1977, Relationship between fracture propagation pressure and pore pressure, SPE 6870, paper presented at the 52ND Annual Fall Technical Conference and Exhibition of SPE held in Denver, Colorado, Oct. 9–12.

Santarelli, F.J., Brown, E.T., and Mawey, V., 1986, Analysis of borehole stresses using pressure-dependent, linear electricity, Int. J. Rock Mech. Min. Sci. and Geomech. Abstr., vol. 23 (6), pp. 445–449.

Schmitt, D.R. and Zoback, M.D., 1989, Poro-elastic effects in the determination of maximum horizontal principal stress in hydraulic fracturing tests — a proposed breakdown equation employing a modified stress relation for tensile failure, Int. J. Rock Mech. Min. Sci. & Geomech. Abstr., 26 (6), pp. 499–506.

Schmitt, D.R., 1992, Professor, Dept. of Physics, University of Alberta, personal communication.

Scott, J.D., 1990, Professor, Department of Civil Engineering, University of Alberta, personal communication.

Shi, A., 1988, Contribution a l'Etude de Stabilite des Forages Petroliers, M. Sc. Thesis, Pub. 264. Faculte Polytech de Mons.

Shoji, T. *et al.*, 1985, Growth behavior of hydraulically created crack and its size evaluation using well logging data-crustal rock fracture mechanics approach, Trans. Geothermal Resources Council, 9, part II, pp. 579–584.

Soliman, M.Y., Hunt, J.L., and Lee, W.S., 1987, Fracture parameters — calculated *versus* designed, paper presented at the 38TH Annual Tech. Meeting of the Petroleum Soc. of CIM held in Calgary, June 7–10.

Springer, J.E., Zoback, M.D., Haimson, B.C., Li, F., and Zhai, Q., 1987, Wellbore breakouts at Jianchuan and their relation to the stress field and tectonics of Yunnan Province, China, EOS, Trans. Am. Geophysical Union, vol. 68, p. 146.

Strubhar, M.K., Fitch, J.L., and Glenn, E.E., 1975, Multiple, vertical fractures from an inclined wellbore — a field experiment, JPT, pp. 641–647.

Sun, Y.L. and Peng, S.S., 1989, Development of *in-situ* stress measurement technique using ultrasonic wave attenuation method — a progress report, Rock Mechanics as a guide for efficient utilization of natural resources, Khair, Ed., Balkema, Rotterdam, pp. 477–482.

Teufel, L.W. and Warpinski, N.R., 1984, Determination of *in-situ* stress from anelastic strain recovery measurements; Proc. 25TH Symposium Rock Mech., Soc. of Mining Eng., pp. 176–185.

Teufel, L.N., Rhett, D.W., and Farrell, H.E., 1991, Effect of reservoir depletion and pore pressure drawdown on *in-situ* stress and deformation in the Ekofisk Field, North Sea, Proc. 32ND U.S. Symposium on Rock Mechanics — Rock Mechanics as a Multi-Disciplinary Science, pp. 63–72.

Thiercelin, M., Jeffrey, R.G., and Ben Naceur, K., 1989, Influence of fracture roughness on the geometry of hydraulic fractures, SPE Production Engineering, pp. 435–442.

Timoshenko, S., 1934, Theory of Elasticity: New York and London, McGraw–Hill.

Toksoz, M.N., Johnston, D.H., and Timur, A., 1979, Attenuation of seismic waves in dry and saturated rocks, Part I: laboratory measurements, Geophysics, vol. 44, pp. 681–711.

Warpinski, N.R., Branagan, P., and Wilmer, R., 1985, *In-situ* stress measurement at U.S. DOE's multiwell experiment site, Mesaverde group, Rifle, Colorado, JPT, pp. 527–536.

REFERENCES

Warpinski, N.R., 1989, Determining *in-situ* stress from hydraulic fracturing through perforations, Int. J. Rock Mech. Min. Sci & Geomech. Abstr., 26(6), pp. 523–531.

Warpinski, N.R., 1991, Hydraulic fracturing in tight, fissured media, J. of Petrol. Tech., February, pp. 146–152 and 208–209.

Whitehead, W.S., Gatens III, J.M., and Holditch, S.A., 1989, Determination of *in situ* stress profiles through hydraulic fracturing measurements in two distinct geologic areas, Int. J. Rock Mech. Min. Sci. & Geomech. Abstr., 26 (6), pp. 637–645.

Winkler, K.W. and Nur, A., 1982, Seismic attenuation effects of pore fluids and frictional sliding, Geophysics, vol. 47, pp. 1–15.

Woodland, D.C. and Bell, J.S., 1989, *In-situ* stress magnitudes from mini-frac records in Western Canada, The Journal of Can. Petrol. Tech., vol. 28, no. 5, pp. 22–31.

Yew, C.H., Schmidt, J.H., and Li, Yi., 1989, On Fracture Design of Deviated Wells, SPE 19722. Paper presented at the 64TH Annual Technical Conference and Exhibition of SPE held in San Antonio, Texas, October 8–11.

Zoback, M.D., Rummel, F., Jung, R., and Raleigh, C.B., 1977, Laboratory hydraulic fracturing experiment in intact and pre-fractured rock, Int. J. Rock Mech. Min. Sci. & Geomech. Abstr., 14 (2), pp. 49–58.

Zoback, M.D. and Haimson, B.C., 1982, Status of hydraulic fracturing method for *in-situ* stress measurements, Proc. 23RD Symposium on Rock Mechanics, held at the University of California, Berkeley, California, Aug. 25–27, Goodman, R.E. and Heuze, F.E., Eds., pp. 143–155.

Zoback, M.D., Moos, D., Mastin, L., and Anderson, R.N., 1985, Wellbore breakouts and *in-situ* stress, J. Geophys. Res., vol. 90, pp. 5523–5530.

APPENDIX A

EXAMPLE CALCULATIONS
OF MINI-FRAC
TEST PARAMETERS

APPENDIX A

EXAMPLE CALCULATIONS OF MINI-FRAC TEST PARAMETERS

A1 TRANSMISSIBILITY CALCULATIONS

To calculate the transmissibility from a mini-frac pressure fall-off test, conventional well test analysis is applied on the data after the fracture closes. The standard log–log and Horner plots are used. From the log–log plot, the end of wellbore storage is estimated. The transmissibility is calculated using the following equation:

$$\text{(A1)} \quad \frac{Kh}{\mu} = \frac{2149QB}{m}$$

where Kh/μ = formation transmissibility (md·m/mPa·s)
K = effective permeability to water (md)
h = effective reservoir flow thickness (h)
μ = reservoir fluid viscosity (mPa·s)
Q = fluid injection rate (m^3/d)
B = formation volume factor
m = Horner semi-log straight line slope (kPa/cycle) and
c = 2149 in metric unit

If the average $Q = 9.57\ m^3/d$, $B = 1$, then from Figure 4–15, when slope $m = 505$, we get

$$\frac{Kh}{\mu} = \frac{2149\,(9.57)\,(1.0)}{505} = 40.7 \text{ md·m/mPa·s}$$

If the formation thickness is estimated to be 8.6 m, then the effective mobility, K/μ, is obtained from (A1) as 4.7 md/mPa·s.

A2 SKIN FACTOR

The skin factor can be calculated by the following:

$$S = 1.151\left[\frac{\left(P_{wf} - P_1\right)}{m} - \log\left(\frac{K}{\left(\mu C_t R_w 2\right)}\right) + 5.1\right]$$

In Figure 4–15,

P_{wf} = flowing pressure = $P(t = 0)$ = 5950 kPa (extrapolated from the figure)
P_1 = pressure for $(t_{inj} + dt)/dt = 1$ from Horner plot = 1600 kPa
m = slope of the Horner plot = 505 kPa/cycle
R_w = wellbore radius = 0.061 m
So, S = $1.151[(5950 - 1600)/505 - \log\{5.9/(0.35)(2.18 \times 10^{-6})\,(0.061)^2\} + 5.1]$ gives $S = 5.14$

A3 CALCULATION OF FLUID LEAK-OFF COEFFICIENT BY NOLTE'S METHOD

The leak-off coefficient, C, is expressed as,

$$C = \frac{P^* H^2 \beta_s}{E' H_p \sqrt{t_o}}$$

where P^* = type curve matching pressure
H = the fracture height
H_p = fluid loss height
β_s = ratio of the average and wellbore pressure at shut-in
t_o = injection time
E' = plane strain modulus and is expressed as $E' = E/(1 - \nu^2)$

where E = elastic modulus
ν = Poisson's ratio

For example,
P^* = 330 kPa
H = H_p = 10 m
β_s = 0.85
E = 1.39 E6 kPa
ν = 0.25
t_o = 4 minutes

Thus, $C = 9.48E^{-4}$ m/min

APPENDIX B

PRESSURE–TIME DATA OF TEST #1B

APPENDIX B

PRESSURE–TIME DATA OF TEST #1B

Actual time	Time since start of inj		Pressure
hr:min:sec	sec	hr	kPa
6:24:46	0	0.0	1295.9
6:25:00	16	0.0044	1341.6
6:25:11	27	0.0075	1415.6
6:25:26	42	0.0117	1762.7
6:25:36	52	0.0144	2831.0
6:25:40	56	0.0156	4417.9
6:25:47	63	0.0175	3693.5
6:25:54	70	0.0194	3480.4
6:26:05	81	0.0225	3338.1
6:33:06	502	0.1394	2998.5
6:38:05	801	0.2225	2938.7
6:43:04	1100	0.3056	2927.0
6:49:08	1464	0.4067	2929.2
6:55:18	1834	0.5094	2938.9
6:55:26	1842	0.5117	2936.9
6:55:29	1845	0.5125	2938.1
6:55:36	1852	0.5144	2939.4
6:55:40	1856	0.516	2938.3
6:55:47	1863	0.518	2933.8
6:55:54	1870	0.5194	2897.6
6:55:56	1872	0.52	2887.9
6:55:58	1874	0.5206	2885.5
6:56:05	1881	0.5225	2883.0
6:56:12	1888	0.5244	2879.5
6:56:20	1896	0.5267	2876.5
6:56:30	1906	0.5294	2871.5
6:56:41	1917	0.5325	2868.9
6:56:56	1932	0.5367	2866.2
6:57:10	1946	0.5406	2862.4
6:57:42	1978	0.5494	2857.0
7:02:05	2241	0.6225	2834.5
7:03:06	2302	0.6394	2830.8
7:08:05	2601	0.7225	2816.6
7:11:05	2781	0.7725	2808.7
7:15:06	3022	0.8394	2797.9
7:20:12	3328	0.9244	2787.6
7:26:12	3688	1.0244	2764.8
7:36:17	4293	1.1925	2727.9
7:46:22	4898	1.3606	2678.6
7:56:30	5506	1.5294	2609.7
8:06:32	6108	1.6967	2523.5
8:16:36	6712	1.8644	2391.2
8:26:30	7306	2.0294	2048.3
8:32:30	7666	2.1294	1850.6
8:34:36	7790	2.1639	1768.3
8:36:32	7906	2.1961	1686.9
8:42:32	8266	2.2961	1577.5
8:48:32	8626	2.3961	1560.6
8:54:32	8986	2.4961	1519.0
9:04:29	9583	2.6600	1474.4

APPENDIX C

DEFINITION OF TERMS

APPENDIX C

DEFINITION OF TERMS

Back stress. Increase in local stress field that can be caused by processes like pore pressure increase, thermal loading, and presence of borehole.

Closure stress. The stress at which two opposing faces of a fracture close completely.

Cohesive strength. Cohesive force that holds grains in contact with each other.

Deformation. Any change in the original form or volume of rock caused by applied forces

Elasticity. The property of a material to return to its original state (shape and size) upon release of the deforming force. The stress–strain relationship of most non-porous elastic materials is linear.

Fluid efficiency. It is the efficiency of an injection fluid to fracture a formation and extend it. Fluid efficiency is affected by the fluid loss into the formation. As the fracture length increases, the total fluid loss along the fracture face increases, consequently, the efficiency during injection decreases with time, assuming the rate is kept the same. The fluid efficiency is greatest in a storage dominated (fluid-filled fracture) case and least in a leak-off dominated case. The fluid efficiency also depends on the nature of the injection fluid (density, viscosity) and the reservoir character (porosity, permeability, reservoir temperature, rock type, *etc*.).

Fracture. A surface of discontinuity within a rock where the cohesive force is zero

Fracture stiffness. Change in stress necessary for a unit change in fracture closure.

Hoop stress. Tangential stress in and around a circular borehole.

Mated fracture. A fracture whose opposing surfaces completely matches on closure. Mated fractures are distinguished from unmated fractures by incomplete closure because of a mismatch of the two opposing surfaces.

Poisson's ratio. The ratio of the linear contraction to the lateral expansion is regarded as Poisson's ratio. Poisson's ratio for most rocks lie between 0.15 and 0.35.

Poro-elasticity. The term is used to designate the elastic behaviour of porous materials. The stress–strain relationship of most porous materials is non-linear. The deformation of a poro-elastic material is expressed in terms of effective stress, σ_{eff}, given by,

$$\sigma_{eff} = \sigma - P_p ,$$

where, σ is the total stress and P_p is the pore pressure. For non-porous materials, $\sigma_{eff} = \sigma$.

Poro-elastic constant. The constant describes the efficiency of the fluid pressure to counteract the total applied stress. The value of the constant varies between 0 and 1 and depends on the pore geometry and the physical properties of the material.

Principal stress. The three mutually perpendicular planes in a state of stress at any point in a body along which only normal stresses act.

Shear strength. Strength of material to overcome failure by shear deformation.

Shear fracture. A fracture that has a sense of displacement parallel to the fracture plane and forms at some acute angle to the maximum principal stress direction. All principal stresses must be compressive.

Tensile fracture. A fracture which has a sense of displacement perpendicular to the fracture plane and forms parallel to the maximum and intermediate principal stress directions and perpendicular to the minimum principal stress direction

Tensile strength. Material strength necessary to overcome failure in tension.

APPENDIX D

NOMENCLATURE

APPENDIX D

NOMENCLATURE

b – Formation volume factor

C, c – Constant

C_t – Total compressibility of the formation

dp – Pressure difference

Δt, dt – Time since shut-in

ΔP – Increase in fluid pressure in the wellbore over the original pressure

E' – Plane strain modulus and is expressed as $E' = E/(1 - \nu^2)$

E – Elastic modulus

g – Acceleration due to gravity

h – Effective reservoir flow thickness/overburden thickness

ISIP – Instantaneous shut-in pressure

k – Formation permeability

m – Slope of a plot

P – Pressure (bottomhole or surface)

P_b – Breakdown pressure

P_f – Fracture extension or propagation pressure

P_p – Pore pressure

P_{re} – Reopening pressure

P_w – Hydrostatic fluid pressure

P_{wf} – Flowing pressure

q – Fluid injection rate

r – Distance from the center of the borehole

r_w, R_w – Wellbore radius

S – Skin factor

T – Tensile strength

T_{inj} – Injection time

T_{injss} – Time to the beginning of pseudo-steady state flow

NOTATION OF SYMBOLS

σ_r – Radial stress

σ_θ – Circumferential stress

σ_h – Horizontal stress

σ_v – Vertical stress

σ_{min}, σ_{max}
– Minimum and maximum principal stress, respectively

$\tau_{r\theta}$, τ_{rz}, $t_{\theta z}$
– Shear stresses

σ_m – Maximum principal stress

σ_{xx}, σ_{yy}, σ_{zz}
– *in-situ* stress components in the Cartesian coordinate system

σ_{xy}, σ_{xz}, σ_{yz}
– *in-situ* stress components in the *xy*, *xz*, and *yz* planes, respectively

ϕ – Porosity

μ – Reservoir fluid viscosity

β_s – Ratio of average and wellbore pressures at shut-in

ν – Poisson's ratio

δ – Dimensionless shut-in time expressed as $\delta = \Delta t/T_{inj}$

θ – Angular coordinate

γ – Angle between a fracture and the well axis

ρ – Average density of the rock-forming materials

CONVERSION OF UNITS

1 psi = 6.895×10^{-3} MPa (1 MPa = 10^3 kPa)

1 foot = 3.048×10^{-1} m

1 liter = 1.00×10^{-3} m^3

SUBJECT INDEX

AUTHOR INDEX

SUBJECT INDEX

absolute permeability; 18, 29, 30
Anelastic Strain Recovery (ASR); 54, 55, 57
annulus; 9, 19

back stress; 12, 35
balanced and underbalanced perforations; 9
bi-linear flow; 24, 26
borehole holographic interferometry; 54 – 56
borehole slotting technique; 54 – 56
borehole televiewer; xxiv, 16, 56
bottomhole pressure gauges; 17
bottomhole pressure; 18, 19, 22, 25, 27, 45
breakdown pressure; 8 – 13, 22, 34 – 36, 40, 44, 46
breakout; 54, 56
bridge plug; 19
brittle failure; 4
bulk compressibility; 11

cased hole testing procedure; 18
cased hole; 9, 13, 16, 18, 46
casing pressure; 18
Christianovich-Zheltov model; 32
circumferential stress; 2, 10, 11, 72
closure pressure; closure stress 8, 13, 23 – 27, 32, 35, 37,
    40, 45, 46, 70
closure time; 27, 32
cohesive strength; 16, 47, 70
compressional wave velocity; 55
crack; 36 – 37, 54
creep; 22, 34

deviated well; 10
Differential Strain Analysis (DSA); 54 – 56
dilation; 31
dipmeter; 56
downhole gauges; 17
drill stem test; 11

effective stress; 2, 32, 70
elastic analysis; 2
elastic constants; 5, 55
elastic modulus; 31

flow meter; 17
flow-back manifold; 17
fluid compressibility; 31
fluid diffusion; 22
fluid diffusivity; 56
fluid viscosity; 30, 56
formation compressibility; 25
formation linear flow; 24
formation transmissibility; xxi, xxiii, 29
fracture azimuth; 56
fracture extension pressure; 9, 13
fracture height; 31, 32
fracture initiation; 9, 10
fracture linear flow; 23, 24, 31
fracture propagation pressure; 15, 35, 46
fracture stiffness; 9
fracture toughness; 36, 37
fracture width; 32
fracture-fluid; 9
frictional forces; 6, 37

G-function; 25, 32

helical perforation pattern; 16
holographic interferometric technique; 56
hoop stress; 8
horizontal fracture; 6, 30, 46
horizontal stress; 2, 3, 9 – 12, 16, 34, 35, 54 – 56
horizontal well; 16, 38
Horner plot; 24, 28, 30, 40, 45, 66
hydraulic fracturing stimulation treatment (HFST); 8
hydraulic fracturing; xxiii, 8, 34, 54 – 57
hydrostatic fluid pressure; 2, 72

impression packer; xxiv, 16, 54, 56
inclined borehole; 3, 4
inclined fracture; 23

SUBJECT INDEX

incomplete breakdown; 12
inflatable packer; 17
injection rate; xxiii, 8, 9, 11, 13, 16, 18, 19, 22, 27, 29 – 31, 34 – 37, 40, 45 – 47, 56, 66, 72
instantaneous shut-in pressure (ISIP); 8, 9, 13, 16, 22–24, 26, 34, 36–38, 40, 46, 47, 55, 72
interference hologram; 55

joints; 35

leak-off coefficient; 31, 66
leak-off; 8, 9, 11, 13, 16, 22 – 26, 31, 32, 36, 70

matrix compressibility; 11
maximum horizontal stress; 13, 54 – 56
maximum principal stress; 10, 70, 72
micro-frac; xxiii, 16, 17, 35, 37
mini-frac testing; 8, 16, 19, 56, 57
mini-frac; xxiii, xxiv, 5, 6, 8, 10 – 13, 16, 17, 19, 22, 23, 29, 31, 32, 34 – 38, 40, 45 – 47, 54 – 56, 66
minimum horizontal stress; 9 – 11, 16, 54 – 56
minimum *in-situ* stress; 8, 10, 12, 13, 16, 17, 22 – 29, 35 – 38, 40, 44, 47, 54, 56, 57
multiple fracture; 10, 37

natural fracture; 35, 56, 57
non-planar fracture; 10

overburden stress; 10, 45, 54 – 57
overcoring technique; 54, 56

packer; 6, 18, 19, 54, 56
perforated cased well; 16, 45
perforation friction effect; 13
Perkins-Kern model; 32
piezometer; 11
plastic analysis; 4
Poisson's ratio; 4, 9 – 11, 31, 56, 66, 70, 72
Pore pressure; 5, 9, 11, 13, 16, 34 – 36, 46, 70, 72
poro-elastic effects; 5, 35
pressure fall-off test; 11, 66
pressure gauges; 11, 17 – 19
pressure gradient; 22, 45, 46
pressure transducer; 17
proppant; 8
pseudo-radial flow; 9, 25
pump-in/flow-back test; 24, 27

quasi-orthogonal fracture; 28

radial stress; 2, 72
reopening pressure; 11, 12, 22, 28, 34, 36, 40, 46, 72
reservoir pressure; 6, 25, 29, 35

S-shaped fractures; 10, 16
shear failure; 13, 31
shear stress; 6, 72
shear wave (V_s); 55
shut-in tool; 18, 19, 29, 31
skin effect; 23, 29, 30
skin factor; xxiii, 30, 45, 66, 72
steam stimulation; xxiii
straddle packer; 16, 17, 19
strain energy; 10, 56
stress gradient; 47
stress intensity factor; 10, 37
surface pressure; 11, 17, 19, 22, 25, 29

tandem square 24, 25, 40
tar sand; 12, 13, 16, 18, 29 – 32, 34, 37, 40, 45, 47, 56, 57
tensile strength; 11, 13, 18, 22, 70, 72
thermal stress; 16
thermo-elastic; 8
tool string; 17
transmissibility; 17, 29, 30, 45, 66

uncased well; 11, 16, 40, 45

vertical fracture; 12, 30, 46
vertical or overburden stress; 10, 45, 47, 54 – 57
vertical well; 16, 17
visco-elastic; 5
visco-plastic; 5, 34
V_p/V_s ratio; 55

waste disposal; xxiii
wave attenuation; 55, 56
wave velocity anisotropy; 54 – 56
wellbore breakout; 54, 56
wellbore effects; 18, 19
wellbore stability; xxiii
wellbore storage; xxiii, 23, 24, 26, 29 – 31, 40, 66
wellhead pressure; 18, 19

Young's modulus; 56

AUTHOR INDEX

Abbas; xxiv
Abou–Sayed; xxiv

Bass; 55
Behrmann; 9
Bell; 47, 54
Bjarnason; 9
Bock; 55
Boone; xxiv, 35
Breckels; 35
Bredehoeft; xxiv
Brown; xxiv, 55
Bush; 34

Cheng; 5
Cheung; xxiv
Christianson; 10
Cinco–Ley; 23
Currie; 47

Daneshy; 9
De Bree; xxiv
Detournay; xxiv, 5, 8, 11
Dey; 55
Doe; 56
Dusseault; xxiv, 46, 47

Earlougher; 30
Elbel; 9
Enever; 36
Everdingen; 30

Fairhurst; xxiv, 56

Gnirk; 4
Gough; 54
Gringarten; 23
Gronseth; xxiv, 8, 16, 19, 22, 23, 36
Guenot; 5

Hagel; xxiv
Hagoort; 35
Haimson; xxiv, 8, 54, 56
Hallam; 10
Hannan; 55
Hassan; xxiv
Hickman; xxiv, 12, 23, 36, 54
Horner; 30
Hubbert; xxiv, 2, 5, 6, 8
Hurst; 30

Ikeda; xxiv
Irwin; 37

Johnson; 4
Jones; 19

Kehle; 6, 8
Kim; xxiv
Kirsch; 2
Kobayashi; 28
Kry; xxiv, 8, 16, 19, 22, 23, 36
Kuriyagawa; xxiv

Last; 10
Layne; 35
Lee; 32
Li; 56
Ljunggren; 9

McLennan; xxiv, 4, 5, 8, 9, 23, 28
Meyer; xxiv, 34
Mizuta; 28
Moos; 55
Morgenstern; 36

Nolte; xxiv, 24, 31, 32
Nur; 55

Peng; 55
Poon; 23
Prats; 34
Pros; 55
Proskin; xxiv, 45

Rabba; 16
Raisbeck; 47
Ramey; 23
Ratigan; xxiv
Roegiers; xxiv, 23, 28, 35, 37
Rosepillar; xxiv

Saltuklaroglu; 13
Salz; 35
Samaniego; 23
Santarelli; 5
Sargeant; 19
Schmitt; 55
Scott; 22
Shi; 4
Shoji; 36
Siriwardane; 35
Soliman; xxiv
Springer; 54
Stesky; 55
Strubhar; 9
Sun; 55

Teufel; 54
Thiercelin; 36
Timoshenko; 2, 5
Tsukahara; xxiv

van Eekelen; 35

Walters; xxiv
Warpinski; xxiv, 16, 34, 37, 54
Whitehead; 28
Willis; xxiv, 2, 5, 6, 8
Winkler; 55
Woodland; 47
Woolterton; 36

Yew; 10

Zoback; 8, 12, 23, 36, 54, 55

N.L.C. - B.N.C.
3 3286 11724638 5

Printed in Canada